Biofabrication Strategies and Engineered In Vitro Systems for Vascular Mechanobiology

Shantanu Pradhan, Omar A. Banda, Cindy J. Farino, John L. Sperduto, Keely A. Keller, Ryan Taitano, and John H. Slater*

The vascular system is integral for maintaining organ-specific functions and homeostasis. Dysregulation in vascular architecture and function can lead to various chronic or acute disorders. Investigation of the role of the vascular system in health and disease has been accelerated through the development of tissue-engineered constructs and microphysiological on-chip platforms. These in vitro systems permit studies of biochemical regulation of vascular networks and parenchymal tissue and provide mechanistic insights into the biophysical and hemodynamic forces acting in organ-specific niches. Detailed understanding of these forces and the mechanotransductory pathways involved is necessary to develop preventative and therapeutic strategies targeting the vascular system. This review describes vascular structure and function, the role of hemodynamic forces in maintaining vascular homeostasis, and measurement approaches for cell and tissue level mechanical properties influencing vascular phenomena. State-of-the-art techniques for fabricating in vitro microvascular systems, with varying degrees of biological and engineering complexity, are summarized. Finally, the role of vascular mechanobiology in organ-specific niches and pathophysiological states, and efforts to recapitulate these events using in vitro microphysiological systems, are explored. It is hoped that this review will help readers appreciate the important, but understudied, role of vascular-parenchymal mechanotransduction in health and disease toward developing mechanotherapeutics for treatment strategies.

Prof. S. Pradhan, O. A. Banda, C. J. Farino, J. L. Sperduto, K. A. Keller, R. Taitano, Prof. J. H. Slater Department of Biomedical Engineering University of Delaware 150 Academy Street, 161 Colburn Lab, Newark, DE 19716, USA E-mail: jhslater@udel.edu Prof. S. Pradhan Department of Biotechnology Bhupat and Jyoti Mehta School of Biosciences Indian Institute of Technology Madras Chennai 600036, India Prof. J. H. Slater Department of Materials Science and Engineering University of Delaware 201 DuPont Hall, Newark, DE 19716, USA Prof. J. H. Slater

Prof. J. H. Slater Delaware Biotechnology Institute 15 Innovation Way, Newark, DE 19711, USA

The ORCID identification number(s) for the author(s) of this article can be found under https://doi.org/10.1002/adhm.201901255.

DOI: 10.1002/adhm.201901255

1. Introduction

Among the current health challenges, cardiovascular diseases, obesity, diabetes, and associated vascular inflammation and dysfunction are attaining pandemic status throughout the world due to changes in dietary habits, lifestyle choices, and environmental exposure, among others.[1,2] Fundamental research into the biological changes associated with these diseases and clinical approaches to prevent, ameliorate, and treat these pathologies are gaining attention.[3] In addition to the biochemical, molecular, and genetic causes of these diseases, the biophysical forces and related mechanobiological events underpinning cardiovascular diseases are of great interest, but probing these events using in vivo or simplified in vitro models is challenging.^[4] Past research has implicated several factors, which regulate vascular structure and function at the cellular and tissue level, including hemodynamic variations, traction forces at the endothesubstratum, extracellular matrix (ECM) characteristics, cell-cell, and cellmatrix interactions, and others.[5-11] Comprehensive mechanistic investigation of

these processes is necessary to understand disease progression and ultimately develop therapeutic strategies to prevent and mitigate chronic and acute vascular pathologies.

In this regard, recent advances in tissue engineering, biomaterials, and biofabrication strategies to generate perfused microphysiological systems have facilitated the development of various in vitro models that closely recapitulate in vivo and native physiology.[12-15] Implementation of macroscale synthetic tissues has improved our understanding of underlying mechanisms of tissue function and related pathology.[16,17] In line with these advances, the need to vascularize synthetic tissue constructs and establish dynamic, fluidic, perfusion cultures has also arisen, thereby opening new avenues for investigating microenvironmental changes that occur during cardiovascular disease.^[18-21] Several microphysiological systems have been developed for disease modeling and drug development.[12,22-25] The demand for employing these platforms is primarily driven by the added benefits of: 1) recapitulation of complex 3D, tissuespecific microphysiology via use of multicellular co-cultures

ADVANCED HEALTHCARE MATERIALS

and ECM-mimetic biomaterials, 2) use of microliter- to picoliter-scale reagents and media, 3) user-defined, programmable, and continuous control of 3D vessel structure and flow, 4) spatiotemporal control over the distribution of biochemical gradients, and 5) the ability to monitor associated cellular and tissue events with high spatial and temporal resolution over extended time periods.

Toward this end, integration of vascularized microfluidic networks within microphysiological systems incorporating multiple cell types in engineered matrices has received significant attention. [13,26-28] Various techniques have been developed to fabricate these systems, which range from simple, linear channels to complex, tortuous, and interconnected networks that mimic the architecture and flow properties of native vasculature. [27,29,30] Studies to model and characterize flow, perfusion, and diffusion phenomena have also been conducted with respect to various organ niches and pathological scenarios.[31-34] Although such studies are becoming increasingly useful for modeling disease progression, drug transport, tissue oxygenation, angiogenesis, cardiovascular pathology, and cancer; the influence of physical flow parameters on the underlying cellular and tissue-level mechanobiology remains relatively underexplored. In the past, 2D substrates and static cultures have been used; but owing to their simplistic and assumption-heavy design, static 2D cultures fail to recapitulate the dynamic, everchanging properties of microvascular flow phenomena. [15,32,34] Hence, there is an urgent need to recreate biomimetic, vascular networks that mimic physiological flow properties and that support macroscale, synthetic tissues as well as facilitate the investigation of flow-associated forces and downstream mechanotransduction events occurring in vascular-parenchymal tissue interfaces.[35,36]

In this review, the need for fabrication of engineered vascular constructs (Section 2) is presented. The role of various structural and functional elements pertaining to vascular hemodynamics and associated mechanotransduction processes is described (Section 3). Multiple strategies for measurement of force and cell and tissue level mechanical properties are discussed (Section 4). The current state-of-the-art techniques for fabricating vascularized tissue constructs and in vitro models are surveyed with emphasis on fabrication efficiency (resolution vs speed), biocompatibility, scalability, and translatability (Section 5). The role of biophysical and hemodynamic forces in the context of pathophysiological processes and organ-specific niches is described (Section 6). Finally, current limitations and future opportunities in studying vascular mechanobiology in engineered systems are discussed (Section 7). This review will help readers appreciate the important role of hemodynamic forces at play within vascularized systems, associated cellular and tissue-level effects in various pathologies, and assist in designing improved microphysiological systems for disease modeling and development of vascular mechanotherapeutics.

2. The Need for Microfluidic & Vascular Networks Embedded In Tissue-Engineered Constructs

Traditionally, the influence of fluid shear stress and associated traction forces and strains on endothelial cell (EC) physiology



Shantanu Pradhan is an assistant professor of biotechnology at the Indian Institute of Technology Madras. He received his B.Tech. from the National Institute of Technology Durgapur and a Ph.D. from Auburn University. He was a postdoctoral researcher in the Department of Biomedical Engineering at the University of Delaware.

His research interests include biomaterials to mimic tumor and vascular microenvironments and in vitro engineered models for drug-testing applications.



Omar A. Banda is currently pursuing a Ph.D. in biomedical engineering at the University of Delaware. He received a B.S. in cell biology and biochemistry at Rice University. His research interests include hydrogel biomaterials, cellular mechanotransduction, and biophysics.



John H. Slater is an assistant professor of biomedical engineering at the University of Delaware. He received a B.S. in mechanical engineering from the University of North Carolina at Charlotte and a Ph.D. in biomedical engineering with a Graduate Portfolio Degree in nanoscience and nanotechnology from the University of Texas. He was a postdoc

in bioengineering at Rice University and a research scientist in biomedical engineering at Duke University. His research interests include biomimetic materials, mechanobiology, and in vitro microphysiological systems.

and function have been studied in reductionist models (e.g., parallel plate flow chambers, 2D substrates, transwell inserts).^[7,8,37,38] These studies have provided significant insights into critical aspects of vascular morphogenesis, differentiation, barrier function, diffusional transport, and paracrine signaling mechanisms. In particular, these models are excellent for decoupling the roles of several interconnected flow parameters with complex associations on vascular processes. For example, although physiological wall shear stress

ADVANCED HEALTHCARE

Table 1. Limitations of current reductionist in vitro vascular models. [15,32,34]

Physiological element	Limitations and challenges	
Cell types	Difficulty in incorporating multiple cell types with a high degree of spatial control to recapitulate local tissue niches and cell–cell interactions	
ECM and vascular architecture	Failure to incorporate tissue-specific ECM composition and complex vascular architecture	
Biomimetic flow	Lack of dynamic, complex variations in flow characteristics and resulting forces at the vascular-parenchymal interface	
Macrotissues	Inability to integrate with complex macroscale tissue constructs	
Cell–ECM Interactions	Lack of well-controlled cell–ECM interactions and associated mechanotransduction processes	

(WSS) and circumferential strain (CS) are known to modulate EC morphology, phenotype, function and gene expression;^[39–45] studies have reported that the asynchronicity between WSS and CS results in a complex, time-varying mechanical force pattern that causes a phenotypic shift in ECs from an atheroprotective/normopathic to an atherogenic/vasoactive behavior.^[46,47] Although useful, these models suffer from certain limitations, which make them unattractive beyond basic mechanistic studies (Table 1).

With the advent of new biofabrication strategies for creating 3D, biomimetic vascular networks, more in-depth mechanistic investigations of hemodynamic forces and vascular mechanobiology have become possible.[48-52] Implementation of hydrogels has facilitated the integration of vascular networks with mesoscale, heterogeneous, tissue-specific constructs with complex flow patterns.^[28,35] Hydrogels used for recreating vascular microenvironments include natural, synthetic, and hybrid blends, which can be tuned to cover a wide range of physical (stiffness, porosity, nanotopography, diffusivity) and biochemical properties (adhesivity, degradability, paracrine signaling cues) to emulate organ-specific ECM composition (Table 2). The vast repertoire of hydrogel materials, recent advances in material design and synthesis, and optimized selection of biofabrication techniques presents significant opportunities to create biomimetic vascularized microphysiological systems that are scalable, reproducible with engineered precision, fabricated in a high throughput manner, and provide a high degree of spatiotemporal and fluidic control. These engineered systems are expected to facilitate detailed

Table 2. Range of hydrogel materials used for engineered in vitro vascular constructs.

Hydrogel	Туре	References
Collagen	Natural	[53–60]
Fibrin	Natural	[61–63]
Hyaluronic acid (HA)	Natural	[64,65]
Poly(lactic-co-glycolic acid) (PLGA)	Synthetic	[66–68]
PEG-peptides	Synthetic	[69–76]
PEG-proteins	Hybrid	[77,78]
PEG-dextran	Hybrid	[79]
Gelatin-blends	Hybrid	[80-84]
Gelatin methacrylate (GelMA)	Hybrid	[85–87]

investigation of vascular mechanobiology and thereby provide comprehensive views of associated pathophysiological events, which can be difficult to achieve using in vivo or simplistic in vitro models.

3. Vascular Hemodynamics and Mechanotransduction

The implementation of in vitro platforms toward hemodynamic modeling and vascular mechanobiology requires a basic understanding of vascular structure, physiology,

and the transient forces in the mechanical microenvironment, which are discussed below.

3.1. Vascular Structure and Physiology

In general, large blood vessels consist of three concentric layers: 1) tunica intima, 2) tunica media, and 3) tunica adventitia (**Figure 1**). The tunica intima is the innermost lining consisting of an EC monolayer supported on a thin basement membrane (BM) (primarily composed of type IV collagen and laminin). Since it is in direct contact with blood flow, the EC lumen regulates the transport of nutrients and other soluble factors from the blood to the parenchymal tissue through a tightly-regulated barrier. EC barrier permeability is controlled by intercellular junctions and adhesion molecules including vascular endothelial cadherin (VE-Cadherin, CD144), platelet EC adhesion molecule (PECAM-1, CD31), and claudin-5 among others, and varies in an organ-specific manner and along the hierarchical structure of the vascular tree.

The EC layer is also responsible for: 1) maintaining vascular tone and blood pressure (via secretion of vasomodulatory factors, e.g., nitric oxide (NO), prostracyclin, and endothelin (ET)-1), 2) vascular homeostasis (via secretion of pro- and anticoagulants, e.g. von Willebrand Factor (vWF), tissue factor and thrombomodulin), 3) angiogenesis (via secretion of growth factors, e.g. VEGF, PDGF, and surface receptor expression, e.g., Ang-1, -2), and 4) inflammation (via induced expression of E-selectin, intercellular adhesion molecule (ICAM)-1, or vascular cell adhesion molecule (VCAM)-1 in response to inflammatory molecules, (interleukin (IL)-1 β , tumor necrosis factor (TNF)- α , interferon (IFN)- γ , or reactive oxygen species (ROS)). [7.8]

The tunica media surrounding the intimal layer is composed of mural cells (pericytes in microvasculature and vascular smooth muscle cells (VSMCs) in larger vessels) embedded within an elastin- and collagen-rich matrix. [88] The medial layer is responsible for dilation and constriction of large vessels in response to endothelial-produced nitric oxide (NO) and maintenance of vascular quiescence for vessel stability. The elastic properties of elastin and the tensile properties of collagen act in a coordinated and balanced manner to ensure tightly regulated vasomodulation. The phenotypic and functional plasticity of mural cells depends on both the metabolic and nutrient transport demands of organ niches and their position along the vascular tree. [89,90]

www.advhealthmat.de

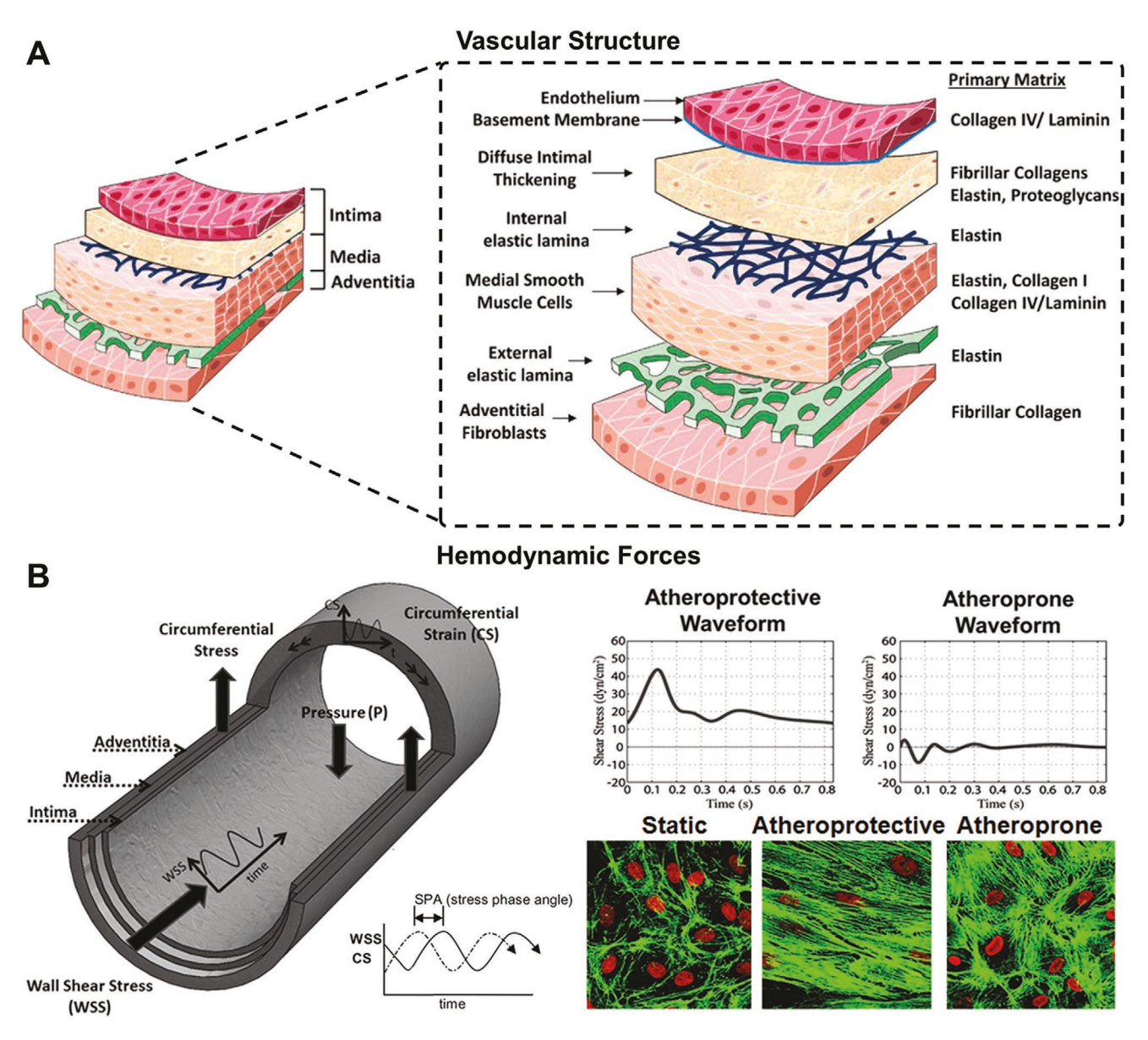


Figure 1. Vascular structure and hemodynamic variables in vascular flow. A) Schematic of the three concentric layers: tunica intima, tunica media and tunica adventitia and associated matrix proteins that constitute a large blood vessel. Adapted with permission. [7] Copyright 2018, American Chemical Society. B) Schematic of the forces acting on blood vessels and the phase lag between wall shear stress (WSS) and circumferential strain (CS) characterized by the stress phase angle (SPA). Adapted with permission. [47] Copyright 2015, PLOS One. Computer-simulated waveforms and cultured EC morphologies under static, atheroprotective and atheroprone conditions (green: F-actin, red: nuclei). Adapted with permission. [99] Copyright 2004, National Academy of the Sciences.

The outermost layer, tunica adventitia, is composed of a fibroelastic connective matrix (made of elastin and type I and III collagen) and hosts a complex milieu of resident cells, including fibroblasts, myofibroblasts, macrophages, T cells, B cells, dendritic cells, mesenchymal, hematopoietic and endothelial progenitors, neural cells, and adipocytes among others.[91] The adventitial layer provides structural support to large vessels, participates in vasomodulation and primary immune responses to inflammation, injury, and repair. Adventitial fibroblasts act as cellular sensors of hemodynamic perturbations and can undergo phenotypic activation toward myofibroblasts, leading to matrix remodeling, altered deposition of matrix proteins, and

changes in vascular tone. Since the medial and adventitial layers act as intermediaries between the inner vessel lumen and the surrounding parenchymal tissue, the mechanical properties of these layers (influenced by protein composition, conformation, alignment, degradation) are critical to a wide range of mechanotransduction processes that ultimately dictate organ-specific function and pathological characteristics. [92,93]

The endothelial glycocalyx, a brush-like, nm-thick layer composed of proteoglycans, glycoproteins, and glycosaminoglycans (GAGs), is present on the luminal EC surface and acts a mechanosensory intermediate between blood flow and the plasma membrane.[7,8,94] The EC luminal surface also hosts reversibly





www.advhealthmat.de

gated ion channels (pores formed by transmembrane proteins), which permit coordinated exchange of Na⁺, Ca²⁺, K⁺, and Cl⁻ ions in response to hemodynamic variations and stretch- and strain-induced perturbations. Mechanical sensing of hemodynamic perturbations is also mediated by the EC plasma membrane via conformational changes in transmembrane proteins and the lipid bilayer, variations in local membrane fluidity and stiffness, engagement of lipid rafts and caveoli, and stimulation of G-protein-coupled receptors (GPCRs).^[7,8]

The basal EC surface is mechanically coupled to the underlying BM via integrin-mediated adhesions. Adhesion ligands present in the constitutive proteins of the BM selectively engage specific integrins and regulate integrin clustering and adhesion site assembly and disassembly, intracellular and intranuclear mechanotransductory signaling processes, and ultimately influence EC morphology and behavior including spreading, alignment, migration, and assembly and function. [38,43,93] The sensory elements of the EC monolayer help transmit mechanical signals from the luminal flow to the intranuclear space via actomyosin contractile machinery mediated by RhoA-Rho kinase (ROCK) signaling and other GTPases. [8,38,93,94]

The cytoskeletal forces transduced to the EC nuclei influence mechanosensitive gene regulation, epigenetic changes (including DNA methylation), and translocation of nuclear and cytoskeletal proteins, resulting in nuclear deformation, stiffening, and alignment. [95] One prominent example of an EC mechanotransducer is Yes-associated protein (YAP) and the transcriptional coactivator (PDZ)-binding motif (TAZ). Changes in blood flow patterns (from laminar to oscillatory regimes) cause activation and cytoskeletal-nuclear translocation of YAP/TAZ, EC proliferation, and a proinflammatory response leading to an atherosclerotic phenotype. Flow-mediated and substrate elasticity-mediated YAP/TAZ translocation is also responsible for vessel maintenance, stability and barrier formation, and inversely, for vascular remodeling and angiogenic sprouting, in a context-dependent manner. [96–98]

The complex vascular microenvironment consisting of multiple cell types, matrix proteins, regulatory biochemical and mechanical cues, and their coordinated, niche-specific presentation and interactions, tightly regulate vascular function and responses to changes in hemodynamics. Alterations in normal structural assembly of cellular and tissue components or expression of signaling molecules can result in various vascular anomalies, which could eventually amplify toward complex pathological conditions.

3.2. Hemodynamic and Mechanical Variables in Vascular Flow

Blood is a dynamic, shear-thinning fluid composed of mechanosensitive cells (red blood cells, white blood cells, platelets) suspended within plasma (proteins, small molecules, and dissolved gases).^[5] The collective synergism of complex blood flow combined with blood vessel characteristics helps maintain mechanical homeostasis in the vascular niche using negative feedback mechanisms. The dynamic mechanical elements associated with blood flow can be grouped into hemodynamic forces (e.g., shear stress, cyclic stretch, and circumferential pressure), vessel wall forces (e.g., BM elasticity and topography)

and intravascular forces (e.g., blood viscoelasticity, RBC deformation, margination) (see Figure 1 in Polacheck et al.^[100] and Figure 3 in James and Allen^[7]). Their regulatory role in vascular homeostasis and function is described below.

3.2.1. Fluid Flow and Shear Stress

Blood flow through vessels is characterized by varying degrees of pulsatility, directionality, and laminarity, depending on the vessel diameter, vessel wall thickness, geometry, and location with respect to the heart and cardiac cycle among other factors.[7] Straight vessels usually encounter unidirectional, laminar flow with higher wall shear stresses (WSS) (1.2-1.5 Pa), while branching or bifurcating vessels can experience transient flow reversals, flow disturbance and turbulence, and lower fluctuating WSS (can drop to 0 Pa). Owing to these complex flow patterns, the magnitude of WSS is described by either the maximum value or the time-averaged value (TAWSS) over the time period of interest. The directionality of flow is described using an oscillatory shear index (OSI) (0 for perfectly unidirectional and 1 for complete reversal) and transverse wall shear stress (transWSS) (extent to which WSS acts perpendicular to uniaxial flow direction).^[7]

EC responses to shear stress have been studied and reviewed extensively. [7,43,93,101,102] In general, physiological shear stress (≈0.448 Pa in the aorta to ≈3.2 Pa in small arteries) associated with sustained unidirectional laminar flow induces directional alignment and elongation of ECs, with reduced turnover (higher quiescence), strengthened cell-cell junctions and cellmatrix adhesions, and lower permeability. Additionally, this flow regime also causes directional remodeling of focal adhesions and actin stress fibers, higher production of NO and expression of endothelial nitric oxide synthase (eNOS), and anti-inflammatory gene expression profiles characteristic of the atheroprotective phenotype.^[103] In contrast, supra- or subphysiological WSS associated with disturbed, bidirectional, or transverse flow is associated with EC rounding, actin stress fiber disassembly or disorganization, weaker cell-cell junctions and cell-matrix adhesions, lower permeability, oxidative stress, EC proliferation, and a proinflammatory expression profile characteristic of the atherogenic phenotype. [7,8,41,99] Differential WSS magnitudes and directionality also affects vasomodulatory regulation of ECs via alterations in angiogenic, chemokine, and inflammatory secretome and activation of VSMCs.[88] Hence, shear stress plays a key role in maintaining EC monolayer structure and function and overall vascular homeostasis.

3.2.2. Circumferential Strain and Cyclic Stretch

In addition to fluid flow, the pulsatile nature of the cardiac cycle and biophysical properties of the blood cause mechanical distention of vessel walls in a complex, transient, and location-dependent manner. Blood pressure exerted on the vessel walls is a combination of four pressure components: 1) ambient pressure (usually considered 0 Pa), 2) hydrostatic pressure (considered 0 Pa at the reference position of the tricuspid valve and varies in proportion to the vertical displacement from this





(Figure 1) dictates the viscoelastic and strain-stiffening behavior of the intimal layer, which affects EC monolayer integrity and function.

position), 3) dynamic pressure (purely drives blood flow and does not affect vessel wall dynamics), and 4) potential energy pressure (the major influencer of vessel wall expansion and contraction caused by cardiac pulsation and dependent on an individual's activity level, state of health, age, and vascular tone). The dynamic nature of blood flow lends a transient quality to lateral blood pressure which varies from 1.3–16 kPa depending on the location. Although most studies have focused on the effects of pulsatile pressure, hydrostatic pressure also influences EC orientation, cytoskeletal reorganization, proliferation, EC-specific protein expression, and altered vaso-modulatory behavior. [93,104,105]

The pulsatile nature of blood pressure results in cyclic stretch (or CS) of the vessel wall, which can be uni- or multiaxial, depending on the blood vessel location and geometry. Uniaxial CS induces EC elongation and alignment perpendicular to the stretch direction, proportionate to the magnitude of applied strain magnitude (up to 10%) and frequency (up to 1.5 Hz), with corresponding changes in actin stress fiber reorganization and focal adhesions. [106] Rotational changes in stretch direction can induce reorientation of ECs to new axes, actin cytoskeletal reorganization, and changes in morphology.[107,108] Similar to shear stress, physiological CS (5-10%) helps maintain fundamental processes including angiogenic sprouting, matrix remodeling via MMP secretion, growth factor and vasomodulatory secretion, and protection from apoptosis via stretchactivated ion channel stimulation, integrin engagement, and downstream mechanotransductive signaling. [42,109,110] However, pathological CS (>20%), caused by hypertension, can result in enhanced ROS and TNF- α production, increased apoptosis, and imbalanced MMP secretion, ultimately affecting EC patency and permeability.[111-114]

Due to the viscoelastic nature of the vessel wall, there is a lag between the applied blood pressure, CS, and WSS during each cardiac cycle. [46,47] The temporal difference between WSS and CS is termed the stress phase angle (SPA), which is an indicator of flow synchronicity in blood vessels (Figure 1). Synchronous flow (SPA = 0°) with steady physiological shear stress helps maintain an atheroprotective EC phenotype, while higher degrees of asynchronicity (maximum SPA = -180°) with fluctuating shear stress, usually observed in vessel branch points and during hypertension, is associated with an increased risk of atherosclerotic plaques.^[46,47] Cyclic stretching of blood vessel walls due to lateral pressure also affects the magnitude of local WSS experienced by ECs, thereby demonstrating the intimate coupling of these factors in hemodynamics. [6,7,45] Hence, tight regulation of CS and blood pressure in coordination with WSS is critical in maintaining healthy vascular tone and function, which is disrupted under pathological conditions.

3.2.3. Basement Membrane Elasticity and Topography

The biophysical features of vessel walls, including BM elasticity, topography, fiber orientation and anisotropy, play a significant role in regulating mechanotransduction processes. The ECM composition of the BM and physical assembly of constitutive proteins (collagen, elastin, laminin, fibronectin, and others)

The influence of matrix elasticity on EC behavior has been investigated using various substrates and elasticity regimes.[57,115] In general, higher BM elasticity leads to increased EC spreading, focal adhesion formation, traction force generation, higher EC contractility, and disruption of cell-cell junctions.[116] Stiffness-mediated YAP/TAZ translocation to EC nuclei also occurs concurrently with changes in EC phenotype, actin cytoskeletal reorganization, and Rho-GTPase activation.^[98] Stiffness-dependent sensitivity of ECs to growth factors, inflammatory molecules, and other small molecules also affects platelet adhesion, endothelial-mesenchymal transition (Endo-MT), and migration. [8,38,117,118] These changes influence matrix deposition and remodeling of the BM, affecting ligand density and distribution, all of which act as a positive feedback loop driving higher vascular permeability and lower patency.[115,119] Changes in ECM composition are associated with age and hypertension where gradual degradation of constitutive elastin and replacement with fibrous collagen leads to stiffer vessels.^[7,8] Of particular interest is the BM topography, which consists of a range of spatial mechanical cues including fiber alignment, pore characteristics, and anisotropy. Investigations on well-defined engineered substrates patterned with grooves, microchannels, or haptotactic gradients demonstrate the role of BM topography on EC alignment, proliferation, migration, and sensitivity to biochemical stimulation.[115,120,121]

Stiffness and topography associated responses of ECs are also coupled to those resulting from shear stress and cyclic stretch.[7,8,122] Application of strain induces alignment and densification of collagen fibers while variations in EC-generated traction forces due to shear stress and cyclic strain cause plastic deformation of collagen networks. Collagen orientation and anisotropy also have synergistic or antagonistic effects on EC behavior based on flow-induced forces. The magnitude of shear stress needed for EC alignment and spreading is inversely correlated to BM stiffness.^[7,8] Lifetime accumulation of pulsatile stretch is also correlated with intimal stiffening and stiffness heterogeneity leading to reduced dampening of pulsatile waveforms in the distal microcirculation.[123] Compounded with increasing stiffness of the parenchymal tissue, the unmitigated transmission of pulsatile pressure to organ-specific niches can eventually promote chronic, age-related disorders including kidney failure and some forms of dementia.[124,125] The hemodynamic effects of stiffness-sensing in ECs influence vascular assembly and function in a complex, transient, and highly regulated manner.

3.2.4. Intravascular Mechanics

Although flow-related and vessel-related properties influence vascular physiology, the mechanical properties of blood, including properties of individual cells and the cell collective, also affect vascular processes.^[5] In particular, variations in cytoskeletal architecture and the presence/absence of nuclei result in mechanical stiffness differences among RBCs, WBCs,



HEALTHCARE
____MATERIALS

and platelets, which dictate elasticity and deformability of individual cell types. [126,127] Intercellular collisions occurring in bloodflow cause margination of stiffer WBCs and platelets toward the vessel wall while the softer RBCs flow in the central space. As a result, the EC monolayer frequently encounters adhesive forces (from platelets) and rolling/shearing forces (from leukocytes and neutrophils). [128,129] Blood viscosity plays a central role in the shear stress exerted on ECs, viscosity being dually coupled to shear rate and hematocrit. Biophysical regulation of blood flow and blood components, including platelet and blood clots, has been investigated and reviewed previously. [5,130,131]

Hemodynamic forces occurring in the multifaceted vascular microenvironment, coupled with the structural assemblage of blood and blood vessel components, significantly influence cellular and tissue function. In-depth investigation of the individual and collective role of these perturbations and decoupling their complex associations is necessary toward mechanistic understanding of various states of health and disease. Engineered models of microvascular networks aim to accelerate these studies and show significant promise in unraveling these independent influences of vascular function.

4. Measuring Cell and Tissue Mechanical Properties for Mechanotransduction Studies

Measurement of hemodynamic forces acting within engineered vascular microenvironments is preceded by the need to quantify mechanical properties of the constituent cells and materials at different length and time scales.[132-134] Developing methods to probe mechanical forces and material properties within vascularized networks poses some unique challenges. Traditionally, mechanical characterization of natural and synthetic cell-laden matrices has been conducted using tensile and compressive testing, where mechanical moduli can be calculated from stress-strain curves gathered from tissuescale samples. In addition, more descriptive and complex moduli describing viscoelastic properties of these materials can be obtained from dynamic tests using similar equipment, as well as from rheological studies.[11,134] Together, these tools have been critical in describing changes occurring in tissues in response to aging and in various pathological conditions (Figure 2).[135,136]

Unfortunately, while many of these existing techniques are suitable for macroscale measurements, they are ill-equipped to characterize nano- to microscale changes in the mechanical environment experienced by cells, rendering them unfavorable for applications in hydrogels containing embedded microfluidic and/or vascular networks. At this scale, mechanical properties, such as tissue stiffness, can vary widely depending on multiple factors including local cellular tension, ECM composition, and flow conditions, leading to inaccuracies in the description of the mechanical environment. [11,135,137,138] The challenges in implementing existing measurement techniques to characterize engineered, vascularized microstissues have hindered the mechanistic understanding of vascular development and vascular disease progression in complex 3D environments. However, novel approaches to measure cell-generated

forces and material properties have emerged that can begin to fill this gap. $^{[132,139-142]}$

Measurements of mechanical properties in engineered microenvironments can be grouped into two general categories:

1) mechanical properties of the substrate /matrix constituting the ECM, and 2) forces acting on, generated in, or propagating through these microenvironments.

4.1. Measuring ECM Mechanical Properties

As a general rule, methods characterizing the ECM employ some means to apply a known force coupled with a method to measure the resulting strain to approximate the modulus or other descriptors of material mechanics. These methods include nano/micro-indentation and optical manipulation approaches.

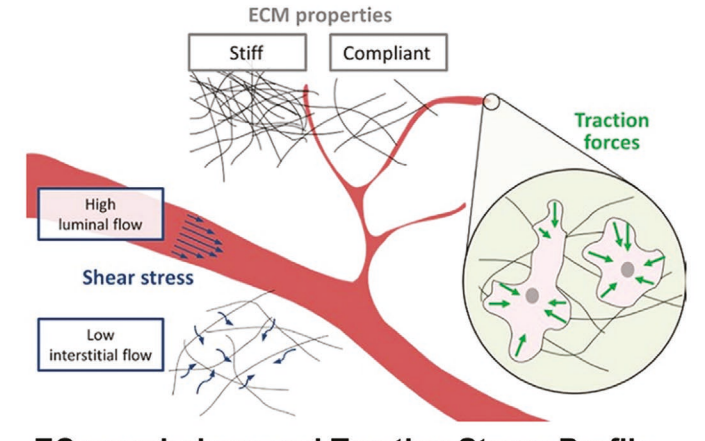
Indentation methods (e.g., atomic force microscope (AFM), nano- and microindenters) use calibrated probes (i.e., with known geometry and elasticity) to indent a surface with unknown mechanical properties.[141,144,145] Depending on the type of indenter, either axial displacement or orthogonal deflection of the indenter is measured as a function of indentation depth. From these data, the stiffness of the material at the surface can be approximated. These approximations require a theoretical model based on the tip geometry (e.g., spherical, pyramidal, etc.) to calculate the force imparted on the sample by the indenter. Additionally, because of the low magnitude moduli often associated with tissue, a thorough characterization of adhesion forces between the sample and the indenter is required. Several models have been developed to incorporate the effects of these adhesion forces.[146,147] A major benefit of indentation systems is the ability to tailor probes specifically to a sample of interest, making them suitable for a wide range of biomaterials and for engineered tissues that model healthy and diseased states.[148-150] Cantilever stiffness as well as the size and shape of the probe tip (affecting the contact area) can be adjusted to measure forces as low as several piconewtons and has been used to approximate the elastic properties of individual protein molecules and polymer chains.^[151,152] Since indentation methods often allow only for the surface of a material to be indented, this approach is often not suitable for in situ measurements. However, for samples where the materials of interest lie near the surface, highly resolved maps of material stiffness can be generated by iteratively indenting the sample throughout an area of interest.

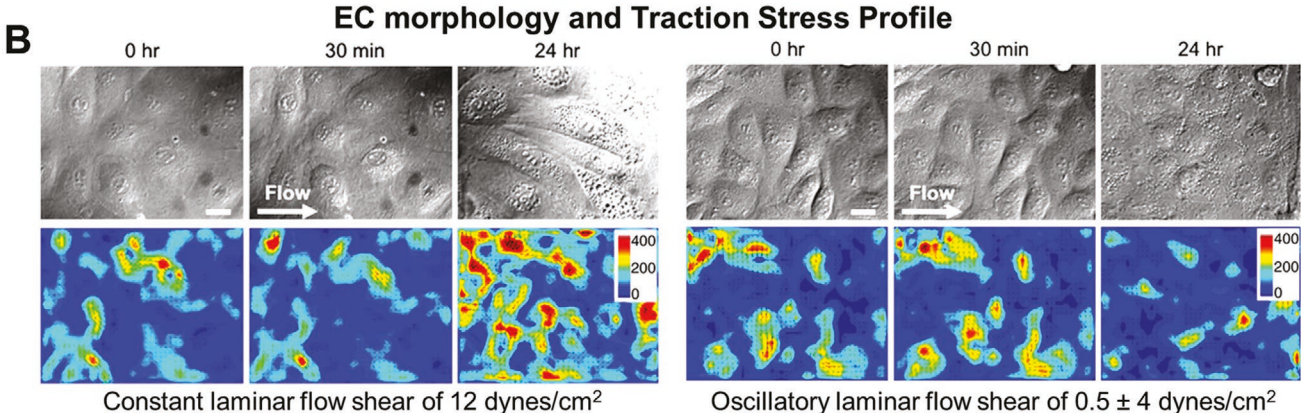
Optical manipulation approaches (e.g., optical tweezers—single-beam gradient force traps) employ focused lasers to impart force on particles near or within the beam path. Monitoring the effect of this force on the motion of a target particle provides information about the surrounding matrix, which can be used to approximate material properties. [132,140,141] Several factors influence the magnitude of force generated on a given particle, including the size and refractive index of the particle, the strength of the electric field created by the beam, and the electric dipole moment of the particle. For use in characterizing biological systems, the combination of laser parameters and particle probes must be calibrated a priori. There are several calibration methods available with differing advantages based

Δ

www.advancedsciencenews.com www.advhealthmat.de

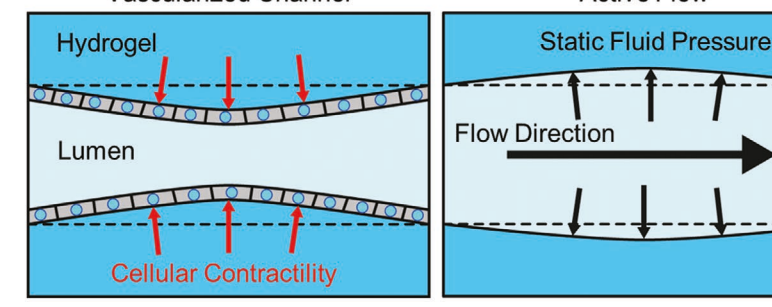
Microenvironmental Forces in the Vascular Environment





Cellular Deformability in Vascularized Constructs

Vascularized Channel Active Flow Flow in Vascular Channel



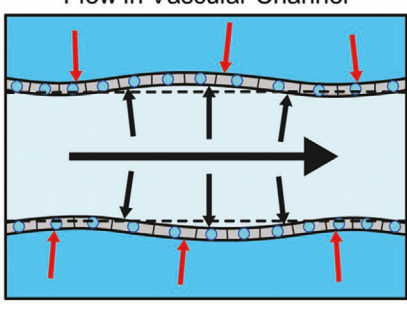


Figure 2. Measurement of endothelial cell forces in the vascular microenvironment. A) Schematic of microenvironmental forces experienced by ECs in blood vessels and generation of traction forces by ECs in response to these cues. Adapted with permission. Opporight 2016, John Wiley & Sons Ltd. B) DIC images and 3D traction stress (Pa) maps of confluent EC monolayers exposed to constant laminar flow with a shear of 12 dynes cm⁻² and oscillatory laminar flow with a shear of 0.5 \pm 4 dynes cm⁻² at different time points reveal a differential EC response (SB = 10 μ m). Adapted with permission. Opporight 2012, National Academy of the Sciences. C) Considerations for approximating cellular contractility in vascularized constructs. ECs in a vascularized channel are contractile and the magnitude of contraction (red arrows) varies based on hydrogel modulus and static pressure in the channel. Depending on the means of generating flow in prefabricated channels, inducing flow in a channel may change static pressure (small black arrows) in the system. To measure material stresses in vascularized networks caused by cells under active flow conditions, a constant pressure head (e.g., a syringe pump) can be used to drive flow so that static pressure can be assumed constant, and changes in material strain can be directly attributed to cell-generated forces.

on the intended system to probe. Some commercially available systems feature built-in calibration systems to stream-line these measures, allowing for rapid characterization of soft materials with high resolution.^[153,154]

4.2. Measuring Cell-Generated Forces

Cell-generated forces play critical roles in the development and function of microvascular networks. In many cases, these forces

www.advhealthmat.de

ADVANCED HEALTHCARE

are used by cells to sense the physical nature of the surroundings to initiate signaling cascades influencing cell behavior and phenotype (Figure 2). Methods to measure these forces include ECM strain tracking and Förster resonance energy transfer (FRET).^[140,155]

ECM strain tracking measures the forces generated by individual cells or cell clusters on their surroundings and typically rely on tracking strain within the substrate and using resulting strain maps to predict the cell-generated forces that induced them. While converting the material strain into stress is straightforward, converting the material stress into cell generated tractions is an ill-posed problem (i.e., with infinite solutions). As a result, force approximations can vary widely depending on the methodology used. Regardless, these methodologies, broadly referred to as traction force microscopy (TFM), continue to yield insightful biological trends linking cell-generated forces to biological phenomena (Figure 2). [141,156–158]

Resolving forces at the scale of individual cells or focal adhesions requires dense measures of material strain to produce accurate strain maps. The most common means to record these strain maps is to use an elastomeric substrate decorated with densely packed nano- to micron-scale fluorescent beads.^[143,159–161] Displacement of the fluorescent beads is calculated by collecting an image of the beads under cellular tension and comparing that image to an image where the cells have been completely relaxed or physically removed. Measured displacements are converted to strain fields, which can be used to approximate cellular tractions. Another common TFM approach employs an array of small elastomeric cylindrical pillars.[139,143,161] The flat upper surface of these pillars is treated with an adhesive protein to promote cell adhesion. Once bound, contracting cells cause the pillars to deflect, and the deflection is used to approximate the cell-generated forces.

A more recent alternative to TFM involves exploiting FRET phenomena to track strain in modified load-bearing proteins or substrates.^[140,141,161] These sensors allow the user to track the separation of chromophores embedded in the tertiary structure of a modified protein, or on separate strands within duplexed DNA. The efficiency of this energy transfer is directly related to the distance between chromophores and can be measured using microscopy techniques capable of resolving the relative fluorescence of donor and accepter chromophores (i.e., the FRET index). A major benefit of using FRET-based sensors is the ability to directly measure strain within a target molecule. Coupled with elasticity data from AFM tests on these probes, strain can be converted into the total force required to separate the chromophores by a known distance. In this way, force applied to modified proteins can be directly measured in real time. Although challenging, a variety of FRET-based sensors have been developed for several load-bearing proteins found within cell-cell adhesions, cell-matrix adhesions, and other load-bearing cellular structures. [140,141,161]

4.3. Translating Current Techniques to Vascularized Constructs

Several challenges exist with respect to measuring cell generated forces in fluidized vascular networks. One of them is the adaptation of 2D traction calculation workflows toward

3D environments. Many studies of traction force approximations rely heavily on the assumption that cellular substrates are planar, which simplifies approximations of in-plane and out-of-plane components of traction forces. 3D environments invalidate this assumption and therefore require thorough characterization of the interface between the cell surface and the underlying substrate (i.e., approximations of surface normals). While this approach has been accomplished for isolated cells embedded in hydrogels or on nonplanar surfaces, [159,162] it needs to be adapted to incorporate the additional complexity of vascularized networks (Figure 2).

In the meantime, foregoing the conversion to traction forces and instead using strain mapping or material stress distributions to describe the mechanical behavior of cells in vascular networks enables studying the relationship between cellinduced material stress/strain and phenomena such as cellular migration and extravasation. [163–165] In this regard, collagenbased hydrogels have been employed to eliminate the need for exogenous fiducial markers, as strains can be measured directly from collagen fibril organization monitored via second-harmonic generation (SHG) microscopy or confocal reflectance (CR) microscopy. [166]

Another major challenge in this regard is consideration of flow-associated forces. Approaches to characterize cell-generated forces relies on highly precise localization of fiducial markers to track material strain. [159,160] which can be disrupted by the application of fluid shear stress in fluidized networks (Figure 2). As a result, measuring traction forces in flow-based systems requires capturing a pre-stressed state of the hydrogel under stable flow conditions, so that additional changes in strain fields can be directly attributed to cellular activity. Studies on planar substrates within fluidized chambers have demonstrated the feasibility of measuring traction forces under flow.[39,43,167-169] ECs cultured under flow undergo changes in cell-cell junction organization and forces, migration and alignment, and traction force magnitudes. Extending these flow-based studies to 3D vascularized networks will likely require highly reproducible networks with well-characterized flow-profiles to achieve a known prestressed state for strain field measures. The magnitude of the impact of flow depends heavily on the elastic properties of the hydrogel being used. Characterizing the elastic properties of the hydrogels under flow will require high precision tools, such as optical or magnetic tweezers, to characterize local changes in material properties due to flow.[140] In addition, 3D microenvironments require considerations of strain propagation between endothelial branches in complex networks, as contracting vessels could potentially change the effective stiffness of the surrounding hydrogel.[170-172] Separating relative contributions of vessel contractility and fluid pressure will be key to accurately measuring cell-generated forces in vascularized tissue constructs.

Where applicable, FRET-based sensors could be invaluable for circumventing several challenges associated with strain tracking in vascularized constructs. [140,173] The ability to directly measure force generation in mechanosensitive proteins removes the need to physically characterize the substrate, greatly simplifying the overall process. 2D studies have demonstrated the feasibility of using FRET-based sensor in active flow conditions, and it is likely that this approach could be directly translated into 3D networks.



www.advhealthmat.de



Relatively few tools are well adapted to study mechanics of 3D vascular networks. Applying existing tools will require significant adaptations of existing workflows to deal with confounding factors such as flow conditions and cell-induced strain propagation, but can potentially yield important new insights into the mechanobiology of vascular networks.

5. Fabrication Strategies to Generate Microfluidic and Vascular Networks in Hydrogels

Over the past few decades, a multitude of strategies have been developed for fabrication of 3D in vitro microfluidic and vascular networks. [27,49–51,174] The major considerations with regard to these techniques are scalability, user-programmability with a high degree of control, reproducibility, throughput, resolution, cost, architectural complexity and intricacy, spatial positioning of multiple cell types, cytotoxicity, material handling and processability, and control over local physical and biochemical cues for rapid vascular morphogenesis and functional integration (see Figure 1 in Bogorad et al.^[29]).

Meso- and macroscale constructs can be achieved in a highthroughput, reproducible fashion using 3D bioprinting and stereolithography, but these techniques also involve higher relative costs and may incur toxicity issues. Additionally, resolution and architectural complexity is often limited with increase in scale and the choice of printable and cytocompatible materials can limit the applicability of these approaches. Micromolding methods are relatively cheap, facile, and easily reproducible but scalability and low complexity limit their implementation to simple, often planar vessel architectures.[51] Laser-based fabrication approaches can achieve high resolution, reproducibility, spatiotemporal control and complexity, although poor scalability and low throughput are major hindrances.^[175] Selfassembly provides a high degree of architectural complexity and vasculomimetic organization, albeit with a high degree of stochasticity and poor reproducibility in terms of producing the exact same architecture each time.[30,35,176,177]

An important operational metric, spatial resolution/time to manufacture (RTM) ratio, was previously defined to provide a comparative analysis of various biofabrication strategies. A higher RTM value indicates a more efficient process (faster production speed with finer spatial details). For most technologies, the RTM ratio remains bound between 0.01 and 1.00, indicating that high-throughput processes are limited in resolution and generating intricate features is time-consuming. In recent advances, combinatorial fabrication strategies employing soft lithography, bioprinting, micromolding, or laser-based degradation integrated with on-chip systems have helped overcome many of these limitations while retaining the inherent advantages offered by individual approaches alone. [13,14,28,178–181] Major features of these techniques and their applicability toward investigation of vascular mechanobiology are discussed.

5.1. Self-Assembly of Microvascular Networks

The most prominent and facile approach for fabrication of 3D vascular networks is self-assembly, which relies on the

ability of ECs encapsulated in hydrogels to organize into neovascular assemblies (via vasculogenesis and lumenogenesis) and gradually undergo vascular morphogenesis (via tubulogenesis) into stable capillary-like microvessels (Figure 3).[182,183] ECs co-encapsulated with mural cell types including fibroblasts, pericytes, mesenchymal stem/stromal cells (MSCs), adipose-derived stem/stromal cells (ASCs) and others within hydrogels have been used for formation of self-assembled networks.^[183–186] Although human umbilical vein endothelial cells (HUVECs) are most prominently used for self-assembly, other EC lines include human induced pluripotent stem cellderived ECs (iPSC-ECs), human endothelial colony forming cells (ECFCs), endothelial progenitor cells (EPCs), and human microvascular endothelial cells (MVECs). [65,78,85,187] Mural cells not only engage in paracrine signaling with adjoining ECs, but also assist in remodeling the ECM through matrix protein deposition, proteolytic degradation, and matrix deformation via cell-generated tension. [90,182,186,188] The formation and organization of vascular lumens and branch points with high vessel density, lacunarity, and network connectivity is closely reminiscent of the "tree-like" capillary beds in organs with high blood vessel density.[30] These networks, during the process of assembly, can be connected to fluid reservoirs and microfluidic systems for cyclic or continuous controlled perfusion, simulative of interstitial flow, which provides additional guidance toward structural and functional maturation.[28,29]

Recognizing the poor user-control over cellular organization, various strategies have been developed to enhance vasculogenesis by exploiting mechanotransduction processes during EC tubule formation, deposition of basement membrane proteins, integrin engagement, and interstitial flow to form stable, patent and perfusable networks that closely recapitulate native microvascular architecture and hemodynamic properties.^[28,29,189,190] These strategies can be broadly grouped into: 1) biophysical, 2) biochemical, and 3) mesoscale structural hydrogel modifications that influence nano- to macroscale self-assembly processes (Figure 3).

Biophysical modification strategies include modulation of hydrogel microarchitecture to obtain defined fibrillar properties, crosslink density, bulk and microscale matrix stiffness/viscoelasticity, and permeability, among others. [55,81] For example, properties of collagen have been tuned via: 1) cold-casting with Matrigel to enhance fibrillar assembly, 2) freeze drying to create anisotropic or aligned pores, 3) crosslinking at varying pH, temperature, concentration, and cell densities to tune stiffness, fiber thickness, length, and density, all of which influence self-assembly of microvasculature. [53–58] Similarly, fibrin gels (which have shorter, thinner, densely meshed fibrils compared to collagen) with modifications to matrix density and induction of uniaxial cyclic pre-stress have been used in sprouting angiogenesis assays. [61,62,190,191]

Natural matrices, although useful, make it challenging to decouple the influence of multiple interdependent matrix properties on vascular network assembly. Hence, synthetic matrices (or hybrid blends) with independently tunable properties are an attractive option. [67,69,70,77,83] Collagen covalently coupled and photocrosslinked with PEGDA yields an amorphous microstructure (as opposed to the fibrillar structure of unmodified collagen), while still preserving the triple-helical

www.advhealthmat.de

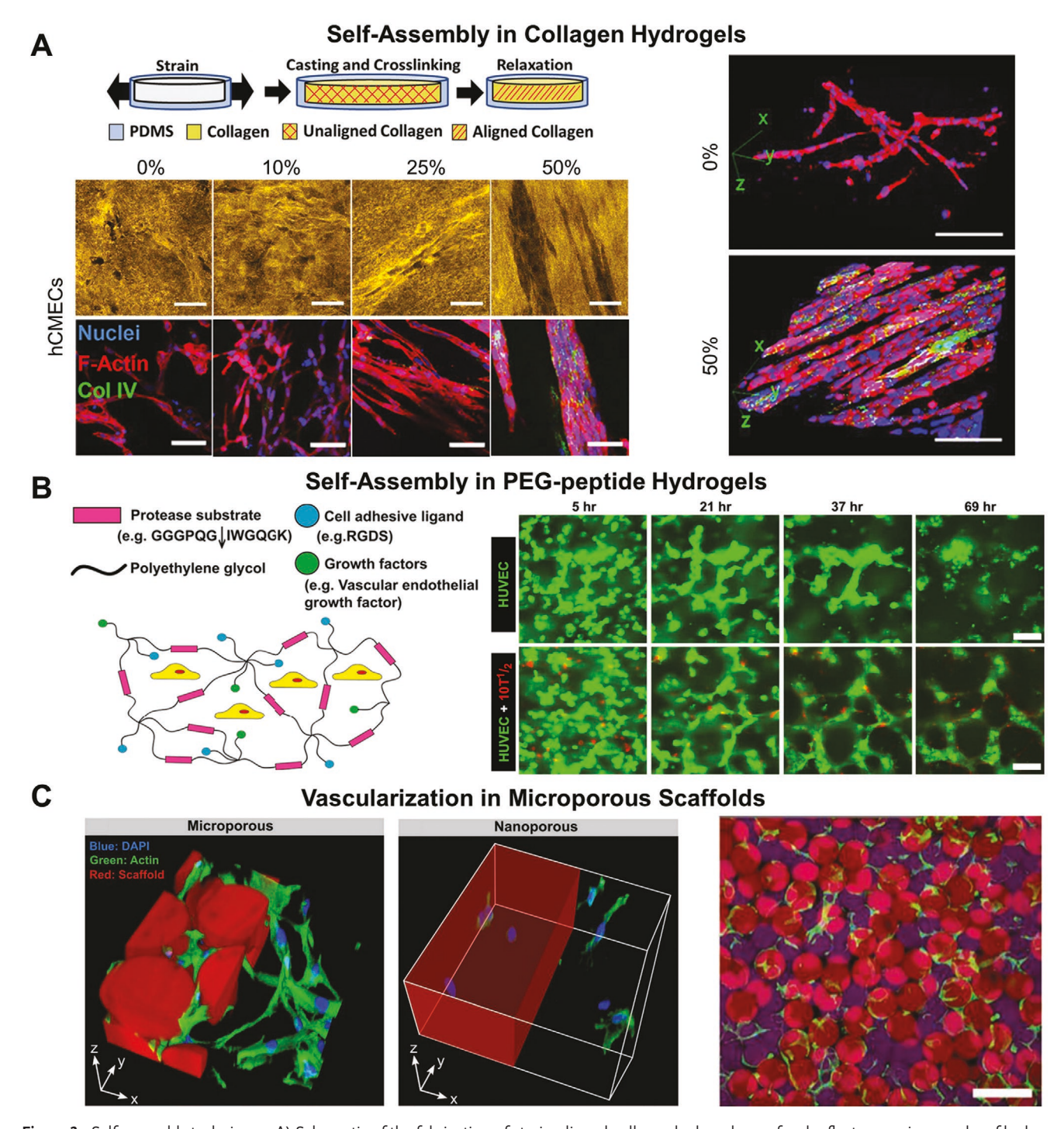


Figure 3. Self-assembly techniques. A) Schematic of the fabrication of strain-aligned collagen hydrogels, confocal reflectance micrographs of hydrogels with encapsulated hCMECs (SB = $100 \mu m$) with confocal micrographs of cells as a function of applied prestrain (SB = $50 \mu m$), and 3D reconstruction of z-stacks demonstrate enhanced vascularization with collagen alignment (SB = $100 \mu m$). Adapted with permission. Copyright 2018, American Chemical Society. B) Schematic of proteolytically degradable and cell-responsive PEG hydrogels and the dynamics of self-assembly of encapsulated HUVECs (green) and 10T1/2 cells (red) demonstrate the stabilizing role of fibroblasts on EC assembly. Adapted with permission. Copyright 2010, Elsevier. C) 3D reconstruction of confocal z-stacks of modularly assembled hydrogel microspheres (red) to form microporous scaffolds that enable enhanced EC infiltration compared to nanoporous scaffolds (red) and confocal micrographs of infiltrated ECs (green) within a combination of soft (purple) and stiff (red) hydrogel microspheres (SB = $200 \mu m$). Adapted with permission. Copyright 2019, Wiley-VCH. Abbreviations— hCMECs, human cerebral microvascular endothelial cells, HUVECs, human umbilical vein endothelial cells, VEGF, vascular endothelial growth factor.



www.advhealthmat.de



nature and native binding sites for integrins, growth factors and cellular proteases.^[77] PEGDA can be added to hydrogel precursors to induce secondary crosslinks, and higher matrix stiffness, thereby leading to mature, stable capillary formation.^[77] Secondary crosslinking of chemically-modified gelatindextran hydrogels using transglutaminase and gelatin-phenolic hydroxyl hydrogels via peroxidase-catalysis has been shown to promote vascular morphogenesis.^[81,82,192]

In addition to elasticity, porosity and pore architecture of engineered matrices can also be tuned via phase separation, sacrificial templating, solvent casting/particle leaching, and gas foaming to enable enhanced vascular infiltration. [55,66,68,193] A major challenge in regulating biophysical matrix properties is to attain a fine balance between the migratory (vascular sprouting, contiguous network coverage) and morphogenic behavior (time-dependent formation of vacuoles, coalescence into lumens, maturation of tubules and anastomosis) of ECs. [182] These behaviors also overlap with differential matrix remodelability of EC lines (via deposition of type IV collagen and laminin, and secretion of MMP-1), source of ECs (blood vs lymph or organ specific), and generation of basal or straininduced traction forces which are dynamically altered over the course of the culture period. [9,11]

Vasculogenesis in EC-laden hydrogels can be further enhanced via addition of soluble factors in the culture media. In one study, decellularized human lung fibroblast-derived matrix coupled with collagen and supplemented with growth factors was used for in vitro vascularization and in vivo wound healing applications.^[194] However, due to the short half-life of these proteins and limited, uncontrolled diffusivity within large matrices, biochemical modification strategies have been developed for precise, user-controlled presentation of these biomolecules to encapsulated ECs. Nanoparticle-clustering or covalent coupling and immobilization of specific factors including vascular endothelial growth factor (VEGF), fibroblast growth factor-2 (FGF-2), and others within engineered matrices, either independently or in a combinatorial fashion, has been used to enhance vascularization both in vitro and in vivo. [71,72,74,195]Synthetic variants of natural proteins, including VEGF-mimetic and collagen-mimetic peptide sequences, can also be considered as alternate choices for conjugation. [69,196,197]

Spatial control of: 1) matrix adhesivity via incorporation of cell-adhesive peptides or selective engagement of $\alpha_3/\alpha_5\beta_1$ integrins over $\alpha_{v}\beta_{3}$ integrins, 2) degradability via incorporation of proteolytic sequences of differential MMP-sensitivities, 3) stiffness via hindered crosslinking to obtain softer matrices, and 4) oxygen tension via induction of hypoxia and activation of MMP secretion, have been used to induce formation of robust vascular networks. [63,70,73,75,80,81,84] Another alternative to the presentation of these bioactive factors is co-encapsulation of ECs with supporting fibroblasts, which provide: 1) distributed pro-angiogenic signaling, proteolytic activity, and matrix remodeling in a dynamic fashion, 2) vessel stabilization and maturation via differentiation into pericyte-like and smooth muscle-like cells (SMCs), and 3) generation of contractile, traction forces that accelerate EC network formation. $^{[71,72,75]}$ However, the optimal ratiometric densities of multiple cell types in the hydrogel matrix must be carefully considered as too high EC/SMC ratio can lead to clustering instead of microvessel

formation while too low EC/SMC ratio can lead to poor network assembly. $^{[182]}$

As an alternate to biophysical and biochemical modifications, supramolecular and mesoscale structuring of hydrogels has been employed for enhanced vascularization, re-epithelialization and wound healing. ECs co-encapsulated with fibroblasts within modular microtissues (100-200 µm diameter, composed on fibrin, collagen, or agarose-hydroxyapatite-fibrinogen) and further encapsulated in larger matrices have been used for studies of vascular sprouting and vessel connectivity.[198-200] Differential density interfaces (denser collagen microspheres embedded in a softer collagen bulk matrix) can be created to facilitate robust EC invasion and assembly.^[59] However, these approaches yield nanoporous matrices, which can make it challenging and slow for encapsulated ECs to tunnel through and form mature cell-cell junctions. This problem can be overcome by employing granular hydrogels composed of microporous annealed hydrogel particles (MAPs) or sub-millimeter modularly assembled hydrogel rods covered with ECs. By changing the size, shape, packing density, void fraction, adhesivity, and local stiffness of these micron-sized hydrogel building blocks, local shear rates and traction forces of ECs can be controlled to facilitate interstitial perfusion through the bulk hydrogel and a high mass transfer coefficient of oxygen and nutrients, leading to quiescent, confluent, and non-thrombogenic EC networks with improved infiltration and coverage. [60,201-203] Multiple fabrication strategies for uniform, high-throughput generation of these modular hydrogel constructs (microspheres, particles, microfibers and others) via microfluidic technologies have also been developed.[48,76,204]

Overall, these matrix modifications strategies have significantly helped improve hydrogel vascularization processes and have been successfully implemented in both mechanistic studies of vascular morphogenesis and applications in injectable local cell delivery for tissue regeneration.^[35,176,205]

5.2. Bioprinting

Bioprinting has emerged as one of the most popular choices in additive manufacturing owing to the availability of a wide variety of cell compatible hydrogel precursors (bioinks), improvements in material handling and dispensing control, and rapid prototyping abilities. [49,51,178,181] Bioprinting can be categorized into two major classes: direct and indirect. Direct printing involves controlled deposition of cell-laden material onto a surface, while indirect printing comprises guided patterning of sacrificial materials, embedding patterns in larger cell-laden matrices and subsequent removal of patterned material yielding constructs with 3D space-filling hollow channels and networks.^[206] Direct printing can be further classified into: 1) ink-jet/drop-based printing (high speed dispensing of femto- to nanoliter drops of cell-laden bioinks), 2) valve-jet printing (non-contact, droplet-based deposition of cells with or without hydrogel carriers using pneumatic pressure and mechanical pulse generators), and 3) extrusion printing/bioplotting (relatively slower dispensing of continuous filaments of cell-laden bioinks via thermal or piezoelectric actuators).

www.advhealthmat.de

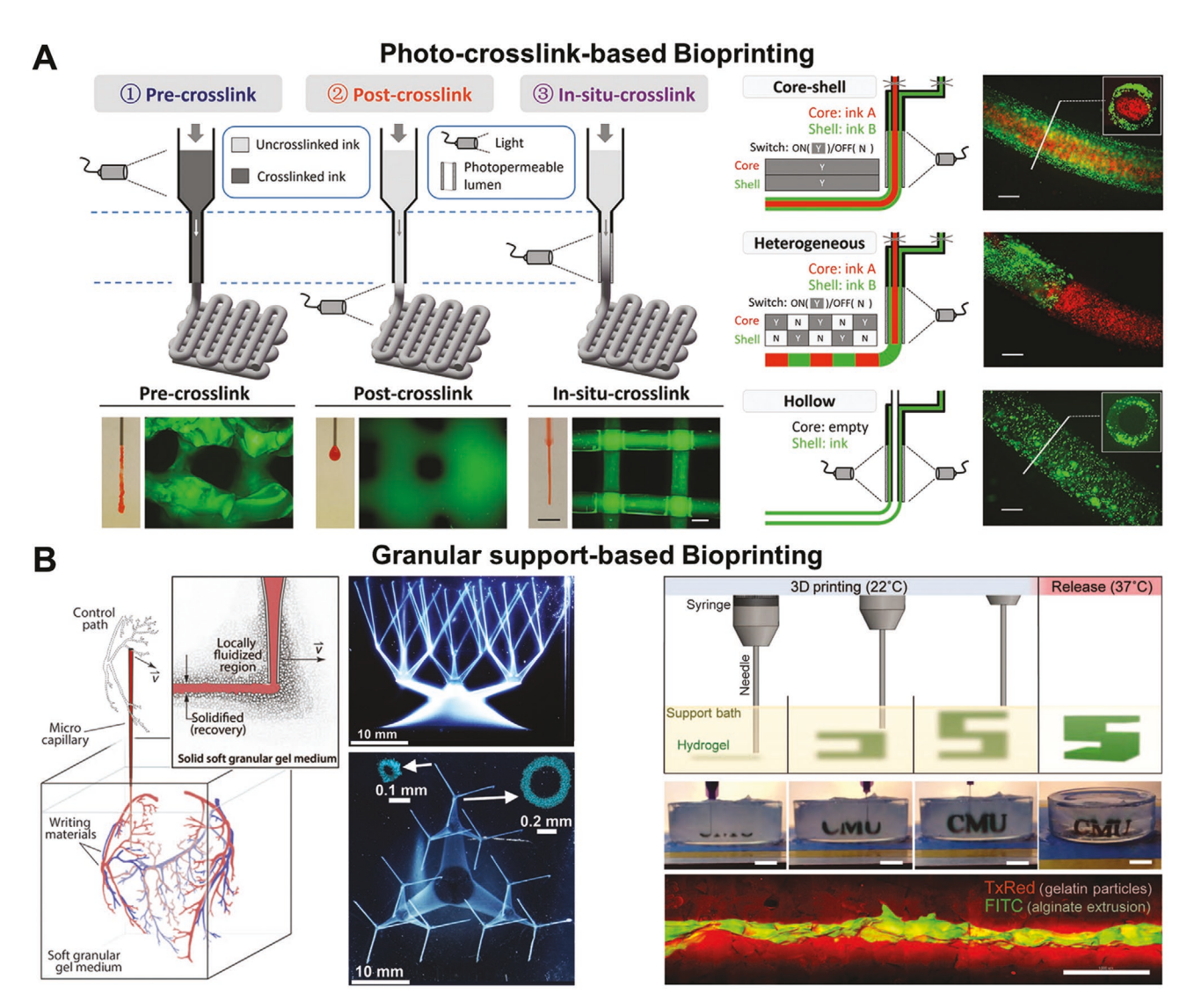


Figure 4. Bioprinting techniques. A) Schematic of three different crosslinking strategies during extrusion bioprinting and representative images of nozzles with extruded material (methacrylated hyaluronic acid) and printed lattice structure (SB: left = 5 mm, right = $500 \mu m$). Complex printed filaments (core—shell, heterogeneous, hollow) with in situ crosslinking approach using one or more fluorescent inks with fibroblasts (SB = $500 \mu m$). Adapted with permission.^[211] Copyright 2017, Wiley-VCH. B) Schematic of 3D printing of complex patterns within granular support gel medium (Carbopol, left and gelatin, right). Hierarchically branched tubular networks and hollow vessels with features spanning several orders of magnitude (insets: confocal cross sections). Adapted with permission.^[217] Copyright 2015, American Association for the Advancement of Science (AAAS). Representative alginate filament (green) embedded within gelatin slurry support bath (red) (SB = 1 mm). Adapted with permission.^[216] Copyright 2015, AAAS.

In ink-jet and valve-jet printing, owing to the high speed of droplet ejection and nozzle/printhead movement in the xy-plane, bioinks need to undergo rapid gelation (to prevent material dispersion postprinting) and have low viscosity (to allow smooth flow through the print nozzle). [207–209] Fibrinogen physically crosslinked with thrombin (yielding fibrin) and sodium alginate—collagen composites ionically crosslinked with calcium chloride (CaCl₂) have been used to print ECs in multiple configurations to yield vascularized constructs. [207–209] However, rapid dispensing comes at the cost of potential cell damage during ejection, nozzle clogging, and formation of cavitation bubbles within the printhead assembly. Some of these limitations are overcome in extrusion-based printing, where lower dispensing fluxes permit the use of a wide variety

of printable and biocompatible materials, including hydrogels, elastomers, and nonviscous inks (**Figure 4**).^[210–212]

Recent material advances have enabled the use of hydrogels (with dual crosslinking, shear-thinning, and rapid self-healing properties formed via reversible guest–host (GH) bonds) in extrusion bioinks. [213,214] Methacrylated hyaluronic acid (MeHA) coupled with adamantane (guest) and β -cyclodextrin (host) can be extruded in a layer-by-layer format; the shear-dependent GH bonds and UV-mediated curing forming dual-crosslinked stable filaments to yield freestanding, hierarchical structures. [213,214] The printing process can be executed within the volume of a support gel either as linear, branched or spiral filaments to create integrated microstructures and the viscosity of the hydrogel bioink can be tuned via in situ photocrosslinking

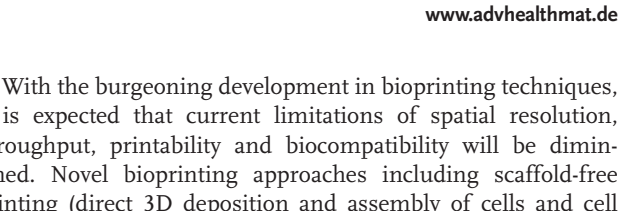


immediately prior to extrusion, thereby yielding stable, selfsupporting assemblies (Figure 4).[215-218] The pattern fidelity of the extrusion-printed structures can be maintained by choosing support gels of optimum supramolecular properties: self-healing hydrogels (MeHA with GH bonds) or granular gels (gelatin microspheres or Carbopol) that locally deform at the focal point of extrusion but rapidly heal around the printed material upon removal of the nozzle, thereby yielding millim-

eter-scale, complex, biomimetic, embedded objects.^[215–217] One variation of extrusion-based printing, coaxial printing, is particularly useful for fabrication of vascular tube-like structures.[219-222] Coaxial printing is based on the simultaneous extrusion of two or more bioinks using core and shell assemblies, the core material being dissolved to result in hollow filaments and perfusable, freestanding and functional microvessels. [220,221] Owing to the need for rapid crosslinking of the extruded shell material that forms the filament walls, CaCl₂induced crosslinking of sodium alginate remains the most popular choice, although MeHA, GelMA, and PEG-based bioinks have also been employed.[222,223] The relative flowrates of the core and shell material and nozzle diameters can be adjusted to obtain hollow filaments with user-controlled filament and lumen diameters and filament wall thickness.^[221,222,224] Modifications in extrusion approaches have also resulted in simultaneous, sequential, or combinatorial multimaterial printing, which facilitates co-printing of multiple cell types in local niches and heterogeneous hierarchical architectures.[211,223]

As an alternate to direct printing methods, indirect printing techniques have also been developed for fabrication of hydrogel-embedded vascular networks. Sacrificial materials used for templating channels and networks in 3D volumes include reversibly crosslinked gelatin, carbohydrate glass, agarose, Pluronic, shear-thinning MeHA hydrogels with GH bonds, freestanding PVA scaffolds, self-healing glucose, and PEGDA hydrogels.^[214,225-231] Carbohydrate glass (glucose. sucrose, and dextran blend) fibers demonstrate excellent versatility with a range of natural and synthetic materials and can be drawn into programmable space-filling lattices or aligned channels with high pattern fidelity post washing. [229,232] Fabricated scaffolds can be connected to microfluidic perfusion systems that allow introduction of ECs into hollow channels and subsequent lumenization. This approach allows vascularization, oxygenation, and angiogenic sprouting of millimeter-scale hydrogel constructs in vitro and engraftment and functional integration of synthetic tissues with host vasculature in vivo.[232]

Although linear channels can be easily fabricated with sacrificial and fugitive inks, recent improvements in material and printing strategies have enabled creation of more complex geometries including constricted channels (for modeling stenosis and thrombosis), spiral channels (for modeling intertwined blood and lymphatic vessels) and perfusable lattice networks (for vascularization of large-volume constr ucts).[214,228,230,231,233] Similar to direct printing in granular or self-healing materials, indirect printing of fugitive inks (Pluronic F-127 and its derivatives) can be implemented in photocrosslinkable MeHA, GelMA, and Pluronic-diacrylate bulk gels (termed omnidirectional printing), resulting in user-defined, heterogeneous, multi-cellular vascular channels.^[234]



it is expected that current limitations of spatial resolution, throughput, printability and biocompatibility will be diminished. Novel bioprinting approaches including scaffold-free printing (direct 3D deposition and assembly of cells and cell spheroids into guided tissue architectures), [235,236] nanoscale matrix fabrication (electrospun fibers in bulk gels for guided EC assembly),[237-242] 4D printing (stimulus-responsive materials that undergo programmed 3D conformational change over time postprinting)[243,244] and acoustophoretic printing (usercontrolled surface acoustic wave forms to pattern cell-laden hydrogels in 3D space)[245,246] can also provide potential opportunities for fabrication of complex vascular networks. Further integration of bioprinted constructs with microfluidic platforms will facilitate the interrogation of vascular mechanobiology in organ-mimetic microenvironments.[178,180]

5.3. Micromolding and Soft Lithography

Techniques to form physically molded and templated microstructures via manipulation of solid, liquid, and viscoelastic materials have been developed for construction of vascular assemblies (Figure 5).[120,247,248] Patterned PDMS molds created from crosslinked SU-8 masters generated via photolithography have been employed for micropatterning, microcontact printing (stamping), and hot embossing of 2D surfaces for EC alignment to create dynamic perfusable microfluidic systems to investigate vascular hemodynamics. [248-253] These techniques have also enabled micromolding of aligned tubular EC cords for in vivo implantation and integration with host vasculature and tissue regeneration.[251]

One facile technique for molding solid geometries involves casting bulk hydrogels (collagen, fibrin, HA) around rigid needles, or flexible wires, filaments, and elastomeric rods, with subsequent removal of these elements to generate templated hollow channels in the matrix.[254-256] Rigid needles of different diameters yield linear cylindrical channels while flexible PDMS rods permit fabrication of branched channels that can be endothelialized, lumenized, and perfused. [257] The removal of rigid needles and flexible rods can result in micron-scale defects at the interface, requiring additional care and precision during removal. This limitation can be mitigated by using PDMS rods capped with iron particles that are magnetically removed (Figure 5)[257,258] or using gold micrometric rods adsorbed with oligopeptide self-assembled monolayers (SAM) that directly transfer ECs from the coated rods to the channel walls on the application of an electric potential. [259] Spatial positioning of vascular and mural cells and bioactive ligands within hollow lumens can also be accomplished via serial injection and crosslinking using bioorthogonal reactions.^[260]

Although these techniques yield simple, planar structures, other novel approaches have led to fabrication of complex branching patterns that more closely resemble native vasculature. These techniques include kidney-mimetic vascular corrosion casts formed using sacrificial PCL[261] and plant leaf venation-mimetic templates.[262-264] Ice-lithography has also been used to generate simple linear 2D patterns on collagen and large-diameter geometrically complex vascular grafts made

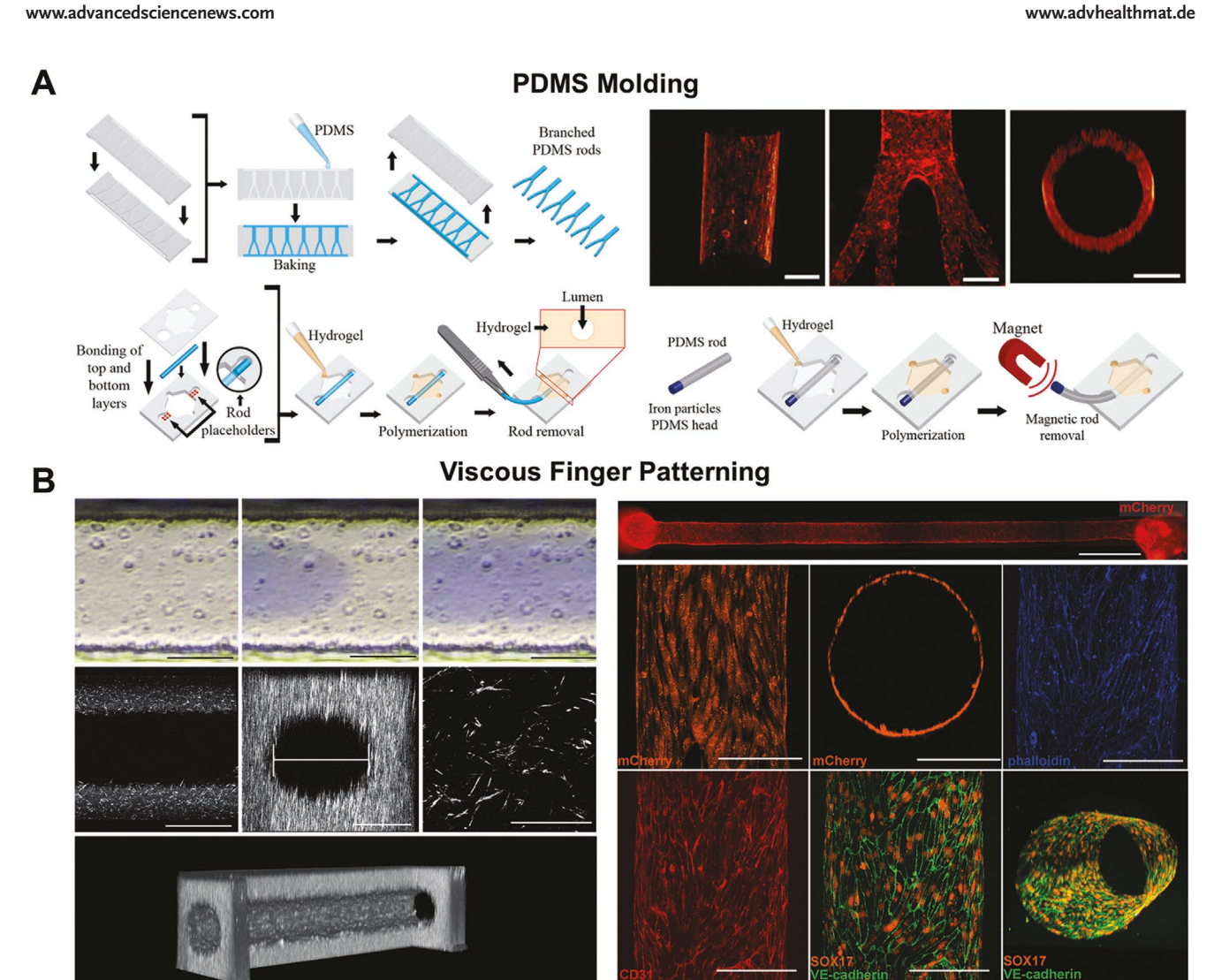


Figure 5. Micromolding and soft lithography techniques. A) Schematic of fabrication of flexible PDMS rods and device assembly to create hollow lumens and magnetic extraction of iron capped-PDMS rods; 3D confocal reconstruction of linear and branched EC-lined lumens (red: F-actin) (SB = 1 mm). Adapted with permission. [257] Copyright 2016, Wiley-VCH. B) Molding of microfluidic channels via viscous finger patterning with blue food dye traveling through collagen solution in a 500 µm wide channel, 2D and 3D reconstruction of two-photon SHG images of patterned channel and collagen scaffold (SB = 200 μm, collagen fibers = 50 μm); 3D culture of hiPSC-ECs (mCherry) for 48 h in static conditions within fabricated collagen channels and confocal views of uniform coverage and lumen structure (blue: F-actin, red: CD31, orange: SOX7, green: VE-cadherin) (SB: top = 1 mm, middle and bottom = 200 μm). Adapted with permission. [247] Copyright 2019, AIP. Abbreviations—hiPSC-EC, human induced pluripotent stem cell derived endothelial cells.

of silk, tropoelastin, PCL, and PDMS.[265,266] In addition to solids, liquid sacrificial bioinks (gelatin, alginate, salt buffer, and others) have been templated with hydrodynamic shaping via microfluidic assembly, coaxial extrusion, and viscous finger patterning to produce flexible and nonlinear, free-standing blood vessel-like channels embedded within larger matrices (Figure 5).[247,267-269]

5.4. Photolithography-Based Approaches

Although self-assembly techniques yield constructs that closely match native microvascular architecture, the cellular organization process is stochastic and sensitive to hydrogel properties, EC line characteristics and variations in fabrication conditions, which can create hindrances in consistency, reproducibility, and engineered precision for in vitro studies. To overcome some of these challenges, photolithography-based fabrication techniques have been developed that allow precise, spatiotemporal, nano- to microscale tuning of local hydrogel properties that lead to directed cellular organization and user-controlled geometric vascular assembly. [50,51,206] These approaches also facilitate the immobilization of controlled concentrations of bioactive molecules to mimic native architectures for investigation of sprouting, EC migration, and vessel formation.[270-272] These techniques can be broadly categorized into: 1) mask-based photolithography, 2) stereolithography, and 3) laser-based lithography.

The most facile photolithography technique incorporates the use of photomasks which selectively control where light





is exposed to 2D light-sensitive substrates or 3D cell-laden hydrogel precursors, thereby transferring defined geometric features onto or into the material. [51] Mask-based photolithography provides precise spatial control of encapsulated cells with high resolution and can be used to guide patterned ECs toward highly aligned vascular assemblies and tubule formation through photocoupling of adhesive moieties or photoinduced changes in matrix elasticity. [273,274] Additional patterning steps can be used to incorporate multiple cell types with ECs in different hydrogel formulations of varying composition, ligand density, and stiffness.^[275] A limitation of traditional mask-based photolithography is the creation of patterns with rectangular cross-sections of user-defined width but fixed height, which often does not match that of native vasculature. [276] To overcome this challenge, a novel technique, backside photolithography, has been developed, which uses an optical diffuser placed in the light path that facilitates feature height gradation as a function of width, thereby yielding features with user-controlled circular cross-sections. [276] This capability is particularly useful when fabricating tortuous, tree-like vascular geometries with bifurcations, loops, and branches to study hemodynamics and deformation of red blood cells (RBCs).[126,127]

Despite facile fabrication and ready availability of photomasks, repeatedly handling and aligning physical masks during fabrication with a high degree of reproducibility and precision can be cumbersome, and the difficulty in controlling the 3D shape of the photopolymerized species has led to the development of maskless photolithography or stereolithography (SL) (Figure 6). [206] The SL working principle is primarily composed of: 1) developing a 3D model of the desired structure using computer-aided design (CAD) software, and for more intricate designs, magnetic resonance imaging (MRI), or computed tomography angiography (CTA); 2) software segmentation of the design into micron-thick layers; 3) image flow of individual layers to the SL apparatus (SLA); 4) light-induced crosslinking of a photosensitive hydrogel one layer at a time; and 5) vertical shifting of the SLA stage to sequentially crosslink the subsequent layers until the entire design is complete.^[51] This workflow can be combined with the use of digital light projection (DLP) involving a commercially available digital mirror device (DMD) system, an array of reflective mirrors, that allows pixelbased image projection over large-area polymer vats thereby yielding complex micron- to millimeter-sized microstructures with precise, user-defined geometries. [277,278] Compared to conventional maskless photolithography, projection-based stereolithography (PSL) offers the advantages of increased throughput and complexity, and precise control over scaffold thickness and feature resolution.[279,280] As proof-ofconcept, hydrogel-encapsulated ECs were spatially positioned in single or multiple layers within defined geometries which resulted in correlated vascular geometries with a mature phenotype and cord-like structures.^[281] Cell-laden hydrogels surrounded by multiple perfusable lumenized vascular channels have also been fabricated using this technique. [282]

The operational bounds of PSL are dictated by the choice of crosslinkable polymers (or curable resins), photoinitiators, photosensitizers, and light exposure conditions. Traditional SL resins suffer from poor biocompatibility and transparency; however, recent improvements in using low-molecular-weight

PEGDA and UV-crosslinkable poly(dimethylsiloxane) (PDMS) coupled with high-efficiency photoinitiators and high-absorbance photosensitizers have been reported. [283,284] Since the xy-resolution is determined by the optical setup and z-resolution by the light attenuating ability of the photoabsorber, creating high fidelity patterns in large hydrogel constructs is challenging with PSL. In a landmark technological advancement, food dye additives (including tartrazine, curcumin, or anthocyanin) or gold nanoparticles (50 nm) were employed as biocompatible potent photoabsorbers for the creation of complex, efficient intravascular microstructures, topologies and networks within large-volume PEGDA hydrogels.[285] This strategy was used to create 3D microfluidic static mixers with integrated fins of alternating chirality, a functional 3D bicuspid valve operating under anterograde and retrograde flows, and entangled fluidic networks designed using mathematical space-filling algorithms. These networks were used to demonstrate the oxygenation of RBCs in a lung-mimetic alveolar model topology, bidirectional blood flow and mixing during air sac ventilation, and functional vascularized implantable hepatic hydrogel carriers.^[285]

As an alternate to PSL, the light path used in photolithography can also be directed via laser-writing and multiphotonbased laser scanning systems. Direct laser-writing (DLW) involves selectively crosslinking in user-defined geometries within bulk 3D polymer precursors, thereby creating patterns with nano- to microscale resolution. [286-288] Linear patterns stacked in multiple layers can be printed to create aligned EC tubule-like structures with co-encapsulated mural cells.[288] Integration of DLW with microfluidic systems allows sequential printing and washing of polymer precursors, thereby yielding multimaterial printing of geometrically complex structures with high spatial control at nanoscale resolution (registration accuracies of 100-200 nm).[286] DLW techniques have also been adapted for controlled deposition of EC patterns using laserinduced forward transfer (LIFT), where the guided laser beam evaporates a gold layer attached to a donor glass slide and the gas pressure generated transfers the underlying EC containing material onto a collector slide. [289,290] The LIFT technique facilitates sequential co-patterning of multiple cell types within microscale niches, thereby creating complex microenvironments that can be implemented for both in vitro studies and in vivo regenerative applications. [289,290] A variation of the LIFT technique, biological laser printing (BioLP), has been used to create guided EC patterns on stackable PLGA biopaper, which was used to form thick 3D vascularized constructs. [291,292] The resolution and optical energy density deposited at the focal point during the writing process can be controlled with the use of femtosecond pulsed lasers, which was demonstrated for in matrix "densification" or laser-guided crosslinking of GelMA hydrogels resulting in EC alignment.^[293]

Technological advances in femtosecond pulsed lasers and multiphoton systems have enabled implementation of laser-scanning lithography (LSL), where pre-registered images are used to guide the laser position and focal intensity, thereby creating 2D and 3D multifaceted biochemical and mechanical patterns with high fidelity, resolution, and spatial gradients (Figure 6). [271,272,294,295] LSL permits guided engagement of EC adhesion, migration, alignment, and organization within bulk hydrogels via nanoscale control of adhesive

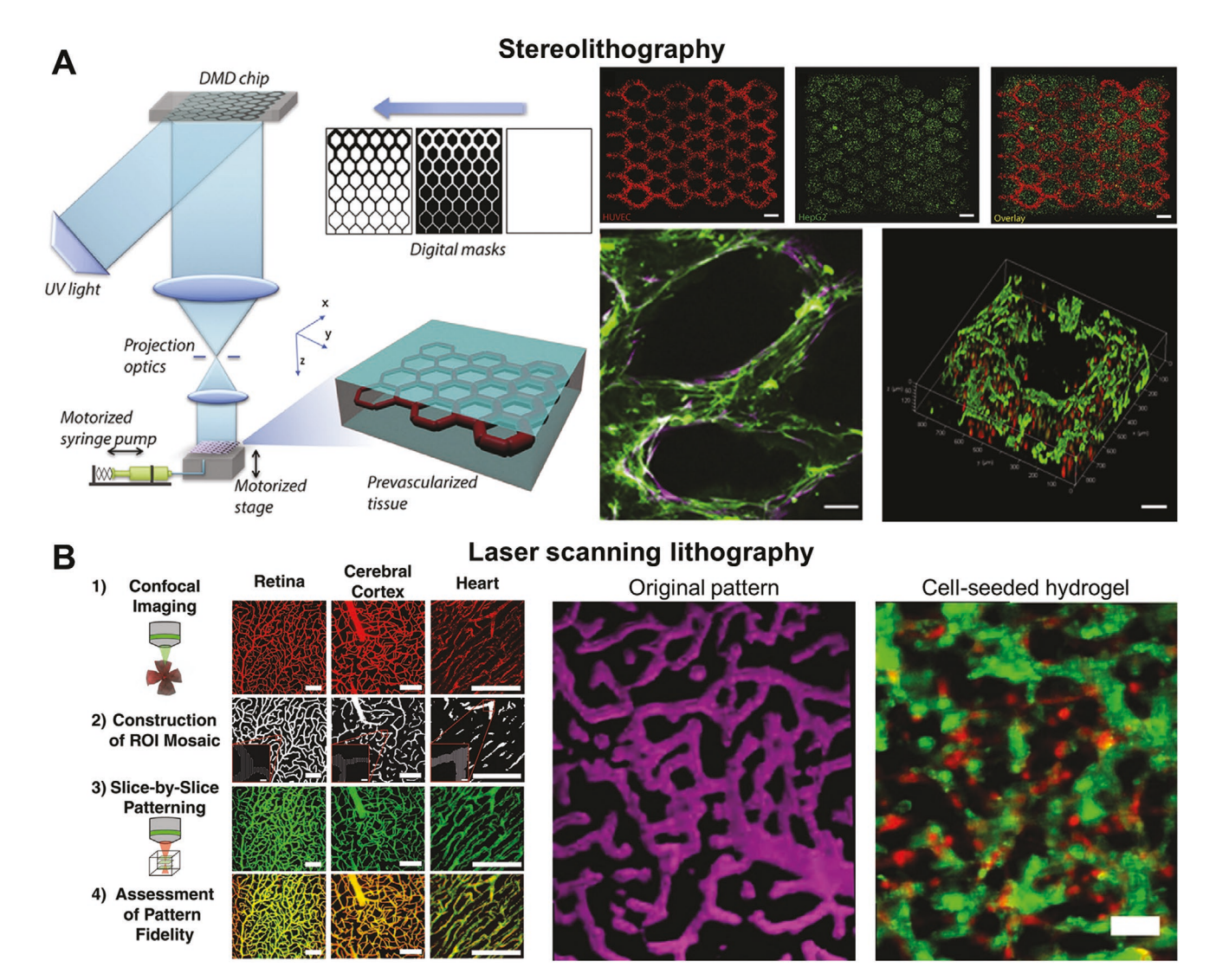


Figure 6. Photolithography-based techniques. A) Stereolithographic projection of channel features to create cell-encapsulated GelMA micropatterns, fluorescent images of heterogeneous tissue constructs with HUVECs (red) and HepG2 cells (SB = 250 μm), confocal slice of network formation after 1-week of coculture of HUVECs (green, CD31) and 10T1/2 (purple, α-SMA) and 3D confocal reconstruction (red: ECs, green: CD31) (SB = 100 μm). Adapted with permission. C278 Copyright 2017, Elsevier. B) Schematic workflow and resulting images from laser scanning lithography of 3D biomimetic vascular patterns within tunable bioactive PEG hydrogels (SB = 100 μm); a degradable PEG-based hydrogel with fluorescent PEG-RGDS pattern (magenta) mimicking the cerebral cortex vasculature and encapsulated HUVECs (green) and 10T1/2 fibroblasts (red) aligned with the RGDS pattern after 24 h (SB = 50 μm). Adapted with permission. C272 Copyright 2012, Wiley-VCH. Abbreviations—GelMA, gelatin methacrylate; HUVECs, human umbilical vein endothelial cells; PEG, poly(ethylene glycol).

ligands and biochemical cues, and integrin and focal adhesion kinase (FAK) activation, ultimately leading to faithful recapitulation of organ-mimetic vascular networks in engineered microenvironments. [272,296,297] Bioactive ligands used in LSL can either be introduced in the bulk hydrogel prior to scanning or incorporated biochemically using a photosensitive moiety that is cleaved upon excitation, thereby allowing the ligand to interact with encapsulated cells. [270,272] The concept of photocleavable presentation of cell-adhesive RGDS ligands has been demonstrated for in vivo vascularization and in vitro studies of light-guided angiogenesis and cell migration. [270,298]

In general, guided projection and positioning of light and the optical properties during photopolymerization can be used to incorporate local biochemical and biophysical cues that can direct scale-spanning cellular and vascular assembly. [271,272] With recent advances in material design and mechanical and optical control, systems including live-cell lithography (laser tweezer-based optical trapping and guided positioning of vascular cells), [299,300] it is expected that photolithographic techniques will generate precisely tailored vascular scaffolds that can be applied for in-depth mechanistic studies.

5.5. Laser-Induced Hydrogel Degradation

Although photolithography-based approaches employ userdirected light paths for additive fabrication of vascular

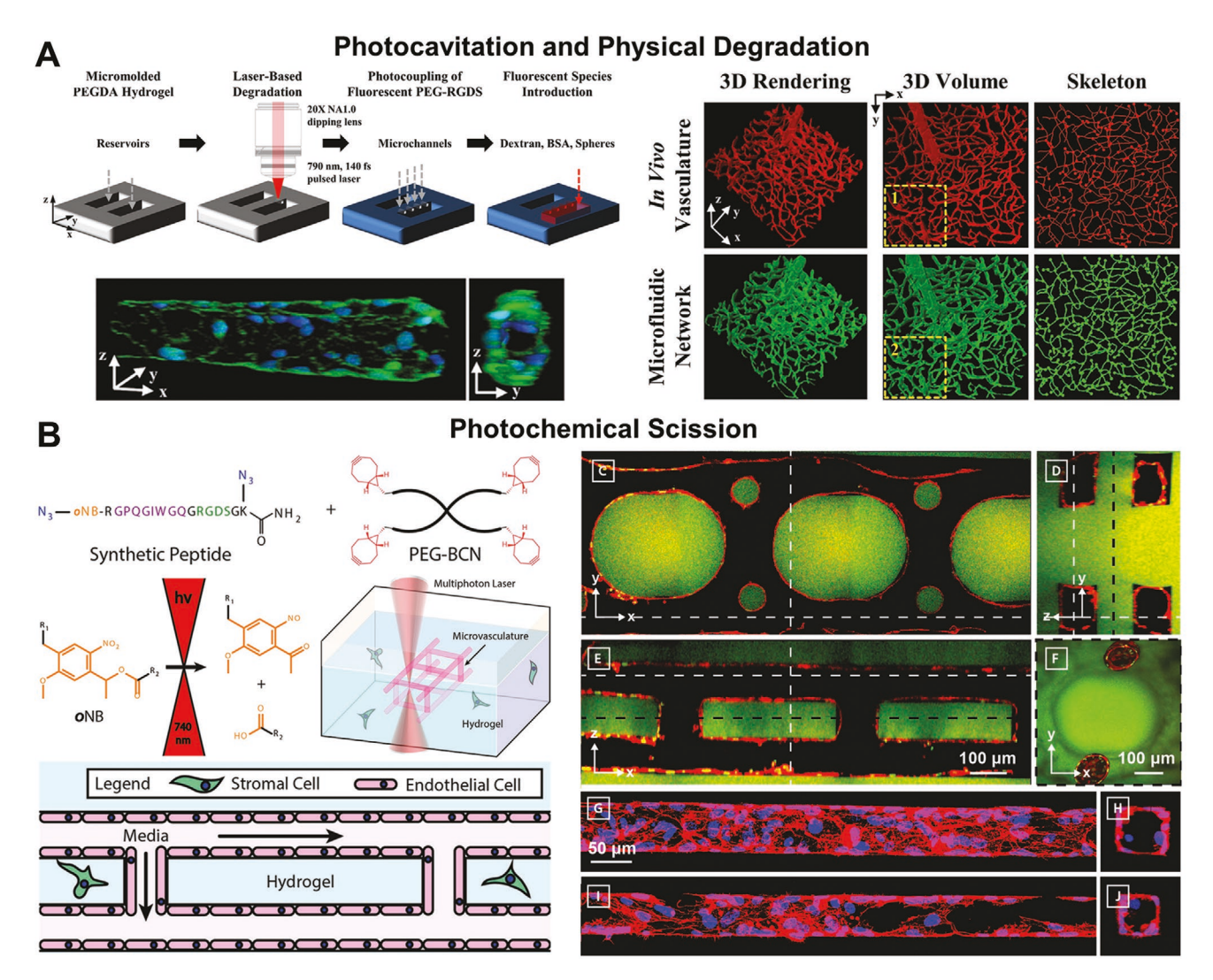


Figure 7. Laser-based degradation techniques. A) Schematic of laser-induced degradation of PEG hydrogel via photocavitation and physical degradation, 3D confocal views of mouse brain ECs forming lumenized channels in laser-degraded channels functionalized with RGDS (green: ZO-1, blue: nuclei) (SB = $50 \mu m$) and fabrication of 3D biomimetic dense, tortuous brain microvasculature. Adapted with permission.^[305] Copyright 2016, Wiley-VCH. B) Schematic of laser-induced scission of photodegradable bioactive PEG hydrogel and seeding of ECs to form perfusable vasculature and confocal views of 3D endothelialized channels of different shape features generated within photodegradable florescent gels (green) (red: F-actin, blue: nuclei). Adapted with permission.^[303] Copyright 2017, Wiley-VCH. Abbreviations—PEG, poly(ethylene glycol); ECs, endothelial cells.

constructs, other subtractive approaches including laser-induced degradation and ablation have also been developed to create user-defined, programmable, highly precise geometries within bulk hydrogel matrices. Nanosecond or femtosecond laser pulses with tuned peak intensities and scan rates can be used to ablate 2D or 3D micron-sized to submicron sized channels with high resolution, millimeter-scale z-depth, and high repeatability for directed cell migration and cell alignment.^[301]

Depending upon the choice of hydrogel material, laser-induced degradation can be executed via: 1) optical heat-assisted evaporation of water trapped within polymer networks leading to bubble formation, expansion, and cavitation; 2) direct plasma ionization and physical degradation of polymer chains constituting the hydrogel matrix and; 3) wavelength-dependent photochemical scission of light-sensitive polymer chains of the hydrogel matrix (**Figure 7**).^[175] Degradation of physically

crosslinked collagen gels can also accomplished by photothermal heating of gel-encapsulated gold nanorods.^[302] These degradation mechanisms dictate the scan speed, laser power, laser source, wavelength, pulse duration, and pulse frequency necessary to achieve the desired features.^[175]

Integration of laser-induced degradation with image-guided laser positioning assists in fabrication of planar or more complex 3D features including organ-mimetic, hierarchical microfluidic networks, intertwined channels mimicking vascular and lymphatic vessels, endothelialized lumens (with mural cells), and in situ, evolvable features permitting dynamic changes in flow paths and biochemical gradients within the 3D hydrogel volume. [303–305] Since the fabricated networks closely mimic the scale-encompassing architecture of the native vascular tree with high fidelity and spatial resolution, this technique, if integrated with microfluidic platforms, has the



www.advhealthmat.de

ADVANCED HEALTHCARE MATERIALS

potential to accurately recapitulate native or abnormal hemodynamics, shear rates, velocities, pressures, and associated mechanical perturbations on the vascular parenchyma. [305–308] Despite the ability to create programmable, precise, biomimetic features and versatility with a wide range of materials, laser-induced degradation is scale-limited, time-consuming, involves multiphoton systems, and can cause laser-induced cell damage in some cases.

Overall, a wide range of techniques have been developed that enable the fabrication of functional vascularized microtissue niches for in vitro mechanistic interrogations. In addition to techniques discussed above, other novel approaches include cell sheet engineering, [240,309,310] magnetic assembly and patterning. [311–316] Implementation of innovative material design (assembled polyelectrolyte hydrogel fibers, [317] thermore-sponsive materials, and others) and integration with microphysiological platforms and sensing technologies can potentially overcome the current limitations of speed, scalability, precision, physiological complexity, and reproducibility and lead to improved platforms for investigation of vascular mechanobiology.

6. Modeling Vascular Mechanopathology in Vascularized Microphysiological Systems

The implementation of various organ-on-a-chip, humanon-a-chip, and disease-on-a-chip platforms to create microphysiological systems have revolutionized the mimicry of human pathophysiology in miniaturized in vitro devices.[12,22,24,179] Microphysiological systems have enabled mechanistic investigations of multiple biological variables on vascular-parenchymal microenvironments as well as testing efficacies and toxicity profiles of therapeutic agents and potential drug candidates. The ability to integrate these systems with other techniques (self-assembly, bioprinting, photolithography, laser-based techniques), compatibility with a wide range of biomaterials, parallelization of fluidic operations in multiplexed culture systems, and high-content imaging have accelerated the commercial translation of these systems for drug discovery applications.^[29,178,180] Historical perspectives of microfluidic device development, applicability toward organ/organoid/tissue/disease modeling and drug delivery, prominent industrial players and their established on-chip platforms, and key challenges in the landscape of licensing and commercial translation have been extensively reviewed previously.[13–15,22,25,32,34,318–320]

Compartmentalization of specific tissue niches coupled with dynamic fluid perfusion facilitates investigation of multiple physiological microenvironments including: 1) vascular units (microvascular networks and arteries);^[321] 2) organ-specific epithelial barriers (lung, small airway, intestinal gut, placenta, retinal barrier, blood-brain barrier, renal proximal unit, and glomerulus);^[318] and 3) parenchymal tissue (cardiac myocardium, skeletal muscle, liver, tumors and others).^[322] Changes in hemodynamics, associated biophysical and mechanical perturbations, and cellular and tissue responses in vascular parenchyma can be replicated in on-chip platforms, providing new insights into vascular mechanobiology and accelerating the discovery of

new targets and drugs. Assessing drug permeability through tissue interface barriers, sequential and interdependent multiorgan metabolism, and stimulatory responses of parenchymal tissue in these devices help improve the predictive power of in vitro models in preclinical studies.

In addition, organ-specific ECM modeled through the use of tissue-mimetic hydrogels enables evaluation of the role of matrix permissivity toward biomolecules, soluble drugs, and nanotherapeutic delivery vehicles. [323–325] Cells and cellular metabolites can also be collected from these devices for processing and analysis, revealing important aspects of metabolism, functional activity, and gene expression influenced by altered hemodynamics. Spatiotemporal variations in biochemical cues (soluble and cell-derived) and induction of gradients with variable flow profiles facilitate dynamic observation and quantification of key cellular processes during multicellular interactions. [326–329]

Although majority of investigations on vascular mechanobiology have been conducted in simple and reductionist models, recent advances in fabrication technologies to generate engineered tissue constructs with vascular networks have aided the close recapitulation of native tissue and organ niches.^[49–51] Particular examples of these niches and the underlying role of vascular mechanobiology driving these processes are discussed below.

6.1. Cardiovascular Diseases

With the progression of age, dysregulation of physiological functions, and accumulation of chronic stress, multiple vascular abnormalities gradually arise, mainly arteriosclerosis, atherosclerosis, thrombosis, and fibrosis. [92,97,330] Arteriosclerosis refers to the stiffening of vessel walls due to reduced production of elastin and substitution with type I collagen in the intimal layer, primarily by VSMCs. Multiple causes including changes in shear stress, cyclic stretch, and prolonged hypertension have been implicated in the phenotypic switching of VSMCs, which also leads to dysregulation of vascular tone.[31,88] Although VSMC plasticity is reversible during short-term injuries and can regenerate back to its physiological phenotype, the chronic accumulation of other vascular insults decelerates this recovery process and drives it toward a pathological state. [31,123] Extracellular lipid pools in the intima consisting of free cholesterol and low-density lipoprotein (LDL) are absorbed and oxidized by VSMCs thereby generating foam cells. Subsequently, chemokine-mediated recruitment of monocytes and differentiation to macrophages leads to the formation of a fibrous cap with a necrotic core and calcification into an atherosclerotic plaque. [88,331] Further remodeling of the plaque due to MMP-mediated degradation can lead to plaque rupture, activation of ECs and platelets, and ultimately clot formation (thrombosis).[88] Migration of fibroblasts, differentiation into myofibroblasts, and deposition of collagen I over time promote fibrosis and scar tissue formation (Figure 8).[332]

Plaque formation in the intima leads to stenosis (narrowing of the vascular lumen), which significantly alters the flow velocity and shear stress profile in poststenotic sites, further

ADVANCED HEALTHCARE MATERIALS

www.advhealthmat.de

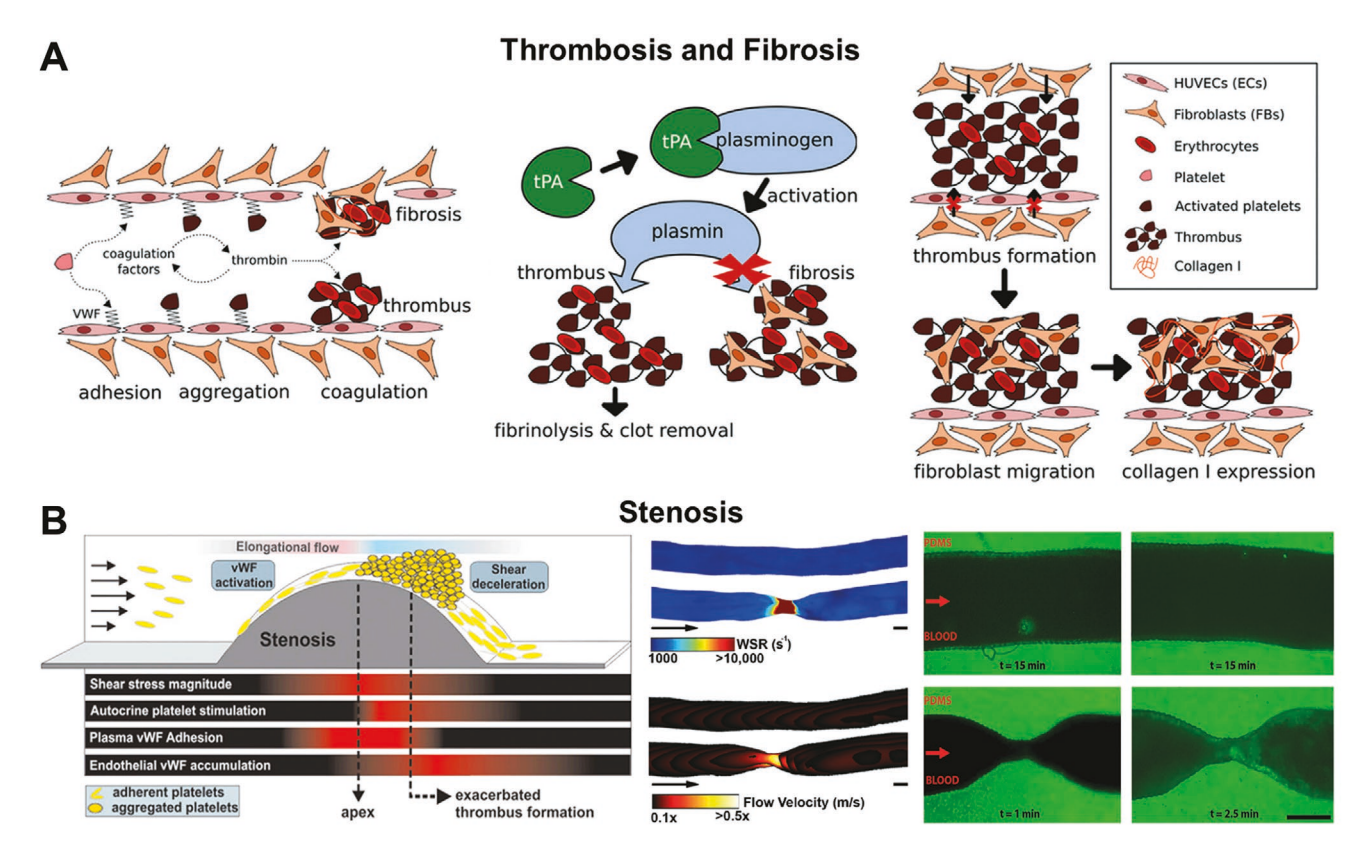


Figure 8. Modeling cardiovascular pathological events in vitro. A) Schematic of the mechanism of thrombus formation and development, including adherence, activation and aggregation of platelets to the damaged endothelium, thrombin-induced coagulation to form a thrombus, tPA induced thrombinolysis, and formation of fibrotic thrombus mediated by fibroblasts. Adapted with permission. Copyright 2016, The Royal Society of Chemistry. B) Schematic of a stenotic geometry that exacerbates thrombus formation through endothelial vWF accumulation, autocrine platelet stimulation, and shear deceleration. Adapted with permission. Copyright 2013, National Academy of the Sciences. Finite element analysis of wall shear rate (WSR) and flow velocity in healthy and stenotic vessels of 67% occlusion, simulated for microfluidic model with input flow of 0.29 mL min⁻¹ and vessel diameter of 400 μm (SB = 200 μm) and platelet aggregation (green: DiOC₆) and thrombosis observed in stenotic geometry after 1 and 2.5 min of blood perfusion, but no aggregation in healthy geometry after 15 min of perfusion (SB = 200 μm). Adapted with permission. Copyright 2017, The Royal Society of Chemistry. Abbreviations—tPA, tissue plasminogen activator, vWF, von Willebrand factor.

increasing the risk of thrombosis. [334,336] Several microfluidic systems have been developed to model stenosis-induced thrombosis and thrombolysis and have shed light on underlying hemodynamic forces and signaling mechanisms driving these events (Figure 8). [333,335,337,338] For example, a sudden increase in sheer magnitude at a stenotic site activates platelets in response to endothelial vWF secretion and integrin-mediated adhesion and aggregation along the decreasing shear gradient via restructuring of filamentous platelet tethers. [334,336] This principle can also be applied in designing microfluidic devices with stenosed flow geometries that can be used for real-time evaluation of clotting function with small blood volumes. These thrombosis- and thrombolysis-on-a-chip models could be used to develop antithrombotic agents and hemostasis monitoring in the clinic. [337,339,340]

In addition to thrombosis, fibrosis has also been modeled in vitro through the application of cyclic mechanical stretching to cell-laden hydrogels, resulting in fibroblast differentiation, matrix protein deposition, ECM stiffening, and remodeling of scar tissue. [332,341,342] These in vitro mechanistic studies which can elucidate the role of biophysical forces in driving aberrant cardiovascular pathologies have significant potential for the

development of life-saving interventions and clinical translation from bench to bedside. [340,343] However, further mechanistic insight into the developmental stages of cardiac disorders needs to be obtained via the use of cardiac-specific ECs or hiPSC-derived ECs differentiated toward cardiac-specific phenotype and their functional incorporation in microphysiological systems.

6.2. Obesity and Diabetes

An imbalance of energy intake and expenditure through lifestyle choices coupled with biological, societal, and environmental factors have prompted obesogenic progression in individuals.^[1] Obesity has been associated with several pathological conditions including insulin resistance, type II diabetes, hypertension, vascular dysfunction, and several forms of cancer.^[2,344,345] Mechanistically, obesity and adiposity are intimately coupled with systemic vasculature via mechanical and biochemical regulation.

Obesity-associated hypertension and insulin resistance causes increases in arterial and capillary stiffness, thickening

HEALTHCARE

www.advhealthmat.de

of the basement membrane, an increase in vessel diameter, and dysregulated vasomodulation. [116,344] Vasomodulation is adversely affected by impaired vasodilation (reduced secretion of and hyposensitivity to vasodilators) or impaired vasoconstriction (elevated secretion of and hypersensitivity to vasoconstrictors), leading to reduced blood flow and reduced functional hyperemia in response to exercise, food intake, or increase in local metabolism. [344,346] This chain of events also correlates with microvascular rarefaction (reduction of blood vessel density), reduced perfusion to peripheral limbs and tissues, and hypoxia, and eventually leads to local ischemia and peripheral vascular disease. [31,344,346]

Obesity is also associated with cholesterol deposition in the vascular intima, which coupled with reduced bloodflow, increases the probability of venous, pulmonary, and cerebral thromboembolism. On a cellular level, obesity leads to altered secretion of pro- and anti-inflammatory cytokines (TNF- α , IL-1 β , -6, -8) and adipokines (adiponectin, leptin) which act synergistically to induce increased vascular permeability, endothelial dysfunction, impaired capillary recruitment, stromal and vascular remodeling, and reduced sensitivity to insulin.[347,348] Mechanical loading on the perivascular adipose tissue resulting from bloodflow also influences its adiposity and downstream regulation of vascular tone. [349] Cyclic uniaxial or biaxial stretch on adipocytes leads to inhibition of adipogenesis while reduced magnitude or frequency of flow or complete static conditions result in enhancement of adipogenesis. [349] Thus, this vicious cycle of adipose regulation of bloodflow and flow-regulated adipogenicity continues in synergism and eventually leads to a host of pathologies in other organs including diabetic vasculopathies, nonalcoholic fatty liver disease (NAFLD), hyperglycemia, and hyperlipidemia, among others.[344,346,350]

Adipogenic dysregulation has been modeled in several in vitro models through the culture and differentiation of adipocytes (with or without endothelial cells), primarily to investigate the secretory profile, immune modulation, and obesityinduced insulin resistance (Figure 9).[322,351,352] Although most studies have focused on biochemical regulation of obesityassociated pathologies, the roles of biophysical forces including shear stress and pressure on adipogenic regulation have been relatively underexplored. However, with increasing appreciation of the role of obesity in driving a wide range of pathologies, it is anticipated that future in vitro and on-chip platforms will incorporate the ability to study the role of mechanical forces in driving these pathologies. These efforts will eventually accelerate development and improvement of the efficacy of antidiabetics, nutraceuticals, and other pharmacogenic agents toward mitigation of obesity and diabetes.

6.3. Pulmonary Niche

The lung and its constitutive small airway and alveolar structures are vital for maintaining gas exchange through the bloodair barrier (BAB). The pulmonary epithelium and the capillary endothelium lining this barrier undergo significant mechanical perturbations due to continuous cyclic distensions and contractions during breathing.^[354] Anatomically, the BAB consists

of the alveolar epithelium (with type I and II epithelial cells), adjoining a thin basement membrane with pericytes, fibroblasts, pulmonary smooth muscle cells, and the pulmonary epithelium. Type I epithelial cells make up 95% of the epithelium and are responsible for diffusive transport of oxygen (O₂) and carbon dioxide (CO₂), while type II epithelial cells secrete a lipoprotein that acts as surfactant and modulates alveolar surface tension during cyclic stretching.[355] Bloodflow through the capillaries is primarily driven by differences in pulmonary arteriolar, venous, and alveolar pressure, while concomitant gas exchange is driven by the partial O2 and CO2 tension across the alveolar interface. These multiple dynamic events are influenced by a host of mechanical forces and their effects on differentiation, cellular proliferation, respiratory function, and disease states of the lung have been investigated in detail.[31,356,357]

In general, physiological mechanical strain on the BAB is necessary for alveologenesis and epithelial and endothelial morphogenesis during lung development. [354] Activation of pericytes in response to cyclic stretch promotes angiocrine signaling and YAP/TAZ-mediated cellular proliferation. [89,357–359] However, accumulation of stretch forces over time can cause transdifferentiation of pericytes and fibroblasts toward a myofibroblast lineage, higher ECM production, basement membrane stiffening, and increased airway resistance, ultimately resulting in pulmonary fibrosis (or chronic lung disease). [89,357,358] Similarly, during ventilator-induced lung injury supraphysiological stretching causes stress failure of the plasma membrane of cells, breakdown of the BAB, release of proinflammatory mediators, and IL-8 mediated neutrophil and leukocyte accumulation. [360]

Several in vitro and on-chip platforms have been developed to recapitulate the dynamics and mechanical deformations occurring at the BAB with particular focus on modeling pulmonary edema, chronic obstructive pulmonary disease (COPD), asthma, lung inflammation, and pulmonary toxicity (Figure 10). [355,361–365] These on-chip platforms (often made of elastomeric PDMS) usually contain a confluent pulmonary epithelium and endothelium separated by a porous support membrane that allows free exchange across the air–liquid interface. Application of vacuum-assisted negative pressure enables stretching of the flexible interface and permits investigation of static versus cyclic stretch conditions on BAB permeability and resistance. [355,363–365]

Intelligent design of platforms can be used to modify the directionality (unidirectional or bidirectional) and axis (uniaxial, biaxial, or triaxial) of the stretch forces to modulate the linear and surface area strain on the cultured cells to decouple the relative contribution of these parameters in maintaining BAB integrity and function. [106,355] In addition, developing complex pulmonary vascular networks around model alveolar assemblies can help identify subtle events including bidirectional flows and RBC mixing and clearance due to cyclic alveolar distension and contraction that is difficult to recapitulate in simplistic models. [285] These platforms have enabled the investigation of the roles that mechanical forces play in gas exchange and pulmonary circulation within the normal and diseased lung; the knowledge of which could be used to develop pulmonary-specific therapeutic interventions.

www.advhealthmat.de

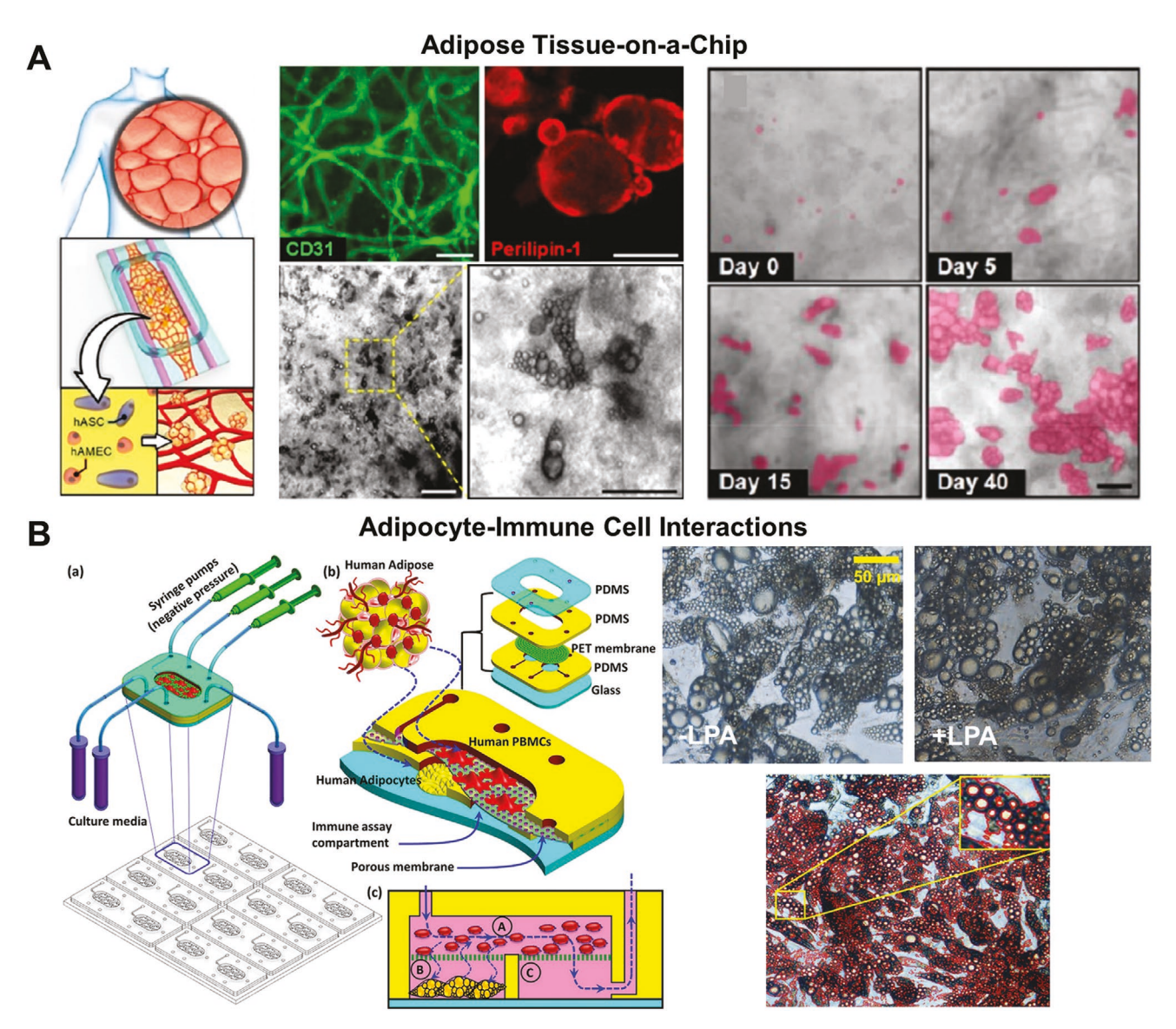


Figure 9. On-chip obesity models. A) Schematic of fabrication of a vascularized human adipose tissue on-chip platform by co-culturing hASCs and hAMECs. hAMECs organize into a 3D vascular network over 2 weeks (green: CD31) and hASCs differentiate into adipocytes bearing intracellular lipid droplets visible in phase contrast and fluorescent micrographs on day 40 (red: perilipin-1) with increase in size and number of droplets (SB = 100 μm). Adapted with permission. Copyright 2019, American Chemical Society. B) Schematic of the setup for studying adipocyte—immune cell interactions during type II diabetes in a microfluidic device with individual compartments for adipocytes and PBMCs, bright-field images and magnified view of lipid droplet accumulation in control and LPA treated adipocyte from adipocyte—PBMC cocultures (SB = 50 μm). Adapted with permission. Copyright 2019, Springer Nature. Abbreviations— hASCs, human adipose-derived stem cells; hAMECs, primary human adipose microvascular endothelial cells; PBMCs, peripheral blood mononuclear cells; LPA, Lipid A from *E. coli* serotype R515.

6.4. Hepatic Niche

The liver, owing to its vital role in nutrient metabolism and toxic clearance, experiences distinct mechanotransductory processes arising out of hemodynamic forces essential to maintaining its function and regeneration potential. The hepatovascular niche (hepatic sinusoids) consists of fenestrated endothelium made of liver sinusoid endothelial cells (LSECs), Kupffer cells (KCs, liver-resident macrophages), hepatic stellate cells (HSCs) in the adjoining Space of Disse, and hepatocytes and cholangiocytes arranged around the bile duct. [31,89,366] Flow

from the hepatic artery and portal vein exerts shear stress and pressure on LSECs, which drives transcellular transport across the fenestrae. The LSEC fenestrae is unique in that it lacks a basement membrane, is highly permeable to macromolecular transport, and has a high endocytotic capacity (necessary for scavenging cellular waste from blood). In addition to common EC mechanosensors, Krüppel-like factor-2 (KLF-2), a shear-sensitive transcription factor present in LSECs and KCs, is responsible for maintaining a flowrate-dependent anti-inflammatory, antioxidant, antithrombotic, and vasoprotective phenotype. [31,366,367]

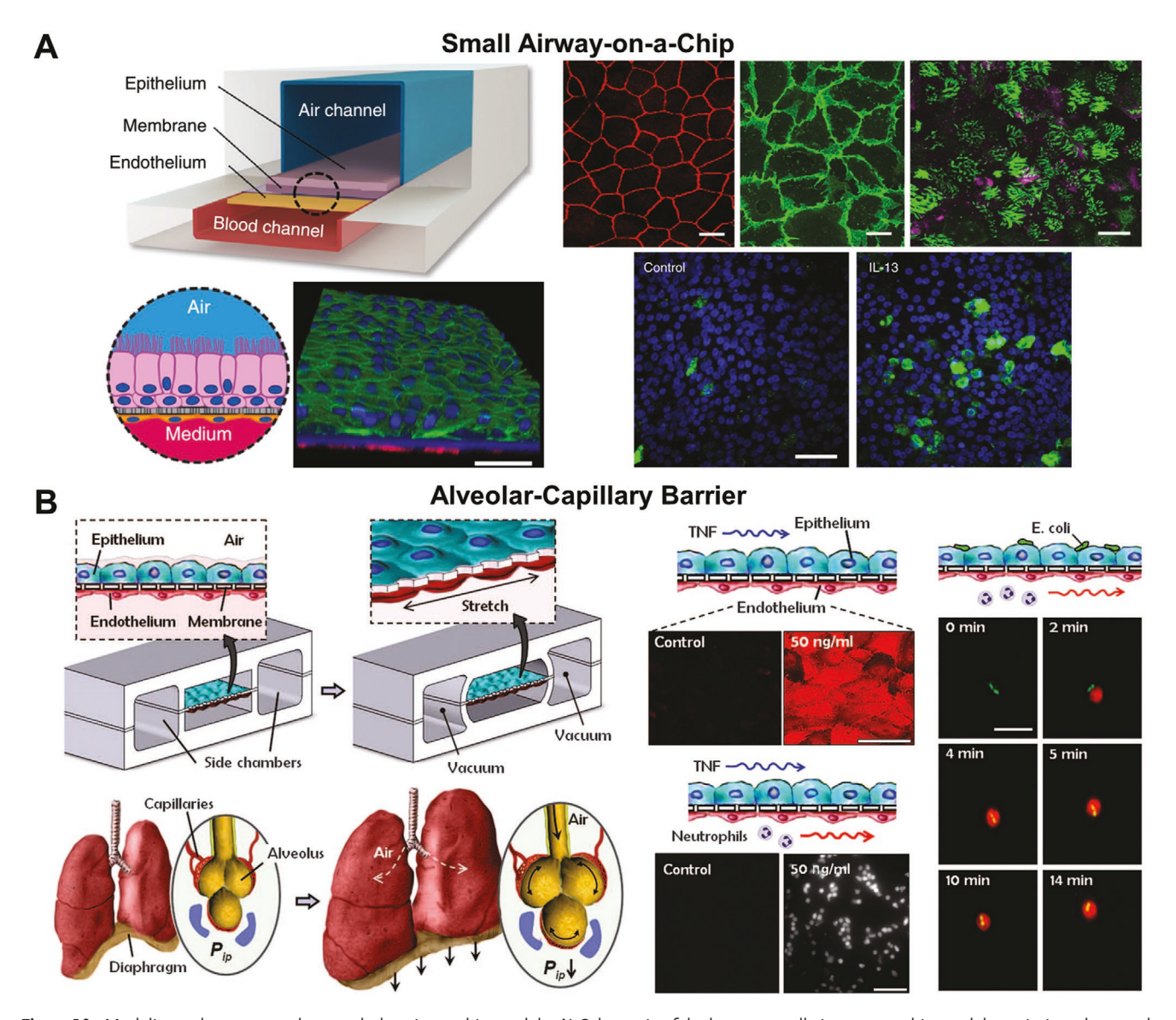


Figure 10. Modeling pulmonary mechanopathology in on-chip models. A) Schematic of the human small airway-on-a-chip model to mimic asthma and lung inflammation with 3D confocal reconstruction of the fully differentiated, pseudostratified airway epithelium formed by hAECs (green: F-actin) with hPMECs (red: F-actin) on either side of the membrane (blue: nuclei) (SB = 30 μm). Demonstration of tight junction formation (red: ZO-1) in hAECs, continuous adherens junctions (green: PECAM-1) in hPMECs, and high numbers of ciliated cells (green: β-tubulin IV) and goblet cells (magenta: MUC5AC) (SB = 20 μm) (top) and confocal micrographs of differentiated airway epithelium cultured on-chip for 4–6 weeks at the air–liquid interface under control or IL-13 treatment (green: MUC5AC, goblet cells, blue: nuclei) (SB = 50 μm) (bottom). Adapted with permission. Copyright 2016, Springer Nature. B) Schematic of the microfluidic device to model the alveolar-capillary barrier with vacuum-assisted mechanical stretching mimicking alveolar distension. Schematic and confocal micrographs of epithelium stimulated with TNF-α upregulating ICAM-1 expression (red) under 10% strain at 0.2 Hz and adhering of human neutrophils to TNF-α activated endothelium (SB = 50 μm). Schematic and fluorescence time-lapse of phagocytosis of two *E. coli* cells (green) on the epithelial surface by a neutrophil (red) that transmigrated from the vascular microchannel to the alveolar compartment (SB = 20 μm). Adapted with permission. Copyright 2010, AAAS. Abbreviations—hAECs, human airway epithelial cells; hPMECs, human pulmonary microvascular endothelial cells; ZO-1, zona occludens-1; PECAM-1, platelet endothelial cell adhesion molecule; MUC5AC, mucin-5; IL-13, interleukin-13; ICAM-1, intercellular adhesion molecule-1, TNF-α, tumor necrosis factor-α.

HSCs play a key role in maintaining flow-mediated sinusoidal tone and stiffness by activation of the RhoA-ROCK pathway, MLC phosphorylation, and stress fiber contraction. Vascular dysfunction arising out of portal hypertension, inflammation or alcoholic damage causes defenestration (or capillarization) of LSECs, deposition of laminin and fibronectin, activation of HSCs toward a proliferative,

procontractile phenotype, reduced NO production, increased ROS generation, and abnormal sensitivity to vasomodulation, thereby hindering oxygenation of hepatocytes. [366,367,369] This eventually leads to necroptosis of hepatocytes and chronic liver disease (cirrhosis). [366,367] Abnormal flow patterns are also associated with platelet recruitment and aggregation, imbalance in pro- and anti-coagulant factors, coagulation and clot formation,

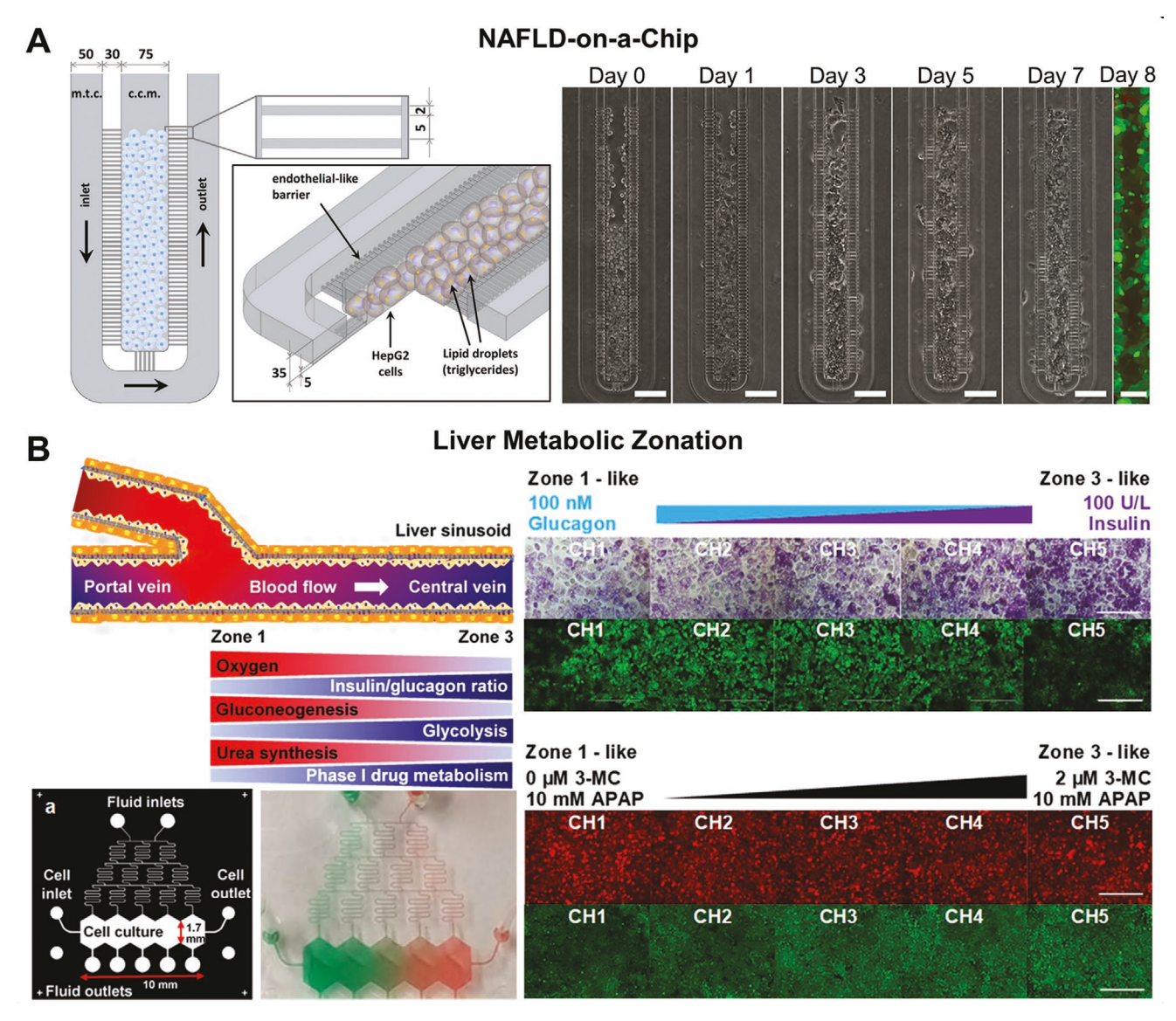


Figure 11. Modeling hepatic microenvironments in in vitro models. A) Schematic of the NAFLD-on-a-chip device design with hepatic cells (m.t.c.: mass transport channel, c.c.m.: cell culture microchamber). Phase contrast micrographs of HepG2 cells inside the microfluidic sinusoid over 0, 1, 3, 5, and 7 d in culture (SB = $100 \, \mu m$) and fluorescence micrograph of cells on day 8 (green: live, red: dead) (SB = $50 \, \mu m$). Adapted with permission. [374] Copyright 2016, PLOS One. B) Schematic of liver circulation and metabolic zonation. Design of the microfluidic gradient generator to mimic hepatic zonal gradients, and gradient of food dyes. Zonation of primary human hepatocytes in carbohydrate metabolism (purple: PAS stain) and nitrogen metabolism (green: CPS1 stain) with gradients of glucagon and insulin (SB = $400 \, \mu m$). Zonation of primary human hepatocytes in drug-induced liver toxicity via exposure to 3-MC and APAP over 4 h (red: tetramethyl rhodamine methyl ester) and drug metabolism (green: CYP1A2 stain) over 24 h (SB = $400 \, \mu m$). Adapted with permission. $^{[375]}$ Copyright 2018, Springer Nature. Abbreviations—NAFLD, nonalcoholic fatty liver disease; CPS1, carbamoyl phosphate synthase-1; 3-MC, 3-methylcholanthrene, APAP, acetaminophen.

and recruitment and adhesion of leukocytes, thereby leading to vessel occlusion and an increase in intrahepatic vascular resistance and pressure. [366,368] Interestingly, recovery from acute liver injury or hepatectomy is also dependent on increases in shear stress and flow, which induces release of NO from LSECs and HSCs and sensitizes hepatocytes to hepatocyte growth factor (HGF) necessary for proliferation and regeneration. [368,370]

Investigation of flow-associated liver function and clearance has been conducted in vitro in several on-chip platforms (Figure 11). [362,371–374] In particular, comparative studies of hepatocyte culture in static versus perfused conditions reveal the important role of flow in albumin and urea secretion, cytochrome P450 metabolism, toxicity modulation of drug compounds, liver zonation, and overall long-term maintenance of hepatocyte viability. [285,375–377] One study uncovered the role of vessel perfusion in stretching of LSECs, activating integrin β_1 and vascular endothelial growth factor receptor 3 (VEGFR3), upregulating HGF secretion, and resulting in increased hepatocyte proliferation and survival. [378] In vitro platforms

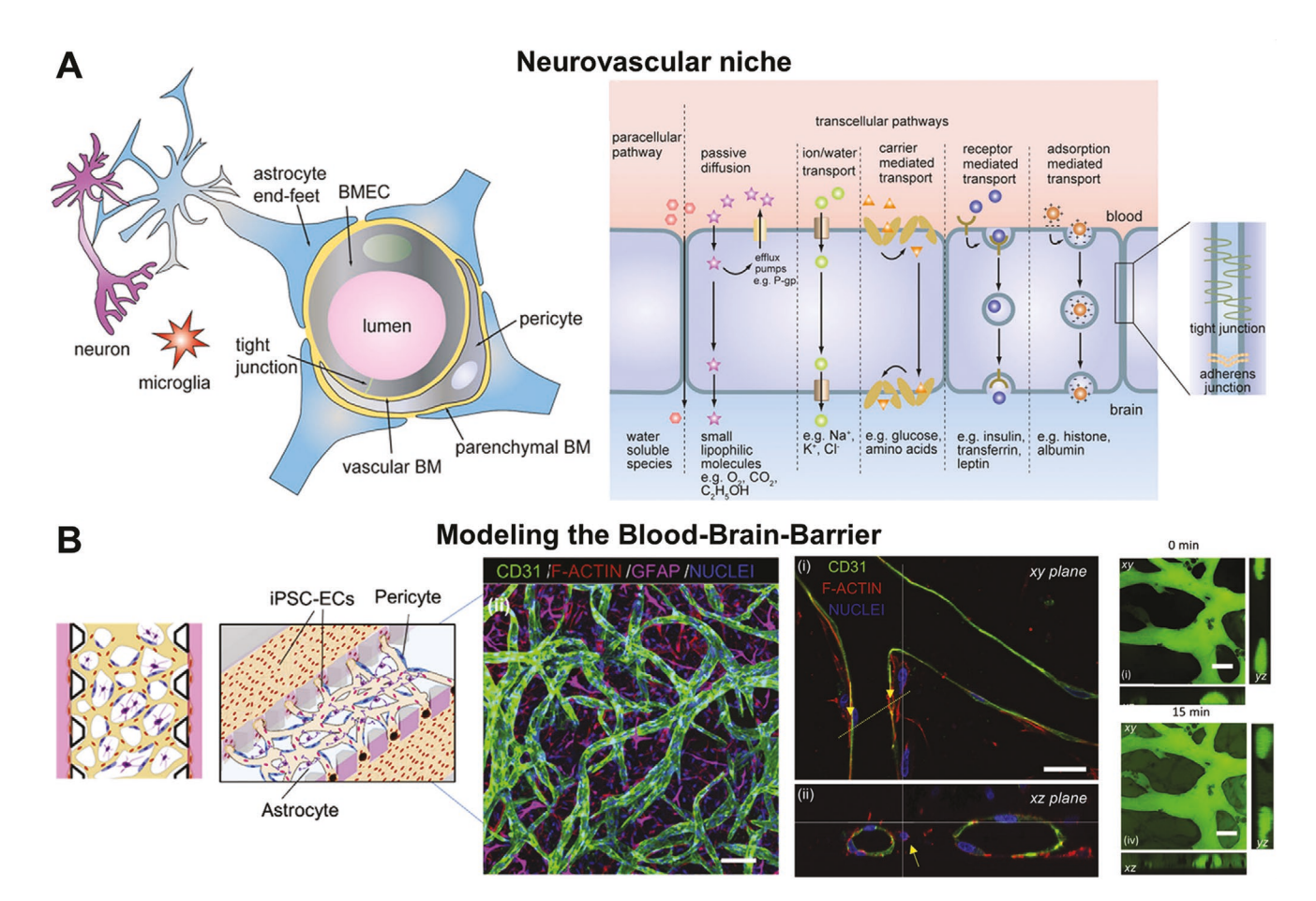


Figure 12. Modeling neurovascular niche in on-chip models. A) Schematic of the structure of the neurovascular unit (NVU) in the blood-brain-barrier (BBB) and molecular transport pathways across the BBB. Adapted with permission. [382] Copyright 2017, Springer Nature. B) Schematic of the BBB-on-a-chip and confocal image of self-assembled iPSC-ECs (green: CD31), pericytes (red: F-actin), astrocytes (magenta: GFAP) (blue: nuclei) (SB = $100 \, \mu m$). Confocal image and projection of stable hollow lumens formed by pericytes enveloping iPSC-EC-derived microvasculature (SB = $20 \, \mu m$), (iv) Maximum intensity projections of 40 kDa FITC-dextran at times 0 and 15 min postperfusion. Adapted with permission. [383] Copyright 2018, Elsevier. Abbreviations—BMEC, brain microvascular endothelial cells, BM, basement matrix.

recapitulating the complex hepatic niche offer a roadmap toward testing first-pass metabolism and toxicity of candidate drugs, and mechanistic insights into liver regeneration. [362,371] However, decoupling the individual roles of shear stress, cyclic stretch and pressure on different cell types in the liver sinusoid within complex hepatic microenvironments is necessary to develop liver-specific mechanotherapeutics and warrants further investigation. In addition, the role of the lymphatic vasculature in the hepatic niche is also understudied and could potentially be recapitulated in microphysiological systems.

6.5. Neurovascular Niche

The cerebrovascular system is responsible for providing oxygen and nutrients to the energy-intensive neural tissue in the brain, while maintaining ionic and fluidic homeostasis enabling physiological brain function. These functions are accomplished by the neurovascular unit (NVU) consisting of the cerebral capillaries, wrapped with pericytes, and adjoining astrocytes, glial cells, and neurons in the neural parenchyma

(Figure 12).^[381] Brain microvascular ECs (BMECs) constituting cerebral microvasculature form a tightly regulated blood–brain barrier (BBB) that controls paracellular and transcellular transport of ions, nutrients, metabolites, and biomolecules.^[379,380] While paracellular transport is mediated by tight junctions (claudins, occludins) and adherens junctions (VE Cadherin) between BMECs, transcellular transport is mediated by BMEC-specific ion pumps, surface receptors, and protein transporters.^[379,380] The synergistic regulation of BBB integrity and permeability by BMECs, pericytes and astrocytes in the presence of hemodynamic variations and continuous neuronal signaling is critical toward maintaining normal blood perfusion, preventing neuroinflammation and immune responses, and inhibition of xenobiotic and pathogenic infiltration, thereby maintaining neuronal health.^[31,379–381]

The BMECs constituting the cerebral microvasculature exhibit high specificity toward BBB functional integrity and phenotypic differences from ECs in other organs. Under the effect of shear stress, BMECs do not undergo cytoskeletal remodeling, elongation or alignment, and maintain a cobblestone morphology, which is necessary to maintain junctional



www.advhealthmat.de



homeostasis.^[384,385] However, shear stress is necessary to upregulate BMEC junctional protein expression, maintain BMEC metabolism, quiescence and low turnover, and physiological levels of hydraulic conductivity, permeability and transendothelial electrical resistance (TEER).^[380,386] This intricately balanced BBB integrity is sensitive to a wide range of hemodynamic perturbations, resulting from age-related deterioration and dietary habits.^[380,387,388] High arteriolar perfusion pressure, due to hypertension and age-related changes in matrix stiffness and elasticity, can result in reduced dampening of the pulsatile cardiac waveform in the cerebral capillaries, leading to chronic accumulation of neuronal shock.^[125,389]

These events also affect adjoining pericytes and astrocytes; pericytes gradually dropout, weaken capillary integrity and reduce blood flow while astrocytes withdraw their end feet, causing neurovascular decoupling, imbalanced vasomodulation, microglial activation, and neuronal and synaptic dysfunction. [125,379,390] Age-related dysregulation in cerebral blood flow and vascular damage is also associated with accumulation of toxic moieties, neuroinflammation, amyloid- β angiopathy, tau pathology, amyotrophic lateral sclerosis (ALS), dementia, cognitive impairment and Alzheimer's disease (AD). [125]

Under acute circumstances, occlusion or hemorrhage of cerebral capillaries can lead to ischemic stroke due to hypoxia with a surrounding transient penumbral layer of injured neuronal tissue. [391,392] This condition is exacerbated by reperfusion injury caused by normalization of bloodflow, which results in sudden generation of ROS downstream of the ischemic site and subsequent neuronal death. [392] Blunt head trauma can also cause a sudden reduction in bloodflow, cellular compression, neurite and axonal swelling, immune infiltration and inflammatory response leading to increased cranial pressure and cerebral edema. [166]

A majority of on-chip studies modeling the NVU have focused on establishing tight BBB integrity by co-culture of ECs. pericytes and astrocytes (or their hIPSC-derived counterparts) within compartmentalized microniches (Figure 12).[383,393-397] Validation of barrier function is demonstrated by evaluation of the TEER value achieved and molecular permeability, expression of junctional proteins and response to neuroinflammatory agents.[398,399] Development of new platforms or extension of existing ones is expected to provide insights into molecular mechanisms underlying pathogenesis of neurodegenerative diseases and facilitate drug delivery through the BBB.[155,395,400-402] However, mechanisms of structural and functional degeneration of the NVU and BBB due to fluctuations in shear stress, cyclic stretch, or pressure and associated changes in strain induced in the vascular wall and adjacent tissue warrant further investigation within these microengineered systems, owing to their important role preceding multiple neural pathologies. In addition, the potential role of the gut microbiota in driving neuronal disorders through changes in vascular permeability and systemic inflammation could also be recapitulated in microphysiological systems.

6.6. Renal Niche

The kidneys are involved in flow-activated filtration and active reabsorption of water, ions and other biomolecules, thereby

maintaining blood pressure, osmolality, and pH homeostasis of the blood. The functional unit of the kidney, the nephron, has a complex architecture, involving multiple renal cell types, organized in a 3D network surrounded by niche-specific ECM and complex vasculature. [403] Two particular interfaces present in the nephron, the glomerular unit and the renal-vascular tubule unit, are of particular interest with regard to exchange of fluids and ions in the presence of hemodynamic forces. [403]

Hydrostatic pressure in the tortuous convoluted structure of the glomerulus drives filtration of fluids and solutes to the adjoining Bowman's capsule. Podocytes present in the glomerulus experience flow-induced shear stress and tensile stretch due to glomerular ultrafiltrate flow and glomerular capillary pressure respectively, which induce extension of podocyte foot processes at the basolateral surface, coverage over renal capillaries, and integrity of the glomerular filtration barrier. [31,404,405] Increased renal blood flow or hypertension can cause hyperfiltration leading to glomerular hypertrophy and chronic kidney disease. [403,406,407]

The renal-vascular tubule unit, responsible for active reabsorption, lies downstream of the glomerular unit and is also influenced by several flow-associated mechanical forces that affect kidney function. [408] Brush border proximal tubule epithelial cells are arranged as microvilli that sense shear stress through bending and respond via reorganization of cytoskeletal actin stress fibers, focal adhesions, and tight junctions. [409,410] Similarly, primary cilia on the cortical collecting ductal cells and endothelial glycocalyx also respond to shear stress via opening of stretch-activated ion channels and vasomodulatory secretion. [408,410] These collective and coordinated responses ultimately help maintain optimum glomerulotubular balance, water, Na⁺, and HCO₃⁻ reabsorption and blood pH and osmolality. [411]

This tightly regulated balance is disturbed in pathological states (due to local inflammation, thickening of basement membrane, high blood sugar, and others), resulting in renovascular hypertension (secondary regulation of blood pressure due to renal hormone secretion), diabetic nephropathy (protein loss in urine and low blood serum albumin), and general glomerulonephritis. [124,407,412] In addition, drug-induced nephrotoxicity is also commonly encountered during pharmacotherapy and metabolic passage. [412–414]

Several studies have been conducted to model key renal processes including macromolecular diffusion and permeability, drug-induced nephrotoxicity, inflammatory cytokine secretion, and the role of strain in podocyte-endothelial crosstalk, among others (Figure 13). [412-418] In particular, application of fluid flow (or flow coupled with 10% cyclic strain) induced differentiation of hiPSCs into mature and functional podocytes, ensured better luminal coverage, extension of podocyte feet processes to the underlying glomerular endothelium, cell type-specific deposition of collagen IV basement membrane protein, ultimately resulting in improved and in vivo-matched urinary clearance.[419] The role of biophysical forces in regulating renal transport processes and barrier function needs to be investigated in detail, which can be achieved by implementation of microfluidic on-chip platforms that permit dynamic biomimetic flow and mechanical perturbations matching pathological renal states.

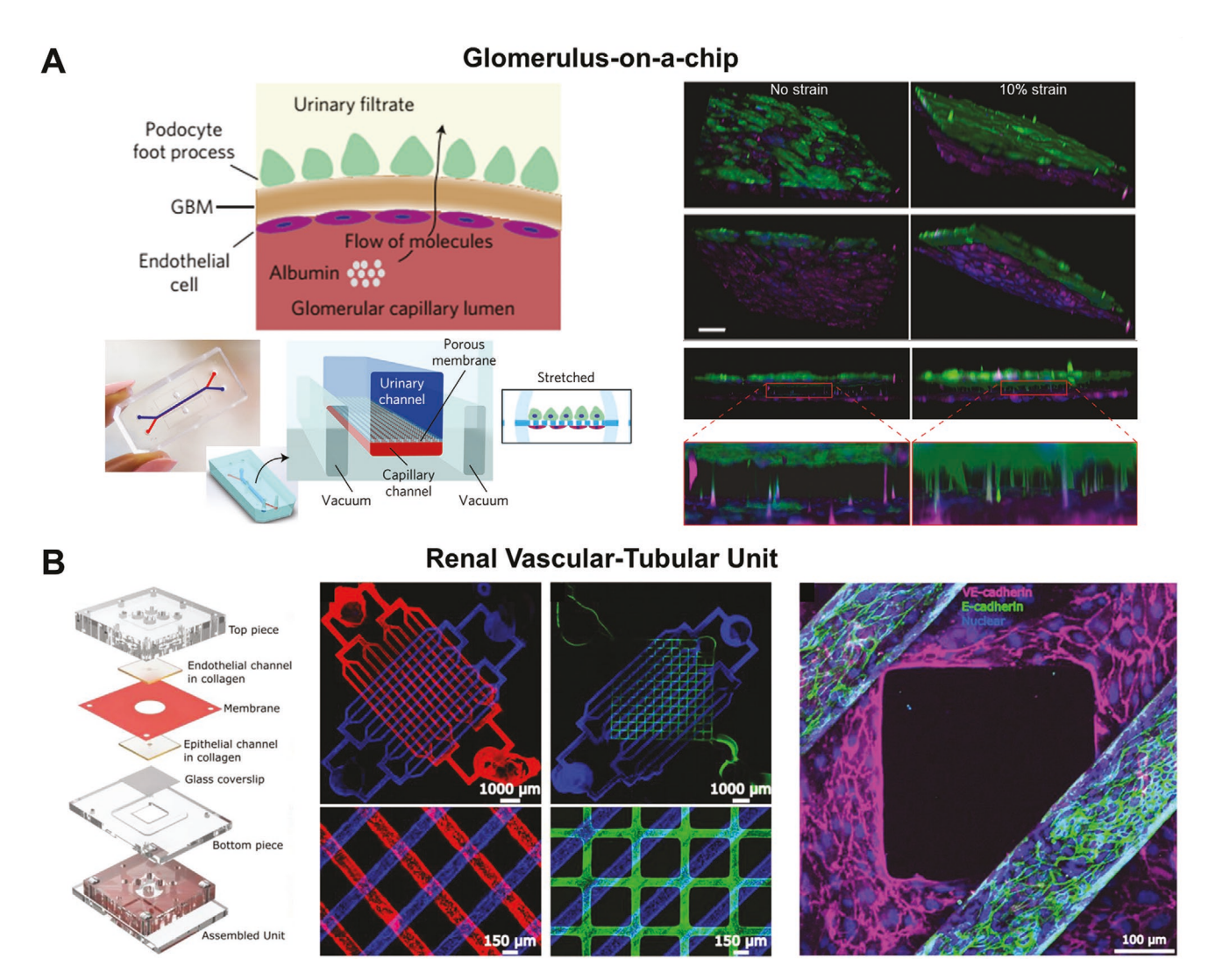


Figure 13. Modeling renal vascular interfaces in on-chip models. A) Schematic of the glomerular capillary wall with hiPSC-derived podocytes and human glomerular ECs separated by the glomerular basement membrane (GBM), photograph and schematic of a microfluidic glomerulus-on-a-chip with vacuum-assisted cyclic stretching of the flexible membrane. Confocal 3D reconstruction of the interface between hiPSC-podocytes (green) and glomerular ECs (magenta) demonstrating enhanced extension of podocyte cell processes through the pores of the flexible membrane and insertion into abluminal surface of the underlying glomerular endothelium with application of 10% strain (SB = $100 \, \mu m$). Adapted with permission. ^[419] Copyright 2017, Springer Nature. B) Schematic of the assembly of the human renal vascular-tubular unit (hRVTU) with parallel-channel geometry for the bottom layer and either parallel-channel or grid geometry for the top layer visualized with perfused fluorescent beads (SB: top = 1 mm, bottom = 150 μm). Confocal 3D projection of channels seeded with HUVECs (magenta: VE-Cadherin) and human renal cortical epithelial cells (green: E-Cadherin) after 14 d of culture demonstrate close proximity of cellularized channels (SB = $100 \, \mu m$). Adapted with permission. ^[418] Copyright 2018, Wiley-VCH.

6.7. Intestinal Niche

The small intestine is primarily responsible for absorption of nutrients from the digestion products in the intestinal lumen and its transport through the intestinal lymphatic to the hepatic portal vein. In addition, commensal microbiota residing in a symbiotic relationship with the intestinal epithelia are also involved in immune surveillance, food antigen tolerance, and infection control (**Figure 14**). The gut epithelium consists of specialized cells (goblet cells, enterocytes, and others) arranged in the form of villi and crypts, which together with the basement membrane and interstitial matrix form the functional gut barrier. This barrier experiences a wide range of forces including pressure

and shear from the endoluminal chyme, peristaltic muscular contraction and relaxation, and cyclic strain induced by rhythmic villous motility, among others. [421,422] These mechanical forces influence epithelial stretching, proliferation, and migration, in a similar manner as the wound healing response cascade. [421] The influence of these forces also propagates to the underlying lacteal lymphatic ECs, collecting lymph vessels, and mesenteric capillaries. [421,422] However, the relative extent to which these endoluminal biophysical forces influence vascular and lymphatic function compared to existing hemodynamic forces arising out of cardiac pulsation is yet to be elucidated.

The normal gut barrier function is often subject to external perturbations arising from inflammatory responses, obesity,



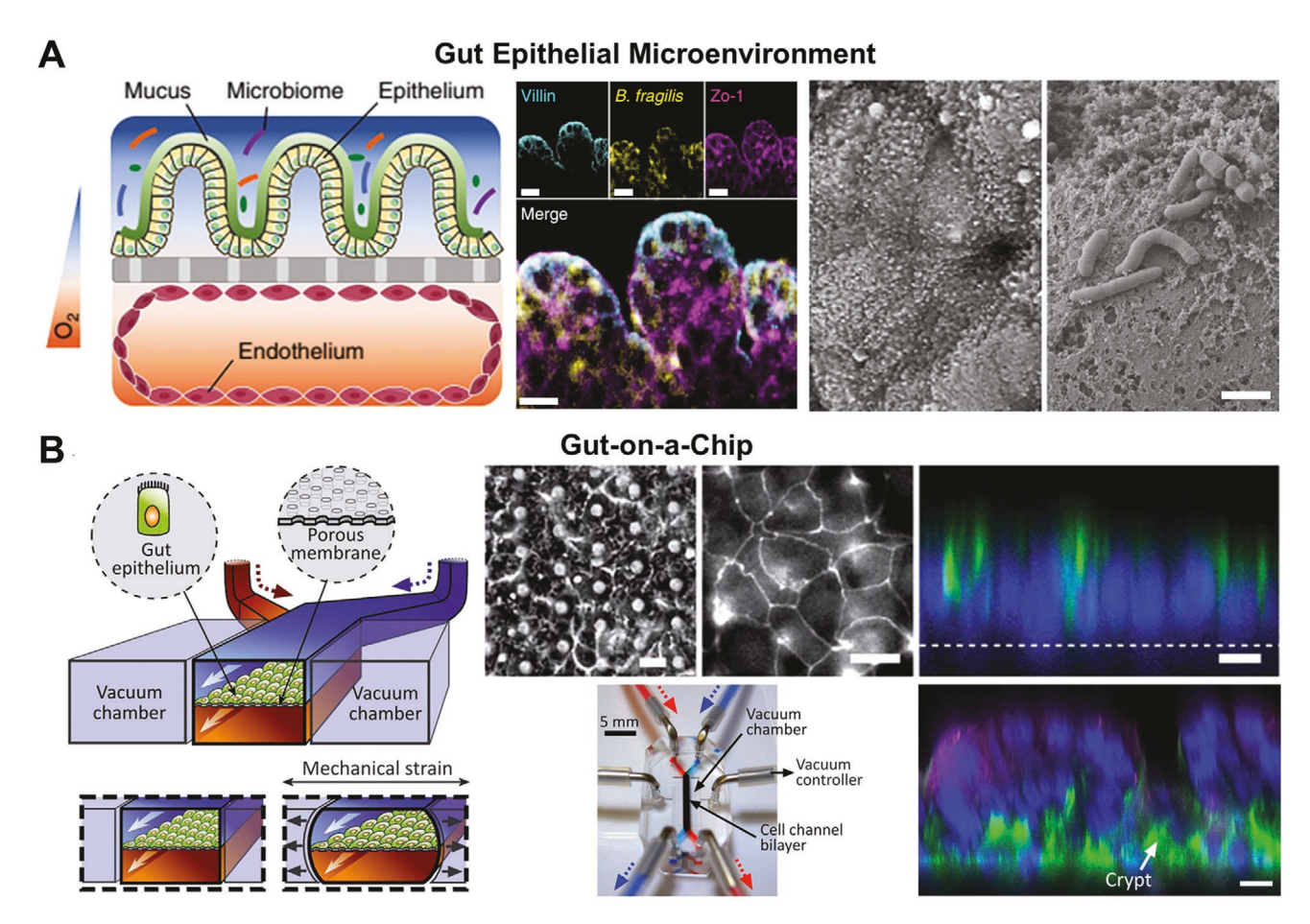


Figure 14. Modeling intestinal/gut vascular microenvironment in on-chip models. A) Schematic of the human intestinal epithelium overlaid with mucus layer and complex gut microbiota and the underlying vascular endothelium. Confocal cross-sectional view of the intestinal epithelium–microbiome interface with co-culture of epithelial cells and *B. fragilis* (cyan: villin, yellow: *B. fragilis*, magenta: ZO-1) (SB = $50 \mu m$). Scanning electron micrographs of the apical surface of the Caco2 epithelium on day 4 of culture before mucus layer accumulation and after day 12 of culture after mucus layer formation and *B. fragilis* addition (SB: = $2 \mu m$). Adapted with permission. (A23) Copyright 2019, Springer Nature. B) Schematic of the gut-on-a-chip device with vacuum-assisted mechanical stretching of the flexible membrane with photograph of the device with perfused dyes. Micrographs of cells under application of cyclic mechanical strain (10%, 0.15 Hz) and flow for 3 d. Phase contrast image of epithelial cells and fluorescence images of ECs (occludin) demonstrate tight junction formation. Confocal cross-section of the interface (green: F-actin, blue: nuclei) (SB = $20 \mu m$) and cross-section view of undulating epithelium at 170 h confirming the presence of villi lined by consistently polarized columnar epithelial cells separated by a crypt (green: F-actin, magenta: mucin, blue: nuclei) (SB = $20 \mu m$). Adapted with permission. (424) Copyright 2012, The Royal Society of Chemistry.

and colonic malignancies.^[425] Imbalance in the basement matrix composition and stiffness, coupled with abnormal pressure and strain amplitudes exerted on the intestinal epithelia can cause unwarranted proliferation, migration, dysbiosis of the gut microbiota, ROS generation, inflammation, and disruption of the gut barrier, ultimately propagating to mesenteric and hepatic organ niches.^[422,425–427]

To that end, there has been increasing interest in modeling this complex milieu within microfluidic on-chip platforms, which can recapitulate the mechanical and biochemical responses of flow and paracrine signaling via coculture of intestinal epithelium, underlying vasculature and commensal bacterial strains (Figure 14). [423,424,428–431] Although such studies are limited, they provide valuable insight into the roles of shear stress, strain, hypoxia (aerobic vs anaerobic microenvironments), inflammatory cytokines, and others in regulating the gut barrier function. [423,426,432] Ultimately, these engineered

models are expected to improve strategies for oral drug delivery, metabolic processing of molecules and pharmaceutics, and development of microbiome-related therapeutics and probiotics.

6.8. Ocular Niche

The human eye consists of two prominent vascular interfaces: 1) the blood-aqueous-barrier (tight junction complex of the ciliary epithelium supported by ECs of the iris vasculature and the Schlemm's canal) and 2) the blood-retinal-barrier (BRB) (located between the retinal tissue and the ocular vascular bed). The BRB is further composed of an outer barrier (oBRB, regulated by the choroidal endothelium and tightly junction bound retinal pigment epithelium) (Figure 15) and an inner barrier (iBRB, composed of tightly bound retinal endothelium coupled with pericytes, astrocytes and Müller cells). [433–435]

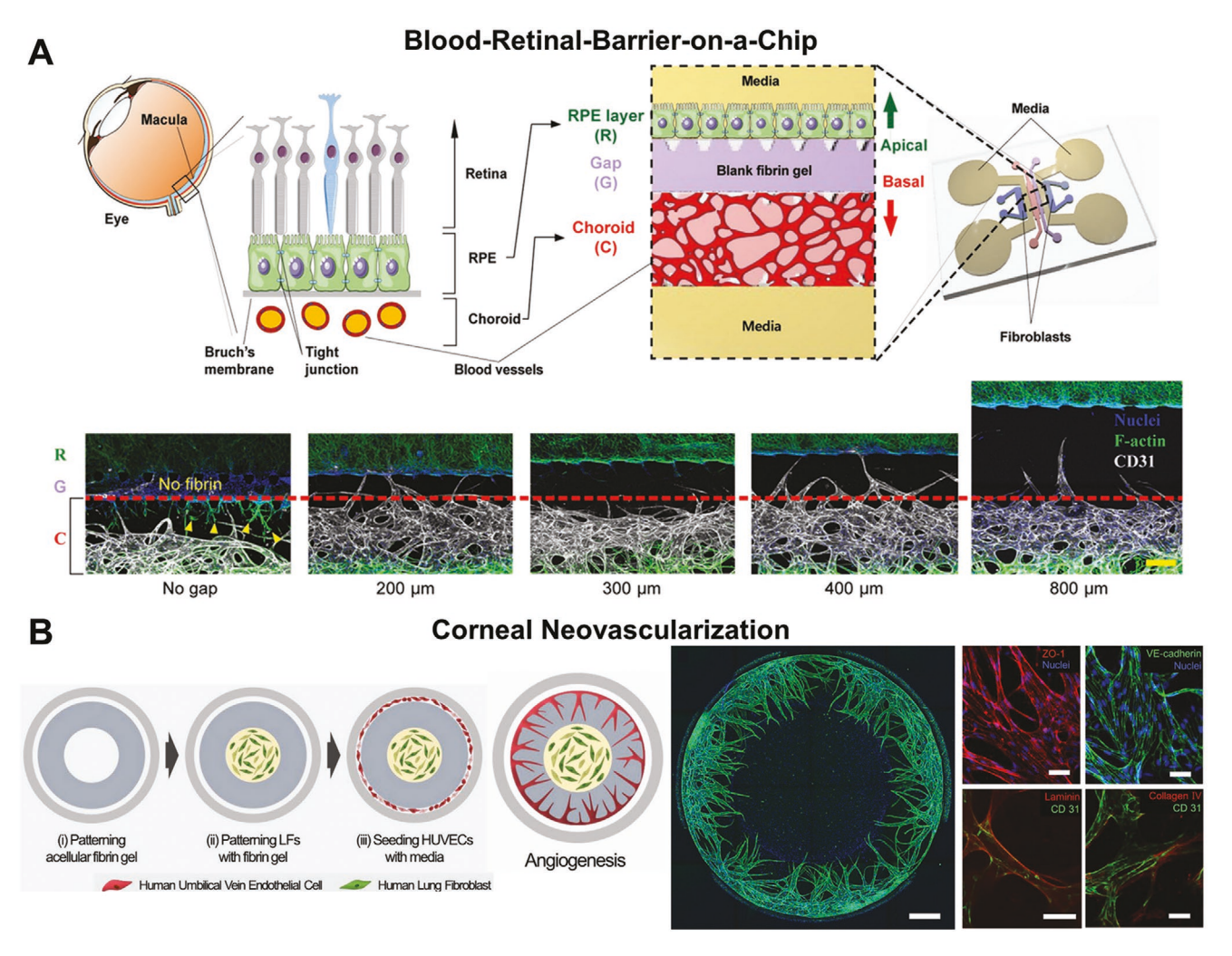


Figure 15. Modeling ocular microenvironment in in vitro models. A) Schematic of the outer blood-retinal barrier (BRB) and design of the 3D retinal pigment epithelium (RPE)-choroid structure on a microfluidic eye-on-a-chip model. ARPE-19 cells were attached to a micropatterned 3D fibrin ECM, with ECs and supporting fibroblasts forming a perfusable vessel network mimicking choroidal vessels. Gap channels of various widths tested to optimize the device design with 400 μm wide channels demonstrating angiogenic sprouts from the unstabilized vessel (green: F-actin, white: CD31, blue: nuclei) (SB = 200 μm). Arrowheads indicate unstable RPE migration without the gap channel. Adapted with permission. (446) Copyright 2018, Wiley-VCH. B) Schematic of corneal neovascularization via patterned seeding of HUVECs and fibroblasts within zonal regions. Confocal micrograph of overall architecture of angiogenic sprouting on day 4 (SB = 500 μm) and characteristic markers demonstrating microvascular assembly (red: ZO-1, green: VE-Cadherin, CD31, red: laminin, collagen IV, blue: nuclei) (SB = 50 μm). Adapted with permission. (447) Copyright 2019, Wiley-VCH.

The blood-aqueous-barrier regulates the flow of ions and solutes from the stromal circulation, aided by ion transporters through the gap junctions, to maintain osmolality of the aqueous humor. Aqueous humor outflow is regulated via the trabecular meshwork (TM) and Schlemm's canal (SC) endothelium, resulting in well-controlled intraocular pressure (IOP). [433,436,437] The blood-aqueous-barrier also serves as an immunoregulatory gateway, regulating infiltration of leukocytes, T lymphocytes, and natural killer (NK) cells into the aqueous humor, and preventing destructive inflammation. [435,438]

The intricate balance between the inflow and outflow of aqueous humor that maintains the IOP is influenced by a number of factors including flow-sensing of trabecular ECs, wall and shear stresses in the vascular endothelium, and basement membrane composition of trabecular lamellae (collagens-I, III, and elastin). [436,438] In combination with IOP, which

exerts compressive forces on the surrounding structures, these factors help regulate local homeostasis through a highly complex interactive network in the anterior eye chamber. [434,436] Imbalance of flow-induced forces, disintegration of the tight barrier due to inflammation, or age-related deterioration of mechanosensory elements can lead to elevated IOP, eventually leading to glaucoma. Hence, maintenance of physiological IOP, either through surgical or biochemical intervention to reduce aqueous humor production or increase outflow, is critical in maintaining ocular homeostasis. [436]

The BRB helps maintain homeostasis between the blood perfusion pressure (PP, induced by retinal arterial blood supply) and the IOP, while regulating fluidic, ionic, and molecular transport between the choroid plexus and retina. [436,439] The junctional and functional integrity of the BRB is sustained by autonomic regulation of retinal vascular flow resistance,



www.advhealthmat.de

which is in turn mediated by several factors including balance between PP and IOP, vessel tone, blood viscosity and shear stress, among others. [439,440] Abnormal regulation of these variables due to age, diabetes, or inflammation can lead to progressive ocular disorders.^[441] Higher blood viscosity, lower flowrate and shear stress, and high blood glucose associated with age and diabetes can cause retinal vein occlusion, basement membrane stiffening, reduced molecular transport, reduced partial oxygen pressure and local hypoxia in the inner retina. [116,441,442] Hindered bloodflow is associated with increased risk of thrombus formation, pericyte dropout, metabolic and vasomodulatory imbalance, and enhanced leukocyte adhesion and infiltration.[31,443-445] These effects can also be exacerbated with elevated PP due to hypertension. Increased hypoxia induces proangiogenic signaling and switching of retinal vasculature from a stable, quiescent phenotype to an activated, angiogenic phenotype leading to neovascular sprouting and BRB dysfunction, which ultimately lead to diabetic retinopathy (DR), age-related macular degeneration (AMD) and macular edema.[116,434,436]

Some studies have aimed at modeling the ocular interfaces, in particular the BRB, using microfluidic culture systems (Figure 15).[322,446,448] Recapitulation of choroidal/retinal and corneal angiogenesis to model AMD and BRB disruption have been conducted with cocultures of retinal endothelial cells (or HUVECs as a substitute), retinal pigment epithelial cells, and intermediately located cells of neuronal origin.[446,447,449,450] These platforms can also be used for testing the efficacy of antiangiogenic agents toward the prevention of diabetes- and age-related vascular disorders.[446,447,449] In addition to BRB, the corneal epithelium (cornea-on-a-chip), which experiences blinking-induced pulsatile forces and cyclic rehydration of lachrymal fluid in an air-liquid interface, has also been used to investigate the differentiation of corneal epithelial cells, dry eve disease-induced epithelial stress, and eve drop-assisted drug permeation, lubrication, and mass transport. [451] Overall, the intricate and complex ocular niche presents great potential for further improvement of these microfluidic platforms which could eventually assist in high-content screening of drugs for ocular diseases.

6.9. Lymphatic System

The lymphatic system is responsible for transporting interstitial fluid (IF) (water, salts, plasma proteins, and WBCs) from the extracellular space via the lymphatic vessels and lymph nodes back to the cardiovascular circulation, thereby maintaining finely balanced tissue fluid homeostasis and molecular trafficking. The transport occurring through the lymphatic vasculature is mediated by various structural and functional elements including vasomodulation by lymphatic endothelial cells (LECs) and lymphatic smooth muscle cells (LSMCs), mechanoreceptors that sense lymph flow-mediated forces, intrinsic and extrinsic pumping of lymph, and bicuspid valves that prevent lymph backflow, among others. [347,452]

In addition, LSMC-mediated cyclic pulsatile contractions ensure unidirectional forward movement of the lymph through the lymphatic vessel.^[452] In addition to lymph transport, the

lymphatic system is also responsible for reverse cholesterol transport and immune surveillance.^[347] Hindrances in lymph flow (due to leakiness in lymph vessels, imbalanced NO signaling, basal membrane stiffening, adipose tissue accumulation, and obesity-induced inflammation) can lead to elevated IF pressure and lymphedema.^[452]

Of particular importance in this regard is the role of IF-induced pressure and shear stress in lymph vessel development and in the tumor microenvironment. [454-457] Lymphangiogenesis is initiated by IF-pressure induced LEC stretching, $\beta 1$ integrin activation, VEGFR3 phosphorylation, LEC proliferation and eventually lymphatic sprouting. [453,455,456] IF flow dynamics also influence lymph vessel valve formation and maintenance.^[453,454] In the tumor microenvironment, the increased intratumoral fluid pressure is associated with cancer-associated fibroblast (CAF) contraction, ECM alignment and stiffening, lymphangiogenic factor secretion, lymphatic sprouting, lymphatic hyperplasia, and eventually tumor cell dissemination toward metastatic spreading. [457,458] These forces concurrently drive macrophage activation, dendritic cell (DC) trafficking, and T cell regulation along the peritumoral lymphatic vessels and the sentinel/tumor draining lymph nodes.[457,459]

Lymph vessel structure and dynamics and its role in lymphatic pathologies have been modeled in several in vitro and on-chip platforms (Figure 16). [219,254,305,460-462] These include the role of shear stress on T cell-dendritic cell trafficking, tumor-dendritic cell communication, diffusional and perfusional transport dynamics between blood and lymphatic vasculature through the interstitial matrix, IF-guided tumor cell migration, lymphatic morphogenesis and immune organoid development. [219,305,460,462-464] These studies aim to shed light on the various interstitial forces and associated biochemical signaling mechanisms that drive various pathologies including lymphedema, inflammation, and tumor cell dissemination.

However, there still exist inherent challenges in microphysiological systems, e.g., incorporating functional immune systems in in vitro platforms, achieving realistic IF-induced flowrates and shear, fabricating valvular structures within artificial lymphatic channels, and incorporating pumping actions to drive lymphatic flow among others. Current established microphysiological systems that lack lymphatic drainage may suffer from build-up of interstitial pressure and decrease of transmural pressure leading to vascular delamination. Additionally, hydraulic conductivity of hydrogel matrices used in on-chip devices needs to be matched to that of parenchymal tissue to ensure relevant IF flow velocity ($\approx 10~\mu m~s^{-1}$). [456] Overcoming these challenges will be critical for investigations of lymphatic disorders and their underlying mechanobiology.

6.10. Cancer

The role of vascular mechanobiology in tumor progression has been studied and reviewed extensively in the context of invasion and migration, epithelial–mesenchymal transition (EMT), metastatic dissemination, survival of circulating tumor cells (CTCs) in vasculature, enhanced chemoresistance, and selection of the cancer stem cell (CSC) phenotype. [465–467] Growing tumor masses are characterized by

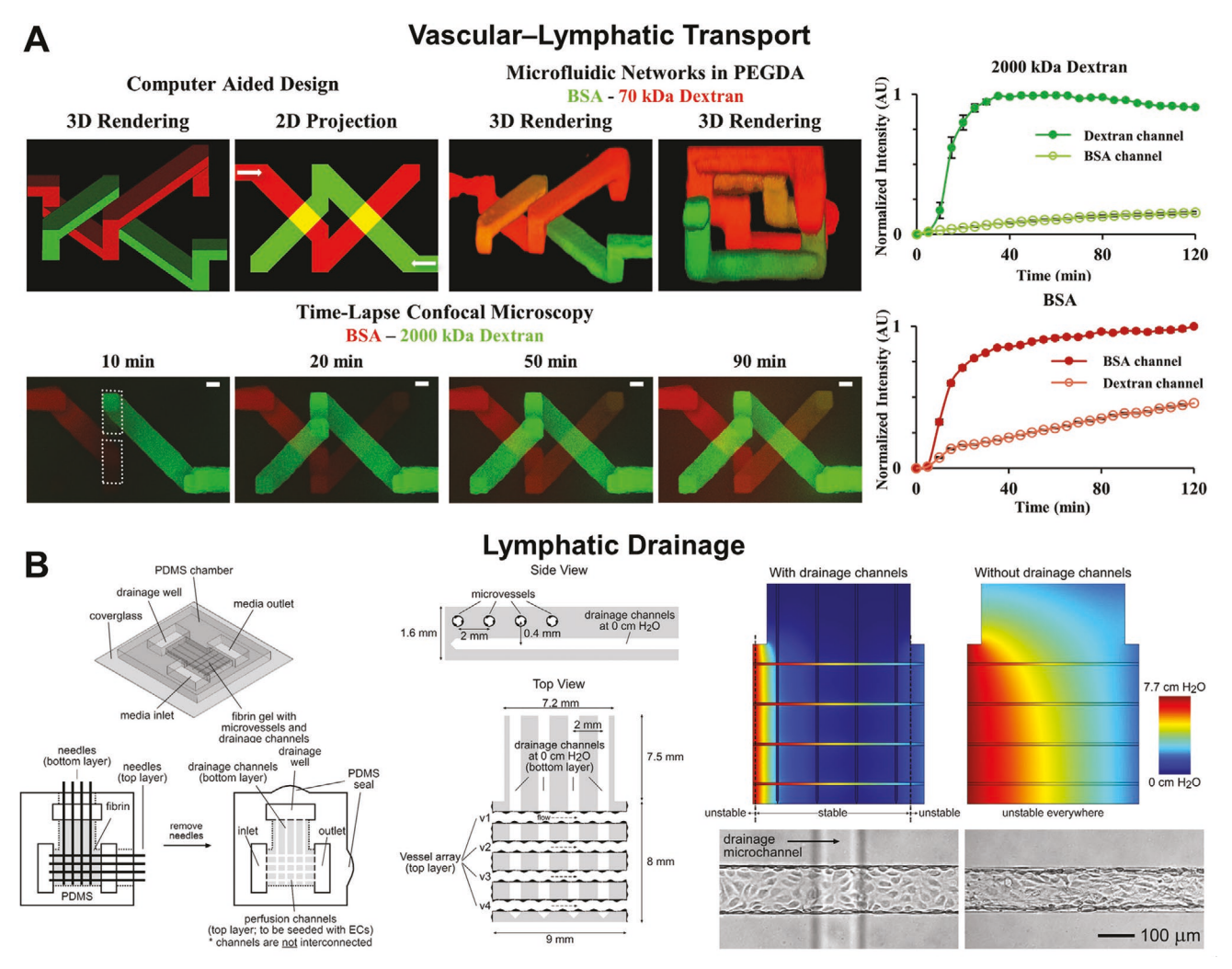


Figure 16. Modeling lymphatic processes in vitro. A) Modeling vascular-lymphatic transport via fabrication of 3D intertwining microchannels in PEGDA hydrogels (channel spacing = 15 μm). Computer aided design and confocal time-lapse imaging of perfused bovine serum albumin (BSA) (red) and 2000 kDa dextran (green) over 90 min demonstrate transport through the hydrogel into the adjacent channel (SB = 20 μm). Quantification of fluorescence intensity of perfused species in both microchannels over time. Adapted with permission. [305] Copyright 2016, Wiley-VCH. B) Schematic of the microfluidic device design with fibrin scaffolds and perfusion and drainage channels micromolded with 120 μm needles. Numerical prediction of pressure profiles and vascular stability in the presence and absence of drainage microchannels predict improved drainage in the presence of lymphatic channels. Corresponding bright-field images of endothelialized channels on day 9 post-seeding (SB = 100 μm). Adapted with permission. [254] Copyright 2013, Wiley Periodicals Inc.

an angiogenic hypervascularized network and lymphatic drainage system, which have distinct phenotypic and genotypic differences from their physiological counterparts. [468] The abnormal angiocrine signaling, metabolic demands and dysregulated flow balance occurring in the tumor mass also leads to accumulation of intratumoral fluid, which exerts high interstitial hydrodynamic pressure on the constituent cells and vessel networks. [468] Coupled with dynamic stiffening of the tumor matrix and physical and biochemical remodeling of the matrix by cancer-associated stromal cells, the mechanical complexity of this milieu makes it challenging to decouple the role of individual variables towards tumorigenic and metastatic progression. [10,468]

Nevertheless, several mechanistic studies using in vitro and on-chip platforms have been conducted to elucidate the effect

of shear stress, interstitial flow, intratumoral pressure and other mechanical perturbations in tumor mechanotransduction. $^{[163,466,469-475]}$ In particular, abnormal blood flow through leaky, tortuous and looping tumor vasculature results in lower shear stress leading to poor diffusional transport and hypoxia. This in turn leads to selection of cells with higher invasion potential and survivability. Additionally, intratumoral fluid pressure induces integrin β_1 -mediated reorganization of matrix adhesions, cytoskeletal architecture, paxillin-dependent protrusion formation, and rheotaxis. $^{[165,476,477]}$ In general, cancer cells have lower cytoskeletal stiffness and increased cellular and nuclear deformability, which enables their migration through size limiting pores of the basement membrane and restricted capillary channels. $^{[478-480]}$ After intravasation in blood vessels, CTCs experience several different hemodynamic forces and

ADVANCED HEALTHCARE MATERIALS

interactions with intravascular cells that both limit their survivability and circulation half-life as well as select for cells with high metastatic seeding potential in distant secondary organs (**Figure 17**).^[478,481] Considering that different organs have widely varying local shear stress and intravascular pressure

profiles, the preferential ability of CTCs to survive postextravasation and form metastatic seeds in an organ-tropic manner deserves special attention. [164,481–483] Interestingly, these CTC characteristics can be used to investigate cancer biophysics at single-cell resolutions. [484]

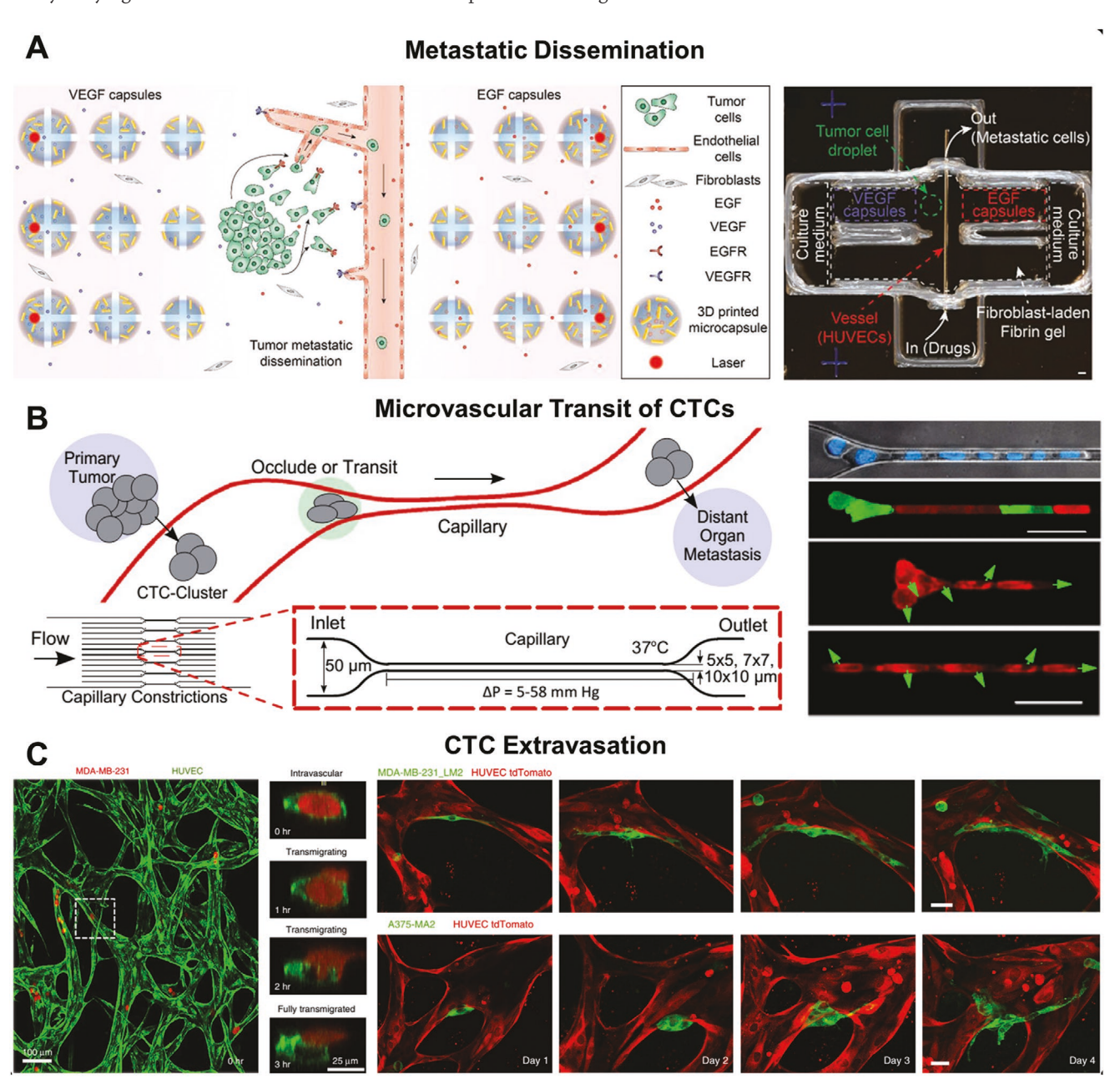


Figure 17. Modeling tumor-vascular interactions in on-chip models. A) Schematic of an in vitro tumor model mimicking metastatic dissemination with integration of tumor cells, EC-lined channels within a fibroblast-laden fibrin gel with photograph of the microfluidic culture chamber for guided tumor cell dissemination. EGF and VEGF gradients are dynamically generated by laser ablation of 3D printed programmable release capsules. (SB = $500 \,\mu m$). Adapted with permission. (F94) Copyright 2019, Wiley-VCH. B) Schematic of circulating tumor cells (CTC) clusters occluding or transiting through capillary to seed metastases and design of a microfluidic capillary device to model the phenomena. Micrographs of an eight-cell cluster of MDA-MB-231 cells (green and red, blue: nuclei) and six-cell LNCaP cluster (red) transiting through 5 μm capillary constriction (SB = $50 \,\mu m$). Adapted with permission. (F78) Copyright 2016, National Academy of the Sciences. C) Confocal projection of a representative region of tumor-perfused (red) self-assembled microvascular network (green) in fibrin gels and cross-sectional views of a single transmigrating tumor cell (in dotted white box) (SB: left = $100 \,\mu m$, right = $25 \,\mu m$). Representative time-lapse images of MDA-MB-231-LM2 cells (top) and A375-MA2 cells (bottom) on day 1 proliferating close to the abluminal side of the lumen over 4 days after transmigration (SB = $20 \,\mu m$). Adapted with permission. (497) Copyright 2017, Springer Nature. Abbreviations: EGF, epidermal growth factor, VEGF, vascular endothelial growth factor.



www.advhealthmat.de



In addition to cancer cells themselves, tumor-associated ECs (TECs) play a vital role in modulating vascular mechanotransduction in the tumor microenvironment. [485,486] In contrast to normal ECs, TECs exhibit higher baseline activity of Rho-ROCK signaling, altered cytoskeletal orientation in response to uniaxial cyclic strain, and altered adhesion and retractability on ECM substrates. [486-488] TEC capillaries are characterized by large intracellular holes, abnormal sprout formation, higher permeability and higher basal inflammation driven by tumorsecreted factors. [486,487,489] These structural deformities, coupled with altered ECM properties, shear stress profiles and mechanochemical signaling from cancer-associated fibroblasts, leads to endothelial-mesenchymal transition and plasticity, which subsequently requires vessel normalization strategies to enable effective penetration and delivery of drugs through the tumor vasculature.[117,490,491] Key differences between healthy vasculature (aligned, hierarchical architecture, uniform flow pattern) versus tumor blood vessels (tortuous, leaky, looped, highly branched and irregular flow pattern) and resulting influence on enhanced permeability and retention (EPR) effect can be modeled for passive targeting of drug carriers.[324,487,492] Investigation of phenotypic and genotypic differences between healthy and tumor-associated ECs can also yield insights for targeting tumor vasculature.[487]

Owing to the significant attention toward modeling of cancer in biomaterials-based microfluidic platforms. several insights have been elucidated mechanistic (Figure 17).[219,460,493-496] This knowledge has in turn enabled the screening and development of anticancer drugs and therapeutic agents to target tumor cell proliferation, migration, invasion, and other events occurring during the metastatic cascade. Some important areas in in vitro tumor modeling that merit future consideration include the role of biophysical and hemodynamic forces in regulating tumor dormancy, metastatic recurrence, tumor-immune cell interactions, tumor lymphatic clearance, CSC-phenotype maintenance, the role of obesity in tumor progression and gut microbiota-mediated tumor control among others. In addition to treatment of cancer, the side effects of various chemotherapeutic agents on the cardiovascular system and associated parenchymal tissue also need to be investigated to improve the safety of administered drugs.

7. Current Limitations and Future Opportunities

Although vascularized, tissue engineered systems for investigating vascular mechanobiology have been developed, many limitations have made it challenging for translation toward high-throughput, facile, and reliable systems for systematic investigations; some of which are discussed below.

7.1. Fabrication and Implementation of Vascularized Microphysiological Systems

While a number of biofabrication strategies have been developed to generate hydrogel-embedded vascular systems, it still remains difficult to recreate the highly dense, tortuous, and complex architecture of microvasculature. Coupling

microvascular architecture with the branching architecture of larger vessels is even more challenging. The ability to achieve this level of complexity will require the development of new fabrication strategies or the integration of multiple fabrication strategies, coupled with self-assembly processes, to generate 3D vascular architectures that mimic the full "tree" of macroto microvasculature. [30] Additionally, incorporating desired parenchymal cells along with the vasculature and gentle biofabrication strategies that limit cell injury need to be utilized.

Media formulations that support optimal function of multiple cell types need to be further developed. This consideration is particularly necessary for organ-specific microphysiological systems and translation toward human-on-a-chip systems in which the proper "routing" is needed so that cells in multiple niches can communicate via soluble factors in the correct sequence and at physiological concentrations. [498] These approaches could be challenging for a single lab, but not impossible, and the involvement of a consortium to direct such a concerted effort between multiple labs could greatly facilitate this process.

With gradual technological advances, microphysiological systems offer promising routes for yielding high-quality, large datasets through integration with electrochemical sensors (to monitor spatiotemporal changes in cellular responses) and incorporation of patient-derived cells/organoids (toward development of personalized medicine). Additionally, validation of on-chip devices with in vivo studies and standardization of experimental protocols and design via academic-industrial collaborations may be necessary to improve relevance. [14,319]

7.1.1. Translation and Commercialization

Despite their advantages, the path of on-chip devices from academic labs to large-scale industrial manufacturing is beset with challenges. Current production methods involving soft lithography are expensive, time-consuming, prone to error, and involve multiple assembly steps. Advances in 3D printing of elastomeric materials may facilitate rapid prototyping and single-step assembly, thereby improving reproducibility and error tolerance.[180] When considering device translation, the ease-of-manufacture is critical to any product establishing widespread use within a market. For the purposes of cell culture, thermoplastic-based products including petri dishes, well-plates, and transwells manufactured via injection-molding enabling mass manufacturing, while also being amendable to a myriad of biological and chemical assays. In contrast, most microphysiological systems have silicone-based designs specific to a single or few applications that involve manufacturing via multiple labor- and time-intensive steps.

Although focused applications and specialized methods have their distinct, important advantages, ideally they should not impede the rapid prototyping/manufacturing of on-chip devices. Toward this goal, a few high-throughput manufacturing processes have been implemented including laser-cutting, [502,503] xurography, [504] micromilling, [505] and the aforementioned injection-molding [506,507] to produce on-chip devices but these methods are less common than soft-lithography and 3D-printing. In the future, researchers designing on-chip





www.advhealthmat.de

devices must carefully consider the range of available fabrication technologies to ensure facile, scalable, and adaptable manufacturing of their devices.

7.1.2. Device Interfacing

Macro-to-microfluidic interfacing is crucial in on-chip devices for generating rigorous and reproducible results. The predominant method for interfacing macrofluidics with microfluidics is inserting connectors (e.g., needles, tubing, or fittings) directly into the ports of the chips (usually made of PDMS). However, these connectors and the resulting interfaces are prone to problems. First, connecting them into the chip ports displaces substantial fluid within the microchannels and generates high transient pressure, both of which can damage the hydrogel matrix and/or the seeded vasculature. Second, these connections may not be robust; they can be finicky and often leak under high pressure and long-term perfusion.

The strength of the interface between the hydrogel and the encompassing microfluidic device remains largely unaddressed and characterized. It is necessary to demonstrate a strong, robust polymer–elastomer interface and validate that this interfacing does not affect or damage the device and the cultured cells within. Since the presence of tiny leaks can have significant effect on device performance, it is imperative to ensure the strengths of seals, bonds, and interfaces.^[508] Even small studies can require several devices for experimental replicates, hence every small loss of effort spent troubleshooting sensitive and unreliable interfacing will compound to lost time and labor, poor results, and wasted resources.

7.1.3. Experimental Considerations

Maintaining sterile and consistent fluidic conditions in on-chip devices is crucial to their successful implementation. Small discrepancies in flow, pressure, and sterility can have major impacts, which are often hard to measure or observe directly, on the performance and generated results of on-chip devices. Although several studies demonstrate fluidic perfusion at given flowrates and/or pressures, quantitative validation using particle-image-velocimetry, particle-tracking-velocimetry, or similar methods is often lacking. Additionally, details regarding aseptic macro-to-microfluidic interfaces, housings, and handling necessary to perfuse the devices and maintain long-term sterile conditions is often missing, making it challenging to replicate or adopt various device designs. Hence, greater focus should be placed on establishing the experimental rigor necessary for wide-scale adoption of on-chip devices, similar to that of traditional platforms.

Generating and maintaining dynamic conditions (e.g., flow, pressure) within on-chip devices can be implemented via four broad strategies, each with their respective advantages, disadvantages, and challenges listed below (Table 3). The optimum choice of perfusion method depends on the application. Experiments requiring a confluent endothelium and relatively low pressure, flow, and shear, are well-suited for rocking, where throughput, ease-of-use, and simplicity far exceeds all other

methods. Experiments requiring higher flow and pressure are better suited for a syringe-pump, peristaltic-pump, or hydraulic head. Those requiring precise, reliable, and defined control of dynamic conditions are best suited for pressure-controllers, albeit at a loss of throughput and overall ease-of-use. When choosing from these methods, researchers must carefully balance throughput and ease-of-use with control and physiological relevance, thereby ensuring maximum parallelization of sample handling and operations.

7.1.4. Measuring Mechanobiological Events in Complex Engineered Tissues

Although a number of methods exist to measure the bulk or local mechanical properties of heterogenous tissues, variations of these methods or new techniques must be developed to accurately and quickly map the temporal and spatial differences that occur in complex tissues. Furthermore, deconstruction of the multiple combined strain fields induced by hemodynamic properties and cells will need advancements in strain field mapping techniques as well as computational, numerical, and finite element modeling methods to accurately determine the contributions from each mechanical input in complex geometries. Achieving these goals will require close collaboration between engineers, materials scientists, physicists, and experts in mathematical modeling. Conversion of strain fields to stresses and forces will be quite a challenge in these complex systems and relying on strain alone will likely have to suffice in the near future. Experimental decoupling of the temporal strain fields induced by hemodynamics and cell generated forces will require a multitude of intense experimental controls and will likely be very time consuming and extensive.

7.1.5. Choice of Relevant Endothelial Cells

With regard to designing an in vitro vascularized model, the choice of appropriate EC types depends upon the intended application and translatability of the model. HUVECs were the first human EC type to successfully be isolated and cultured in vitro and being relatively inexpensive and proliferative, are a good benchmark useful in early stages of device or model development.^[509,510] However, due to inherent differences, HUVECs may not be applicable for the investigation of organ-specific vascular mechanobiology.

For example, in a study of diabetic hyperglycemia-induced endothelial dysfunction, HUVECs and HMVECs showed significant differences in gene expression, hydrogen peroxide production, and mitochondrial membrane polarization, demonstrating that EC choice does have an influence on the results and interpretation of disease-based EC studies.^[511] Differences in adhesion molecule and gene expression profiles exist between macro- and microvascular, arterial and venous, and organ-specific ECs.^[512,513] Organ-specific ECs have also been shown to vary in their barrier properties in vitro, forming continuous, fenestrated, or sinusoidal endothelium in vivo.^[31,514] EC angiogenic potential, metabolic rate, and susceptibility to shear stress can also vary from organ to organ.^[510,514] These



 Table 3. Approaches for microfluidic perfusion in on-chip devices.

Method	Advantages	Disadvantages	Limitations
Hydraulic Head	SimpleExpensiveRequires no pumps or controlConsistent and reliable flow/pressure	 Conditions vary with time, often by an order-of-magnitude Requires frequent media replenishment 	 Cumbersome to use for long-term perfusion Varying conditions are not physiological
Syringe Pump	Consistent and reliable flow/pressure.InexpensiveScalable with multiple devices	 Requires high volumes of media due to absence of recirculation Cannot change pressure independent of flow 	 Requires substantial footprint Imaging can be low-throughput and cumbersome Difficult to maintain sterility
Peristaltic Pump	 Requires low volumes of media due to recirculation Inexpensive Small footprint Easy to maintain sterility 	 Flow and pressure pulse/oscillate with time and require dampening to eliminate Cannot change pressure independent of flow 	 Throughput better than syringe- pumps, but still low overall Sterility easier to maintain than syringe-pump and pressure-controller
Rocking	 Requires low volumes of media Inexpensive Small footprint Easy to maintain sterility High-throughput Can control transmural pressure independent of flow Requires no interfacing with a macrofluidic system 	 Limits to pressure, flow, and shear Flow oscillates back-and-forth with time Requires daily replacing of media due to evaporating 	Difficult to induce shear higher than 5 dyne cm ⁻²
Pressure-Controller	 Precise control of conditions Can change flow and pressure independently Requires low volumes of media Small footprint Scalable with multiple devices 	 Expensive Some systems do not recirculate media Requires calibrating for each specific device 	 Low throughput Limited number of commercial systems available Often requires custom programming and calibrating

findings are not surprising when considering the functional differences between organs and the physiological requirements of organ-specific endothelium.

A number of immortalized EC lines have been developed. including Ea.Hy926 and HMEC-1; however, many of these lines fail to exhibit important endothelial characteristics such as expression of vWF, CD31, CD34, and various adhesion molecules including E-selectin, VCAM-1, and ICAM-1. Of the EC lines developed. HPMEC-ST1.6R shows the most similarity to primary human microvascular ECs in vitro. [515] Human induced pluripotent stem cells (hiPSCs) could potentially provide an option, having been directed toward EC phenotype; efforts are ongoing, however, to obtain more mature and functional organ-specific behavior and gene expression.^[516] The use of patient-derived cells for individualized medicine has also gained traction as a method to more accurately recapitulate in vivo conditions of ECs in in vitro devices; a recent study cultured patient-specific renal cell carcinoma tumor-derived and normal kidney ECs in in vitro vascular models to screen antiangiogenic therapies on an individualized basis.[517]

Additionally, different EC types have varying propensity to form self-assembled networks within hydrogel scaffolds. Although HUVECs, ECFCs, and EPCs (being of the early progenitor type) are amenable to forming patent microvascular networks within collagen, fibrin and other natural hydrogels, other EC types (particularly mature lines) require more careful consideration and fine tuning of matrix properties to ensure a high degree of interconnectivity in the network. In this regard, an

important distinction needs to be made between vasculogenic potential (ability to self-assemble into networks) and angiogenic potential (ability to form new sprouts from existing networks) of EC types. Several microphysiological systems capitalize on the vasculogenic or angiogenic ability of ECs to investigate the pathophysiology of interest. However, the relevance of the in vitro observations to that occurring in native physiology is often overlooked or understudied. Future studies need to consider the inherent 3D phenotypic behavior of ECs (e.g., apicobasal polarity, mechanism of EC–EC junction formation, matrix confinement of EC) as well as vessel architectural features (e.g., tortuosity, lacunarity, branching density) in order to validate in vitro results to that observed in vivo or in native conditions.

Overall, EC phenotypic and genotypic heterogeneity should be taken into account when designing in vitro vascularized models and future efforts should focus on using primary adult organ-specific ECs as they become commercially available to improve model relevance.

8. Conclusion

The emergence of vascularized, in vitro microphysiological systems to model various organ and organ-specific pathologies has been a great leap toward translation of mechanistic data obtained in the lab to implementation in clinical settings. Coupled with the use of intelligently engineered materials and a host of biofabrication techniques, these systems



____ /VIAIEKIAL3

can recapitulate niche-level or microenvironmental physiologies with a high degree of physiological accuracy. Although not discussed in this review, investigation of other microvascular physiological niches including pancreatic islets, [351,518–522] musculoskeletal niche, [523–526] and the placental barrier, [318] among others, are also gaining prominence. Recent efforts to integrate individual organ-niches into multiorgan microphysiological systems have provided insight into metabolic and biochemical crosstalk between separate compartments, toxicological assessment of candidate drug compounds, and their biodistribution in preclinical studies. [33,34,498,527]

In addition to functional organ-specific cells, the role of ECs in determining organ functions, through both biochemical signaling and biophysical forces via mechanotransductory pathways, is gaining attention.^[7,8,510,528] The incorporation of organ-specific or disease-specific ECs (to model the phenotype and function of native microvasculature) along with niche-specific functional (or dysfunctional) cells imparts high degree of physiological context to the generated data.^[31,510,514] Although vascular biochemical signaling is well-documented, biophysical forces arising from hemodynamic perturbations, age-related phenomena, and immune engagement also play vital role in health and disease.^[7,8,10]

In general, the role of shear stress, cyclic stretch, and pressure exerted on the endothelium and vascular parenchyma has been studied, [6–8,38,331] but further implementation of complex flow patterns and force fields is only possible with recently developed 3D biomimetic microvascular networks. [285,305] Detailed investigation of endothelial and vascular mechanobiology using these engineered microfluidic systems is therefore necessary to obtain a comprehensive picture of the mechanical microenvironment in various niches, which could potentially be used for developing mechanotherapeutic strategies toward personalized medicine. [529]

Acknowledgements

This work was supported by grants from the National Cancer Institute (R21CA214299), the W.M. Keck Foundation (15A00396), the Delaware Bioscience Center for Advanced Technology (15A01570), the University of Delaware Research Foundation (17A00429) and a National Science Foundation CAREER Award (1751797). O.A.B and J.L.S. were supported by NSF IGERT Fellowships (1144726). C.J.F was supported by a University of Delaware Graduate Scholar Award. K.A.K. was partially supported by a University of Delaware Dissertation Fellowship.

Conflict of Interest

The authors declare no conflict of interest.

Keywords

endothelial cells, hydrogels, mechanotransduction, microfluidic devices, microphysiological systems, organ-on-a-chip, shear stress, tissue engineering

Received: September 5, 2019 Revised: January 24, 2020 Published online:

- [1] M. Blüher, Nat. Rev. Endocrinol. 2019, 15, 288.
- [2] C. García-Jiménez, M. Gutiérrez-Salmerón, A. Chocarro-Calvo, J. M. García-Martinez, A. Castaño, A. De la Vieja, Br. J. Cancer 2016. 114, 716.
- [3] G. Srivastava, C. M. Apovian, Nat. Rev. Endocrinol. 2018, 14, 12.
- [4] D. E. Ingber, Ann. Med. 2003, 35, 564.
- [5] Y. Qiu, D. R. Myers, W. A. Lam, Nat. Rev. Mater. 2019, 4, 294.
- [6] D. Lu, G. S. Kassab, J. R. Soc., Interface 2011, 8, 1379.
- [7] B. D. James, J. B. Allen, ACS Biomater. Sci. Eng. 2018, 4, 3818.
- [8] F. W. Charbonier, M. Zamani, N. F. Huang, Adv. Biosyst. 2019, 3, 1800252.
- [9] G. E. Davis, D. R. Senger, Circ. Res. 2005, 97, 1093.
- [10] D. E. Jaalouk, J. Lammerding, Nat. Rev. Mol. Cell Biol. 2009, 10, 63.
- [11] G. A. Hoffmann, J. Y. Wong, M. L. Smith, Biochemistry 2019, 58, 4710.
- [12] O. Yesil-Celiktas, S. Hassan, A. K. Miri, S. Maharjan, R. Al-kharboosh, A. Quiñones-Hinojosa, Y. S. Zhang, Adv. Biosyst. 2018, 2, 1800109.
- [13] H. Liu, Y. Wang, K. Cui, Y. Guo, X. Zhang, J. Qin, Adv. Mater. 2019, 31, 1902042.
- [14] B. Zhang, A. Korolj, B. F. L. Lai, M. Radisic, Nat. Rev. Mater. 2018, 3, 257.
- [15] S. Ahadian, R. Civitarese, D. Bannerman, M. H. Mohammadi, R. Lu, E. Wang, L. Davenport-Huyer, B. Lai, B. Zhang, Y. Zhao, S. Mandla, A. Korolj, M. Radisic, Adv. Healthcare Mater. 2018, 7, 1700506.
- [16] J. Leijten, J. Rouwkema, Y. S. Zhang, A. Nasajpour, M. R. Dokmeci, A. Khademhosseini, Small 2016, 12, 2130.
- [17] R. H. Harrison, J.-P. St-Pierre, M. M. Stevens, *Tissue Eng.*, Part B 2014, 20, 1.
- [18] J. Fu, D.-A. Wang, Trends Biotechnol. 2018, 36, 834.
- [19] E. C. Novosel, C. Kleinhans, P. J. Kluger, Adv. Drug Delivery Rev. 2011, 63, 300.
- [20] J. Rouwkema, N. C. Rivron, C. A. van Blitterswijk, Trends Biotechnol. 2008, 26, 434.
- [21] M. Lovett, K. Lee, A. Edwards, D. L. Kaplan, *Tissue Eng.*, *Part B* 2009, 15, 353.
- [22] T. Osaki, V. Sivathanu, R. D. Kamm, Curr. Opin. Biotechnol. 2018, 52, 116.
- [23] D. Caballero, S. Kaushik, V. M. Correlo, J. M. Oliveira, R. L. Reis, S. C. Kundu, *Biomaterials* 2017, 149, 98.
- [24] A. Sontheimer-Phelps, B. A. Hassell, D. E. Ingber, Nat. Rev. Cancer 2019, 19, 65.
- [25] K. Ronaldson-Bouchard, G. Vunjak-Novakovic, Cell Stem Cell 2018, 22, 310
- [26] S. E. Park, A. Georgescu, D. Huh, Science 2019, 364, 960.
- [27] A. Malheiro, P. Wieringa, C. Mota, M. Baker, L. Moroni, ACS Biomater. Sci. Eng. 2016, 2, 1694.
- [28] X. Zhang, L. Li, C. Luo, Lab Chip 2016, 16, 1757.
- [29] M. I. Bogorad, J. DeStefano, J. Karlsson, A. D. Wong, S. Gerecht, P. C. Searson. *Lab Chip* **2015**. *15*. 4242.
- [30] M. A. Traore, S. C. George, Tissue Eng., Part B 2017, 23, 505.
- [31] H. G. Augustin, G. Y. Koh, Science 2017, 357, aal2379.
- [32] E. W. Esch, A. Bahinski, D. Huh, Nat. Rev. Drug Discovery 2015, 14, 248
- [33] Y. I. Wang, C. Carmona, J. J. Hickman, M. L. Shuler, Adv. Healthcare Mater. 2018, 7, 1701000.
- [34] S. H. Lee, J. H. Sung, Adv. Healthcare Mater. 2018, 7, 1700419.
- [35] H. Bae, A. S. Puranik, R. Gauvin, F. Edalat, B. Carrillo-Conde, N. A. Peppas, A. Khademhosseini, Sci. Transl. Med. 2012, 4, 160ps23.
- [36] D.-H. Kim, P. K. Wong, J. Park, A. Levchenko, Y. Sun, Annu. Rev. Biomed. Eng. 2009, 11, 203.
- [37] P. Dan, É. Velot, V. Decot, P. Menu, J. Cell Sci. 2015, 128, 2415.

- [38] S. Li, N. F. Huang, S. Hsu, J. Cell. Biochem. 2005, 96, 1110.
- [39] S. S. Hur, J. C. del Alamo, J. S. Park, Y.-S. Li, H. A. Nguyen, D. Teng, K.-C. Wang, L. Flores, B. Alonso-Latorre, J. C. Lasheras, S. Chien, *Proc. Natl. Acad. Sci. USA* 2012, 109, 11110.
- [40] M. L. C. Albuquerque, C. M. Waters, U. Savla, H. W. Schnaper, A. S. Flozak, Am. J. Physiol.: Heart Circ. Physiol. 2000, 279, H293.
- [41] Y. Tardy, N. Resnick, T. Nagel, M. A. Gimbrone, C. F. Dewey, Arterioscler., Thromb., Vasc. Biol. 1997, 17, 3102.
- [42] X. Liu, K. J. Peyton, W. Durante, Am. J. Physiol.: Heart Circ. Physiol. 2013, 304, H1634.
- [43] R. Steward, D. Tambe, C. C. Hardin, R. Krishnan, J. J. Fredberg, Am. J. Physiol.: Cell Physiol. 2015, 308, C657.
- [44] J. W. Song, L. L. Munn, Proc. Natl. Acad. Sci. USA 2011, 108, 15342.
- [45] R. Sinha, S. Le Gac, N. Verdonschot, A. van den Berg, B. Koopman, J. Rouwkema, Sci. Rep. 2016, 6, 29510.
- [46] M. B. Dancu, D. E. Berardi, J. P. Vanden Heuvel, J. M. Tarbell, Arterioscler., Thromb., Vasc. Biol. 2004, 24, 2088.
- [47] R. Amaya, A. Pierides, J. M. Tarbell, PLoS One 2015, 10, 0129952.
- [48] B. G. Chung, K.-H. Lee, A. Khademhosseini, S.-H. Lee, Lab Chip 2012, 12, 45.
- [49] L. Moroni, T. Boland, J. A. Burdick, C. De Maria, B. Derby, G. Forgacs, J. Groll, Q. Li, J. Malda, V. A. Mironov, C. Mota, M. Nakamura, W. Shu, S. Takeuchi, T. B. F. Woodfield, T. Xu, J. J. Yoo, G. Vozzi, *Trends Biotechnol.* 2018, 36, 384.
- [50] A. Morss Clyne, S. Swaminathan, A. Díaz Lantada, Biofabrication 2019, 11, 032001.
- [51] P. Bajaj, R. M. Schweller, A. Khademhosseini, J. L. West, R. Bashir, Annu. Rev. Biomed. Eng. 2014, 16, 247.
- [52] A. D. Bannerman, R. X. Ze Lu, A. Korolj, L. H. Kim, M. Radisic, Curr. Opin. Biomed. Eng. 2018, 6, 8.
- [53] M. G. McCoy, J. M. Wei, S. Choi, J. P. Goerger, W. Zipfel, C. Fischbach, ACS Biomater. Sci. Eng. 2018, 4, 2967.
- [54] M. G. McCoy, B. R. Seo, S. Choi, C. Fischbach, Acta Biomater. 2016, 44, 200.
- [55] A. Berdichevski, M. A. Birch, A. E. Markaki, Mater. Lett. 2019, 248, 93.
- [56] V. L. Cross, Y. Zheng, N. Won Choi, S. S. Verbridge, B. A. Sutermaster, L. J. Bonassar, C. Fischbach, A. D. Stroock, *Biomaterials* 2010, 31, 8596.
- [57] N. Yamamura, R. Sudo, M. Ikeda, K. Tanishita, *Tissue Eng.* 2007, 13, 1443.
- [58] J. T. Morgan, J. Shirazi, E. M. Comber, C. Eschenburg, J. P. Gleghorn, *Biomaterials* 2019, 189, 37.
- [59] K.-B. Celie, Y. Toyoda, X. Dong, K. A. Morrison, P. Zhang, O. Asanbe, J. L. Jin, R. C. Hooper, M. R. Zanotelli, O. Kaymakcalan, R. J. Bender, J. A. Spector, *Acta Biomater.* 2019, 91, 144.
- [60] A. P. McGuigan, M. V. Sefton, Proc. Natl. Acad. Sci. USA 2006, 103, 11461.
- [61] B. A. Juliar, M. T. Keating, Y. P. Kong, E. L. Botvinick, A. J. Putnam, Biomaterials 2018, 162, 99.
- [62] C. M. Ghajar, X. Chen, J. W. Harris, V. Suresh, C. C. W. Hughes, N. L. Jeon, A. J. Putnam, S. C. George, *Biophys. J.* 2008, 94, 1930
- [63] S. Li, L. R. Nih, H. Bachman, P. Fei, Y. Li, E. Nam, R. Dimatteo, S. T. Carmichael, T. H. Barker, T. Segura, Nat. Mater. 2017, 16, 953.
- [64] D. Hanjaya-Putra, V. Bose, Y.-I. Shen, J. Yee, S. Khetan, K. Fox-Talbot, C. Steenbergen, J. A. Burdick, S. Gerecht, *Blood* 2011, 118, 804.
- [65] S. Kusuma, Y.-I. Shen, D. Hanjaya-Putra, P. Mali, L. Cheng, S. Gerecht, Proc. Natl. Acad. Sci. USA 2013, 110, 12601.
- [66] M. C. Ford, J. P. Bertram, S. R. Hynes, M. Michaud, Q. Li, M. Young, S. S. Segal, J. A. Madri, E. B. Lavik, *Proc. Natl. Acad. Sci.* USA 2006, 103, 2512.

- [67] B. Akar, B. Jiang, S. I. Somo, A. A. Appel, J. C. Larson, K. M. Tichauer, E. M. Brey, Biomaterials 2015, 72, 61.
- [68] L. D. Harris, B. S. Kim, D. J. Mooney, J. Biomed. Mater. Res. 1998, 42, 396.
- [69] P. J. Stahl, T. R. Chan, Y.-I. Shen, G. Sun, S. Gerecht, S. M. Yu, Adv. Funct. Mater. 2014, 24, 3213.
- [70] Y. J. He, D. A. Young, M. Mededovic, K. Li, C. Li, K. Tichauer, D. Venerus, G. Papavasiliou, Biomacromolecules 2018, 19, 4168.
- [71] J. J. Moon, J. E. Saik, R. A. Poché, J. E. Leslie-Barbick, S.-H. Lee, A. A. Smith, M. E. Dickinson, J. L. West, *Biomaterials* 2010, 31, 3840
- [72] J. E. Saik, D. J. Gould, E. M. Watkins, M. E. Dickinson, J. L. West, Acta Biomater. 2011, 7, 133.
- [73] R. M. Schweller, J. L. West, ACS Biomater. Sci. Eng. 2015, 1, 335.
- [74] J. E. Leslie-Barbick, C. Shen, C. Chen, J. L. West, *Tissue Eng., Part A* 2011, 17, 221.
- [75] E. B. Peters, N. Christoforou, K. W. Leong, G. A. Truskey, J. L. West, Cell. Mol. Bioeng. 2016, 9, 38.
- [76] J. M. de Rutte, J. Koh, D. Di Carlo, Adv. Funct. Mater. 2019, 29, 1900071.
- [77] R. K. Singh, D. Seliktar, A. J. Putnam, Biomaterials 2013, 34, 9331.
- [78] W. J. Seeto, Y. Tian, R. L. Winter, F. J. Caldwell, A. A. Wooldridge, E. A. Lipke, *Tissue Eng.*, *Part C* 2017, 23, 815.
- [79] G. Sun, Y.-I. Shen, S. Kusuma, K. Fox-Talbot, C. J. Steenbergen, S. Gerecht, *Biomaterials* 2011, 32, 95.
- [80] M. R. Blatchley, F. Hall, S. Wang, H. C. Pruitt, S. Gerecht, Sci. Adv. 2019, 5, eaau7518.
- [81] M. Blatchley, K. M. Park, S. Gerecht, J. Mater. Chem. B 2015, 3, 7939
- [82] C.-H. Chuang, R.-Z. Lin, H.-W. Tien, Y.-C. Chu, Y.-C. Li, J. M. Melero-Martin, Y.-C. Chen, Acta Biomater. 2015, 19, 85.
- [83] D. Hanjaya-Putra, J. Yee, D. Ceci, R. Truitt, D. Yee, S. Gerecht, J. Cell. Mol. Med. 2010, 14, 2436.
- [84] K. M. Park, S. Gerecht, Nat. Commun. 2014, 5, 4075.
- [85] G. A. Calderon, P. Thai, C. W. Hsu, B. Grigoryan, S. M. Gibson, M. E. Dickinson, J. S. Miller, Biomater. Sci. 2017, 5, 1652.
- [86] Y.-C. Chen, R.-Z. Lin, H. Qi, Y. Yang, H. Bae, J. M. Melero-Martin, A. Khademhosseini, Adv. Funct. Mater. 2012, 22, 2027.
- [87] N. Monteiro, W. He, C. M. Franca, A. Athirasala, L. E. Bertassoni, ACS Biomater. Sci. Eng. 2018, 4, 2563.
- [88] G. L. Basatemur, H. F. Jørgensen, M. C. H. Clarke, M. R. Bennett, Z. Mallat, Nat. Rev. Cardiol. 2019, 16, 27.
- [89] A. Holm, T. Heumann, H. G. Augustin, Trends Cell Biol. 2018, 28, 302
- [90] H. Zhao, J. C. Chappell, J. Biol. Eng. 2019, 13, 26.
- [91] K. R. Stenmark, M. E. Yeager, K. C. El Kasmi, E. Nozik-Grayck, E. V. Gerasimovskaya, M. Li, S. R. Riddle, M. G. Frid, Annu. Rev. Physiol. 2013, 75, 23.
- [92] M. A. Gimbrone, J. N. Topper, T. Nagel, K. R. Anderson, G. Garcia-CardeñA, Ann. N. Y. Acad. Sci. 2006, 902, 230.
- [93] S. Chien, Am. J. Physiol.: Heart Circ. Physiol. 2007, 292, H1209.
- [94] S. Weinbaum, X. Zhang, Y. Han, H. Vink, S. C. Cowin, Proc. Natl. Acad. Sci. USA 2003, 100, 7988.
- [95] K. N. Dahl, A. J. S. Ribeiro, J. Lammerding, Circ. Res. 2008, 102, 1307.
- [96] H. Nakajima, K. Yamamoto, S. Agarwala, K. Terai, H. Fukui, S. Fukuhara, K. Ando, T. Miyazaki, Y. Yokota, E. Schmelzer, H.-G. Belting, M. Affolter, V. Lecaudey, N. Mochizuki, *Dev. Cell* 2017, 40, 523.
- [97] K.-C. Wang, Y.-T. Yeh, P. Nguyen, E. Limqueco, J. Lopez, S. Thorossian, K.-L. Guan, Y.-S. J. Li, S. Chien, *Proc. Natl. Acad. Sci.* USA 2016, 113, 11525.
- [98] G. T. K. Boopathy, W. Hong, Front. Cell Dev. Biol. 2019, 7, 49.
- [99] G. Dai, M. R. Kaazempur-Mofrad, S. Natarajan, Y. Zhang, S. Vaughn, B. R. Blackman, R. D. Kamm, G. Garcia-Cardena,

____ MATERIALS

- M. A. Gimbrone, *Proc. Natl. Acad. Sci. USA* **2004**, 101, 14871
- [100] W. J. Polacheck, R. Li, S. G. M. Uzel, R. D. Kamm, Lab Chip 2013, 13, 2252.
- [101] C. A. Hoesli, C. Tremblay, P.-M. Juneau, M. D. Boulanger, A. V. Beland, S. D. Ling, B. Gaillet, C. Duchesne, J. Ruel, G. Laroche, A. Garnier, ACS Biomater. Sci. Eng. 2018, 4, 3779.
- [102] J. G. DeStefano, A. Williams, A. Wnorowski, N. Yimam, P. C. Searson, A. D. Wong, *Integr. Biol.* 2017, 9, 362.
- [103] Y.-X. Wang, H.-B. Liu, P.-S. Li, W.-X. Yuan, B. Liu, S.-T. Liu, K.-R. Qin, Cell. Mol. Bioeng. 2019, 12, 107.
- [104] V. Prystopiuk, B. Fels, C. S. Simon, I. Liashkovich, D. Pasrednik, C. Kronlage, R. Wedlich-Söldner, H. Oberleithner, J. Fels, J. Cell Sci. 2018, 131, jcs206920.
- [105] T. Ohashi, Y. Sugaya, N. Sakamoto, M. Sato, J. Biomech. 2007, 40, 2399.
- [106] J. H.-C. Wang, P. Goldschmidt-Clermont, J. Wille, F. C.-P. Yin, J. Biomech. 2001, 34, 1563.
- [107] J. Fan, P. Ray, Y. Lu, G. Kaur, J. J. Schwarz, L. Q. Wan, Sci. Adv. 2018, 4, eaat2111.
- [108] A. Livne, E. Bouchbinder, B. Geiger, Nat. Commun. 2014, 5, 3938.
- [109] W. Huang, N. Sakamoto, R. Miyazawa, M. Sato, Biochem. Biophys. Res. Commun. 2012, 418, 708.
- [110] T. Iba, B. E. Sumpio, Microvasc. Res. 1991, 42, 245.
- [111] S. V. S. Gangoda, B. Avadhanam, N. F. Jufri, E. H. Sohn, M. Butlin, V. Gupta, R. Chung, A. P. Avolio, Sci. Rep. 2018, 8, 1689.
- [112] A. Leychenko, E. Konorev, M. Jijiwa, M. L. Matter, PLoS One 2011, 6, e29055.
- [113] A. S. Zeiger, F. D. Liu, J. T. Durham, A. Jagielska, R. Mahmoodian, K. J. Van Vliet, I. M. Herman, *Phys. Biol.* **2016**, *13*, 046006.
- [114] Y. Kubota, J. Cell Biol. 1988, 107, 1589.
- [115] H. Jeon, J. H. Tsui, S. I. Jang, J. H. Lee, S. Park, K. Mun, Y. C. Boo, D.-H. Kim, ACS Appl. Mater. Interfaces 2015, 7, 4525.
- [116] X. Yang, H. A. Scott, F. Monickaraj, J. Xu, S. Ardekani, C. F. Nitta, A. Cabrera, P. G. McGuire, U. Mohideen, A. Das, K. Ghosh, FASEB J. 2016, 30, 601.
- [117] E. Dejana, K. K. Hirschi, M. Simons, Nat. Commun. 2017, 8, 14361.
- [118] R. L. Urbano, C. Furia, S. Basehore, A. M. Clyne, *Biophys. J.* 2017, 113, 645.
- [119] J. A. VanderBurgh, H. Hotchkiss, A. Potharazu, P. V. Taufalele, C. A. Reinhart-King, *Integr. Biol.* 2018, 10, 734.
- [120] P. Gupta, J. C. Moses, B. B. Mandal, ACS Biomater. Sci. Eng. 2019, 5, 933.
- [121] S. Koo, R. Muhammad, G. S. L. Peh, J. S. Mehta, E. K. F. Yim, Acta Biomater. 2014, 10, 1975.
- [122] J. T. Morgan, J. A. Wood, N. M. Shah, M. L. Hughbanks, P. Russell, A. I. Barakat, C. J. Murphy, Biomaterials 2012, 33, 4126.
- [123] N. Thorin-Trescases, E. Thorin, Can. J. Cardiol. 2016, 32, 624.
- [124] N. O. S. Câmara, K. Iseki, H. Kramer, Z.-H. Liu, K. Sharma, Nat. Rev. Nephrol. 2017, 13, 181.
- [125] K. Kisler, A. R. Nelson, A. Montagne, B. V. Zlokovic, *Nat. Rev. Neurosci.* 2017, 18, 419.
- [126] K. Vahidkhah, P. Balogh, P. Bagchi, Sci. Rep. 2016, 6, 28194.
- [127] P. Balogh, P. Bagchi, Biophys. J. 2017, 113, 2815.
- [128] S. Prithu, P. M. K, C. L. Siu-Lun, K. Konstantinos, L. Klaus, *Biorheology* 2011, 48, 1.
- [129] Z. M. Ruggeri, J. Thromb. Haemost. 2003, 1, 1335.
- [130] O. V. Kim, R. I. Litvinov, M. S. Alber, J. W. Weisel, *Nat. Commun.* 2017, 8, 1274.
- [131] K. R. M., S. Bhattacharya, S. DasGupta, S. Chakraborty, Lab Chip 2018, 18, 3939.
- [132] P.-H. Wu, D. R.-B. Aroush, A. Asnacios, W.-C. Chen, M. E. Dokukin, B. L. Doss, P. Durand-Smet, A. Ekpenyong, J. Guck, N. V. Guz, P. A. Janmey, J. S. H. Lee, N. M. Moore, A. Ott, Y.-C. Poh, R. Ros,

- M. Sander, I. Sokolov, J. R. Staunton, N. Wang, G. Whyte, D. Wirtz, Nat. Methods 2018, 15, 491.
- [133] A. M. Kloxin, C. J. Kloxin, C. N. Bowman, K. S. Anseth, *Adv. Mater.* **2010**, *22*, 3484.
- [134] K. S. Anseth, C. N. Bowman, L. Brannon-Peppas, *Biomaterials* 1996, 17, 1647.
- [135] C. Bonnans, J. Chou, Z. Werb, Nat. Rev. Mol. Cell Biol. 2014, 15, 786
- [136] D. T. Butcher, T. Alliston, V. M. Weaver, *Nat. Rev. Cancer* **2009**, *9*,
- [137] J. L. Young, A. W. Holle, J. P. Spatz, Exp. Cell Res. 2016, 343, 3.
- [138] C. Matellan, A. E. del Río Hernández, J. Cell Sci. 2019, 132, jcs229013.
- [139] W. R. Legant, A. Pathak, M. T. Yang, V. S. Deshpande, R. M. McMeeking, C. S. Chen, *Proc. Natl. Acad. Sci. USA* 2009, 106, 10097.
- [140] P. Roca-Cusachs, V. Conte, X. Trepat, Nat. Cell Biol. 2017, 19, 742.
- [141] C. Matellan, A. E. del Río Hernández, ACS Biomater. Sci. Eng. 2019, 5, 3703.
- [142] F. A. Gegenfurtner, B. Jahn, H. Wagner, C. Ziegenhain, W. Enard, L. Geistlinger, J. O. Rädler, A. M. Vollmar, S. Zahler, J. Cell Sci. 2018, 131, jcs212886.
- [143] L. Boldock, C. Wittkowske, C. M. Perrault, Microcirculation 2017, 24, e12361.
- [144] W. Y. Wang, C. D. Davidson, D. Lin, B. M. Baker, Nat. Commun. 2019, 10, 1186.
- [145] S. van Helvert, P. Friedl, ACS Appl. Mater. Interfaces 2016, 8, 21946
- [146] S. Sen, S. Subramanian, D. E. Discher, Biophys. J. 2005, 89, 3203.
- [147] J. H. Wen, L. G. Vincent, A. Fuhrmann, Y. S. Choi, K. C. Hribar, H. Taylor-Weiner, S. Chen, A. J. Engler, Nat. Mater. 2014, 13, 979.
- [148] V. Vyas, M. Solomon, G. G. M. D'Souza, B. D. Huey, Cell. Mol. Bioeng. 2019, 12, 203.
- [149] Y. Abidine, A. Constantinescu, V. M. Laurent, V. Sundar Rajan, R. Michel, V. Laplaud, A. Duperray, C. Verdier, *Biophys. J.* 2018, 114, 1165.
- [150] I. Acerbi, L. Cassereau, I. Dean, Q. Shi, A. Au, C. Park, Y. Y. Chen, J. Liphardt, E. S. Hwang, V. M. Weaver, *Integr. Biol.* 2015, 7, 1120.
- [151] L. Andolfi, S. L. M. Greco, D. Tierno, R. Chignola, M. Martinelli, E. Giolo, S. Luppi, I. Delfino, M. Zanetti, A. Battistella, G. Baldini, G. Ricci, M. Lazzarino, *Acta Biomater.* 2019, 94, 505.
- [152] M. P. E. Wenger, L. Bozec, M. A. Horton, P. Mesquida, *Biophys. J.* 2007, 93, 1255.
- [153] D. Gao, W. Ding, M. Nieto-Vesperinas, X. Ding, M. Rahman, T. Zhang, C. Lim, C.-W. Qiu, Light: Sci. Appl. 2017, 6, 17039.
- [154] J. R. Moffitt, Y. R. Chemla, S. B. Smith, C. Bustamante, Annu. Rev. Biochem. 2008, 77, 205.
- [155] M. T. Scimone, H. C. Cramer III, E. Bar-Kochba, R. Amezcua, J. B. Estrada, C. Franck, Nat. Protoc. 2018, 13, 3042.
- [156] O. A. Banda, C. R. Sabanayagam, J. H. Slater, ACS Appl. Mater. Interfaces 2019, 11, 18233.
- [157] M. Bergert, T. Lendenmann, M. Zündel, A. E. Ehret, D. Panozzo, P. Richner, D. K. Kim, S. J. P. Kress, D. J. Norris, O. Sorkine-Hornung, E. Mazza, D. Poulikakos, A. Ferrari, *Nat. Commun.* 2016, 7, 12814.
- [158] H. Jang, J. Kim, J. H. Shin, J. J. Fredberg, C. Y. Park, Y. Park, Lab Chip 2019, 19, 1579.
- [159] W. R. Legant, J. S. Miller, B. L. Blakely, D. M. Cohen, G. M. Genin, C. S. Chen, *Nat. Methods* 2010, 7, 969.
- [160] W. R. Legant, C. K. Choi, J. S. Miller, L. Shao, L. Gao, E. Betzig, C. S. Chen, Proc. Natl. Acad. Sci. USA 2013, 110, 881.
- [161] G. Lee, S.-B. Han, J.-H. Lee, H.-W. Kim, D.-H. Kim, ACS Biomater. Sci. Eng. 2019, 5, 3735.
- [162] J. R. D. Soiné, N. Hersch, G. Dreissen, N. Hampe, B. Hoffmann, R. Merkel, U. S. Schwarz, *Interface Focus* 2016, 6, 20160024.

- [163] J. Escribano, M. B. Chen, E. Moeendarbary, X. Cao, V. Shenoy, J. M. Garcia-Aznar, R. D. Kamm, F. Spill, *PLoS Comput. Biol.* 2019, 15, e1006395.
- [164] M. B. Chen, J. A. Whisler, J. S. Jeon, R. D. Kamm, Integr. Biol. 2013, 5, 1262.
- [165] W. J. Polacheck, A. E. German, A. Mammoto, D. E. Ingber, R. D. Kamm, *Proc. Natl. Acad. Sci. USA* 2014, 111, 2447.
- [166] E. Bar-Kochba, M. T. Scimone, J. B. Estrada, C. Franck, Sci. Rep. 2016, 6, 30550.
- [167] Y.-T. Shiu, S. Li, W. A. Marganski, S. Usami, M. A. Schwartz, Y.-L. Wang, M. Dembo, S. Chien, *Biophys. J.* 2004, 86, 2558.
- [168] C. M. Perrault, A. Brugues, E. Bazellieres, P. Ricco, D. Lacroix, X. Trepat, Biophys. J. 2015, 109, 1533.
- [169] R. H. W. Lam, Y. Sun, W. Chen, J. Fu, Lab Chip 2012, 12, 1865.
- [170] B. P. Helmke, A. B. Rosen, P. F. Davies, Biophys. J. 2003, 84, 2691.
- [171] C. J. Wilson, G. Kasper, M. A. Schütz, G. N. Duda, *Microvasc. Res.* 2009, 78, 358.
- [172] L. Bernardi, C. Giampietro, V. Marina, M. Genta, E. Mazza, A. Ferrari, *Integr. Biol.* 2018, 10, 527.
- [173] W. Xi, T. B. Saw, D. Delacour, C. T. Lim, B. Ladoux, Nat. Rev. Mater. 2019. 4, 23.
- [174] V. Mironov, V. Kasyanov, R. R. Markwald, Trends Biotechnol. 2008, 26. 338.
- [175] S. Pradhan, K. A. Keller, J. L. Sperduto, J. H. Slater, Adv. Healthcare Mater. 2017, 6, 1700681.
- [176] J. Rouwkema, A. Khademhosseini, Trends Biotechnol. 2016, 34, 733.
- [177] Y. Blinder, D. Mooney, S. Levenberg, Curr. Opin. Chem. Eng. 2014, 3, 56.
- [178] A. K. Au, W. Huynh, L. F. Horowitz, A. Folch, Angew. Chem., Int. Ed. 2016, 55, 3862.
- [179] K. Gold, A. K. Gaharwar, A. Jain, Biomaterials 2019, 196, 2.
- [180] N. Bhattacharjee, A. Urrios, S. Kang, A. Folch, Lab Chip 2016, 16, 1720
- [181] I. S. Kinstlinger, J. S. Miller, Lab Chip 2016, 16, 2025.
- [182] Y. J. Blinder, A. Freiman, N. Raindel, D. J. Mooney, S. Levenberg, Sci. Rep. 2016, 5, 17840.
- [183] N. Koike, D. Fukumura, O. Gralla, P. Au, J. S. Schechner, R. K. Jain, Nature 2004, 428, 138.
- [184] V. Suresh, J. L. West, Regener. Eng. Transl. Med. 2019, 5, 180.
- [185] J. M. Sorrell, M. A. Baber, A. I. Caplan, Tissue Eng., Part A 2009, 15, 1751
- [186] L. Evensen, D. R. Micklem, A. Blois, S. V. Berge, N. Aarsæther, A. Littlewood-Evans, J. Wood, J. B. Lorens, PLoS One 2009, 4, e5798.
- [187] E. B. Peters, Tissue Eng., Part B 2018, 24, 1.
- [188] K. E. Scott, K. Rychel, S. Ranamukhaarachchi, P. Rangamani, S. I. Fraley, Acta Biomater. 2019, 96, 81.
- [189] M. P. Cuchiara, D. J. Gould, M. K. McHale, M. E. Dickinson, J. L. West, Adv. Funct. Mater. 2012, 22, 4511.
- [190] T. Matsumoto, Y. C. Yung, C. Fischbach, H. J. Kong, R. Nakaoka, D. J. Mooney, Tissue Eng. 2007, 13, 207.
- [191] R. R. Rao, A. W. Peterson, J. Ceccarelli, A. J. Putnam, J. P. Stegemann, *Angiogenesis* 2012, 15, 253.
- [192] Y. Liu, M. B. Chan-Park, Biomaterials 2009, 30, 196.
- [193] J.-Y. Lai, D. H.-K. Ma, M.-H. Lai, Y.-T. Li, R.-J. Chang, L.-M. Chen, PLoS One 2013, 8, e54058.
- [194] P. Du, M. Suhaeri, S. S. Ha, S. J. Oh, S.-H. Kim, K. Park, Acta Biomater. 2017, 54, 333.
- [195] L. R. Nih, S. Gojgini, S. T. Carmichael, T. Segura, Nat. Mater. 2018, 17, 642.
- [196] T. R. Chan, P. J. Stahl, S. M. Yu, Adv. Funct. Mater. 2011, 21, 4252.
- [197] J. E. Leslie-Barbick, J. E. Saik, D. J. Gould, M. E. Dickinson, J. L. West, *Biomaterials* 2011, 32, 5782.
- [198] A. Y. Rioja, E. L. H. Daley, J. C. Habif, A. J. Putnam, J. P. Stegemann, Acta Biomater. 2017, 55, 144.

- [199] A. Y. Rioja, R. Tiruvannamalai Annamalai, S. Paris, A. J. Putnam, J. P. Stegemann, *Acta Biomater.* **2016**, *29*, 33.
- [200] P. R. A. Chivers, D. K. Smith, Nat. Rev. Mater. 2019, 4, 463.
- [201] D. R. Griffin, W. M. Weaver, P. O. Scumpia, D. Di Carlo, T. Segura, Nat. Mater. 2015, 14, 737.
- [202] L. Riley, L. Schirmer, T. Segura, Curr. Opin. Biotechnol. 2019, 60, 1.
- [203] A. Sheikhi, J. de Rutte, R. Haghniaz, O. Akouissi, A. Sohrabi, D. Di Carlo, A. Khademhosseini, *Biomaterials* 2019, 192, 560.
- [204] M. G. A. Mohamed, S. Kheiri, S. Islam, H. Kumar, A. Yang, K. Kim, Lab Chip 2019, 19, 1621.
- [205] P. S. Briquez, L. E. Clegg, M. M. Martino, F. M. Gabhann, J. A. Hubbell, *Nat. Rev. Mater.* **2016**, *1*, 15006.
- [206] M. D. Sarker, S. Naghieh, N. K. Sharma, X. Chen, J. Pharm. Anal. 2018. 8, 277.
- [207] T. Xu, W. Zhao, J.-M. Zhu, M. Z. Albanna, J. J. Yoo, A. Atala, *Biomaterials* 2013, 34, 130.
- [208] X. Cui, T. Boland, Biomaterials 2009, 30, 6221.
- [209] A. Faulkner-Jones, C. Fyfe, D.-J. Cornelissen, J. Gardner, J. King, A. Courtney, W. Shu, Biofabrication 2015, 7, 044102.
- [210] V. Ozbolat, M. Dey, B. Ayan, A. Povilianskas, M. C. Demirel, I. T. Ozbolat, ACS Biomater. Sci. Eng. 2018, 4, 682.
- [211] L. Ouyang, C. B. Highley, W. Sun, J. A. Burdick, Adv. Mater. 2017, 29, 1604983.
- [212] D. Therriault, S. R. White, J. A. Lewis, Nat. Mater. 2003, 2, 265.
- [213] L. Ouyang, C. B. Highley, C. B. Rodell, W. Sun, J. A. Burdick, ACS Biomater. Sci. Eng. 2016, 2, 1743.
- [214] C. B. Highley, C. B. Rodell, J. A. Burdick, Adv. Mater. 2015, 27, 5075
- [215] A. Lee, A. R. Hudson, D. J. Shiwarski, J. W. Tashman, T. J. Hinton, S. Yerneni, J. M. Bliley, P. G. Campbell, A. W. Feinberg, *Science* 2019, 365, 482.
- [216] T. J. Hinton, Q. Jallerat, R. N. Palchesko, J. H. Park, M. S. Grodzicki, H.-J. Shue, M. H. Ramadan, A. R. Hudson, A. W. Feinberg, Sci. Adv. 2015, 1, 1500758.
- [217] T. Bhattacharjee, S. M. Zehnder, K. G. Rowe, S. Jain, R. M. Nixon, W. G. Sawyer, T. E. Angelini, Sci. Adv. 2015, 1, 1500655.
- [218] C. D. Morley, S. T. Ellison, T. Bhattacharjee, C. S. O'Bryan, Y. Zhang, K. F. Smith, C. P. Kabb, M. Sebastian, G. L. Moore, K. D. Schulze, S. Niemi, W. G. Sawyer, D. D. Tran, D. A. Mitchell, B. S. Sumerlin, C. T. Flores, T. E. Angelini, *Nat. Commun.* 2019, 10, 3029
- [219] X. Cao, R. Ashfaq, F. Cheng, S. Maharjan, J. Li, G. Ying, S. Hassan, H. Xiao, K. Yue, Y. S. Zhang, Adv. Funct. Mater. 2019, 29, 1807173.
- [220] G. Gao, J. Y. Park, B. S. Kim, J. Jang, D.-W. Cho, Adv. Healthcare Mater. 2018, 7, 1801102.
- [221] Q. Gao, Y. He, J. Fu, A. Liu, L. Ma, Biomaterials 2015, 61, 203.
- [222] W. Jia, P. S. Gungor-Ozkerim, Y. S. Zhang, K. Yue, K. Zhu, W. Liu, Q. Pi, B. Byambaa, M. R. Dokmeci, S. R. Shin, A. Khademhosseini, *Biomaterials* 2016, 106, 58.
- [223] C. Colosi, S. R. Shin, V. Manoharan, S. Massa, M. Costantini, A. Barbetta, M. R. Dokmeci, M. Dentini, A. Khademhosseini, Adv. Mater. 2016, 28, 677.
- [224] Y. Zhang, Y. Yu, H. Chen, I. T. Ozbolat, Biofabrication 2013, 5, 025004.
- [225] L. Zhao, V. K. Lee, S.-S. Yoo, G. Dai, X. Intes, Biomaterials 2012, 33, 5325.
- [226] L. E. Bertassoni, M. Cecconi, V. Manoharan, M. Nikkhah, J. Hjortnaes, A. L. Cristino, G. Barabaschi, D. Demarchi, M. R. Dokmeci, Y. Yang, A. Khademhosseini, *Lab Chip* 2014, 14, 2202.
- [227] T.-C. Tseng, F.-Y. Hsieh, P. Theato, Y. Wei, S. Hsu, Biomaterials 2017, 133, 20.
- [228] K. H. Song, C. B. Highley, A. Rouff, J. A. Burdick, Adv. Funct. Mater. 2018, 28, 1801331.

www.adviicaitiiiiat.d

- [229] J. S. Miller, K. R. Stevens, M. T. Yang, B. M. Baker, D.-H. T. Nguyen, D. M. Cohen, E. Toro, A. A. Chen, P. A. Galie, X. Yu, R. Chaturvedi, S. N. Bhatia, C. S. Chen, *Nat. Mater.* 2012, 11, 768.
- [230] M. Hu, A. Dailamy, X. Y. Lei, U. Parekh, D. McDonald, A. Kumar, P. Mali, Adv. Healthcare Mater. 2018, 7, 1800845.
- [231] D. B. Kolesky, K. A. Homan, M. A. Skylar-Scott, J. A. Lewis, *Proc. Natl. Acad. Sci. USA* 2016, 113, 3179.
- [232] T. Mirabella, J. W. MacArthur, D. Cheng, C. K. Ozaki, Y. J. Woo, M. T. Yang, C. S. Chen, *Nat. Biomed. Eng.* 2017, 1, 0083.
- [233] D. B. Kolesky, R. L. Truby, A. S. Gladman, T. A. Busbee, K. A. Homan, J. A. Lewis, Adv. Mater. 2014, 26, 3124.
- [234] W. Wu, A. DeConinck, J. A. Lewis, Adv. Mater. 2011, 23, H178.
- [235] C. Norotte, F. S. Marga, L. E. Niklason, G. Forgacs, *Biomaterials* 2009, 30, 5910.
- [236] K. Jakab, C. Norotte, B. Damon, F. Marga, A. Neagu, C. L. Besch-Williford, A. Kachurin, K. H. Church, H. Park, V. Mironov, R. Markwald, G. Vunjak-Novakovic, G. Forgacs, *Tissue Eng.*, Part A 2008, 14, 413.
- [237] H.-F. Guo, W.-W. Dai, D.-H. Qian, Z.-X. Qin, Y. Lei, X.-Y. Hou, C. Wen, Acta Biomater. 2017, 54, 107.
- [238] J. B. Lee, X. Wang, S. Faley, B. Baer, D. A. Balikov, H.-J. Sung, L. M. Bellan, Adv. Healthcare Mater. 2016, 5, 781.
- [239] S. Bertlein, D. Hikimoto, G. Hochleitner, J. Hümmer, T. Jungst, M. Matsusaki, M. Akashi, J. Groll, Small 2018, 14, 1701521.
- [240] H. Ahn, Y. M. Ju, H. Takahashi, D. F. Williams, J. J. Yoo, S. J. Lee, T. Okano, A. Atala, *Acta Biomater.* 2015, 16, 14.
- [241] J. J. Stankus, L. Soletti, K. Fujimoto, Y. Hong, D. A. Vorp, W. R. Wagner, Biomaterials 2007, 28, 2738.
- [242] X. Li, B. Cho, R. Martin, M. Seu, C. Zhang, Z. Zhou, J. S. Choi, X. Jiang, L. Chen, G. Walia, J. Yan, M. Callanan, H. Liu, K. Colbert, J. Morrissette-McAlmon, W. Grayson, S. Reddy, J. M. Sacks, H.-Q. Mao, Sci. Transl. Med. 2019, 11, aau6210.
- [243] A. Sydney Gladman, E. A. Matsumoto, R. G. Nuzzo, L. Mahadevan, J. A. Lewis, *Nat. Mater.* **2016**, *15*, 413.
- [244] Z. Ding, C. Yuan, X. Peng, T. Wang, H. J. Qi, M. L. Dunn, Sci. Adv. 2017, 3, 1602890.
- [245] D. Foresti, K. T. Kroll, R. Amissah, F. Sillani, K. A. Homan, D. Poulikakos, J. A. Lewis, Sci. Adv. 2018, 4, aat1659.
- [246] B. Kang, J. Shin, H.-J. Park, C. Rhyou, D. Kang, S.-J. Lee, Y. Yoon, S.-W. Cho, H. Lee, *Nat. Commun.* **2018**, *9*, 5402.
- [247] M. N. S. de Graaf, A. Cochrane, F. E. van den Hil, W. Buijsman, A. D. van der Meer, A. van den Berg, C. L. Mummery, V. V. Orlova, APL Bioeng. 2019, 3, 026105.
- [248] A. Tocchio, M. Tamplenizza, F. Martello, I. Gerges, E. Rossi, S. Argentiere, S. Rodighiero, W. Zhao, P. Milani, C. Lenardi, Biomaterials 2015, 45, 124.
- [249] Y. Sun, Q. Jallerat, J. M. Szymanski, A. W. Feinberg, *Nat. Methods* 2015, 12, 134.
- [250] X.-Y. Wang, Z.-H. Jin, B.-W. Gan, S.-W. Lv, M. Xie, W.-H. Huang, Lab Chip 2014, 14, 2709.
- [251] J. D. Baranski, R. R. Chaturvedi, K. R. Stevens, J. Eyckmans, B. Carvalho, R. D. Solorzano, M. T. Yang, J. S. Miller, S. N. Bhatia, C. S. Chen, Proc. Natl. Acad. Sci. USA 2013, 110, 7586.
- [252] J. L. Charest, L. E. Bryant, A. J. Garcia, W. P. King, *Biomaterials* 2004, 25, 4767.
- [253] Y. Zheng, J. Chen, M. Craven, N. W. Choi, S. Totorica, A. Diaz-Santana, P. Kermani, B. Hempstead, C. Fischbach-Teschl, J. A. Lopez, A. D. Stroock, *Proc. Natl. Acad. Sci. USA* 2012, 109, 9342.
- [254] K. H. K. Wong, J. G. Truslow, A. H. Khankhel, K. L. S. Chan, J. Tien, J. Biomed. Mater. Res., Part A 2013, 101A, 2181.
- [255] A. P. Golden, J. Tien, Lab Chip 2007, 7, 720.
- [256] T. Takei, S. Sakai, T. Ono, H. Ijima, K. Kawakami, *Biotechnol. Bioeng.* 2006, 95, 1.

- [257] J. A. Jiménez-Torres, S. L. Peery, K. E. Sung, D. J. Beebe, Adv. Healthcare Mater. 2016. 5, 198.
- [258] P. N. Ingram, L. E. Hind, J. A. Jiminez-Torres, A. Huttenlocher, D. J. Beebe, Adv. Healthcare Mater. 2018, 7, 1700497.
- [259] N. Sadr, M. Zhu, T. Osaki, T. Kakegawa, Y. Yang, M. Moretti, J. Fukuda, A. Khademhosseini, *Biomaterials* 2011, 32, 7479.
- [260] K. T. Dicker, A. C. Moore, N. T. Garabedian, H. Zhang, S. L. Scinto, R. E. Akins, D. L. Burris, J. M. Fox, X. Jia, ACS Appl. Mater. Interfaces 2019, 11, 16402.
- [261] J. Huling, I. K. Ko, A. Atala, J. J. Yoo, Acta Biomater. 2016, 32, 190.
- [262] J. R. Gershlak, S. Hernandez, G. Fontana, L. R. Perreault, K. J. Hansen, S. A. Larson, B. Y. K. Binder, D. M. Dolivo, T. Yang, T. Dominko, M. W. Rolle, P. J. Weathers, F. Medina-Bolivar, C. L. Cramer, W. L. Murphy, G. R. Gaudette, *Biomaterials* 2017, 125, 13.
- [263] J. He, M. Mao, Y. Liu, J. Shao, Z. Jin, D. Li, Adv. Healthcare Mater. 2013, 2, 1108.
- [264] L. Wong, J. D. Pegan, B. Gabela-Zuniga, M. Khine, K. E. McCloskey, Biofabrication 2017, 9, 021001.
- [265] S. Chen, N. Kawazoe, G. Chen, Tissue Eng., Part C 2017, 23, 367.
- [266] R. Wang, J. Ozsvar, B. Aghaei-Ghareh-Bolagh, M. A. Hiob, S. M. Mithieux, A. S. Weiss, Biomaterials 2019, 192, 334.
- [267] K. Kinoshita, M. Iwase, M. Yamada, Y. Yajima, M. Seki, *Biotechnol. J.* 2016, 11, 1415.
- [268] K. A. DiVito, M. A. Daniele, S. A. Roberts, F. S. Ligler, A. A. Adams, Biomaterials 2017, 138, 142.
- [269] L. Jia, F. Han, H. Yang, G. Turnbull, J. Wang, J. Clarke, W. Shu, M. Guo, B. Li, Adv. Healthcare Mater. 2019, 8, 1900435.
- [270] T. T. Lee, J. R. García, J. I. Paez, A. Singh, E. A. Phelps, S. Weis, Z. Shafiq, A. Shekaran, A. del Campo, A. J. García, *Nat. Mater.* 2015, 14, 352.
- [271] M. S. Hahn, J. S. Miller, J. L. West, Adv. Mater. 2006, 18, 2679.
- [272] J. C. Culver, J. C. Hoffmann, R. A. Poché, J. H. Slater, J. L. West, M. E. Dickinson, Adv. Mater. 2012, 24, 2344.
- [273] M. Nikkhah, N. Eshak, P. Zorlutuna, N. Annabi, M. Castello, K. Kim, A. Dolatshahi-Pirouz, F. Edalat, H. Bae, Y. Yang, A. Khademhosseini, *Biomaterials* 2012, 33, 9009.
- [274] H. Aubin, J. W. Nichol, C. B. Hutson, H. Bae, A. L. Sieminski, D. M. Cropek, P. Akhyari, A. Khademhosseini, *Biomaterials* 2010, 31, 6941.
- [275] M. Kazemzadeh-Narbat, J. Rouwkema, N. Annabi, H. Cheng, M. Ghaderi, B.-H. Cha, M. Aparnathi, A. Khalilpour, B. Byambaa, E. Jabbari, A. Tamayol, A. Khademhosseini, Adv. Healthcare Mater. 2017, 6, 1601122.
- [276] M. Fenech, V. Girod, V. Claveria, S. Meance, M. Abkarian, B. Charlot, *Lab Chip* **2019**, *19*, 2096.
- [277] A. P. Zhang, X. Qu, P. Soman, K. C. Hribar, J. W. Lee, S. Chen, S. He, Adv. Mater. 2012, 24, 4266.
- [278] W. Zhu, X. Qu, J. Zhu, X. Ma, S. Patel, J. Liu, P. Wang, C. S. E. Lai, M. Gou, Y. Xu, K. Zhang, S. Chen, *Biomaterials* 2017, 124, 106.
- [279] H. Lin, D. Zhang, P. G. Alexander, G. Yang, J. Tan, A. W.-M. Cheng, R. S. Tuan, *Biomaterials* 2013, 34, 331.
- [280] J. Warner, P. Soman, W. Zhu, M. Tom, S. Chen, ACS Biomater. Sci. Eng. 2016, 2, 1763.
- [281] R. Gauvin, Y.-C. Chen, J. W. Lee, P. Soman, P. Zorlutuna, J. W. Nichol, H. Bae, S. Chen, A. Khademhosseini, *Biomaterials* 2012, 33, 3824.
- [282] R. Zhang, N. B. Larsen, Lab Chip 2017, 17, 4273.
- [283] A. Urrios, C. Parra-Cabrera, N. Bhattacharjee, A. M. Gonzalez-Suarez, L. G. Rigat-Brugarolas, U. Nallapatti, J. Samitier, C. A. DeForest, F. Posas, J. L. Garcia-Cordero, A. Folch, Lab Chip 2016, 16, 2287.
- [284] N. Bhattacharjee, C. Parra-Cabrera, Y. T. Kim, A. P. Kuo, A. Folch, Adv. Mater. 2018, 30, 1800001.

- www.auviicaitiiiiat.uu
- [285] B. Grigoryan, S. J. Paulsen, D. C. Corbett, D. W. Sazer, C. L. Fortin, A. J. Zaita, P. T. Greenfield, N. J. Calafat, J. P. Gounley, A. H. Ta, F. Johansson, A. Randles, J. E. Rosenkrantz, J. D. Louis-Rosenberg, P. A. Galie, K. R. Stevens, J. S. Miller, *Science* 2019, 364, 458.
- [286] A. C. Lamont, M. A. Restaino, M. J. Kim, R. D. Sochol, *Lab Chip* 2019, 19, 2340.
- [287] Z. Wang, X. Jin, Z. Tian, F. Menard, J. F. Holzman, K. Kim, Adv. Healthcare Mater. 2018, 7, 1701249.
- [288] Y. Nahmias, R. E. Schwartz, C. M. Verfaillie, D. J. Odde, Biotechnol. Bioeng. 2005, 92, 129.
- [289] R. Xiong, W. Chai, Y. Huang, Lab Chip 2019, 19, 1644.
- [290] R. Gaebel, N. Ma, J. Liu, J. Guan, L. Koch, C. Klopsch, M. Gruene, A. Toelk, W. Wang, P. Mark, F. Wang, B. Chichkov, W. Li, G. Steinhoff, *Biomaterials* 2011, 32, 9218.
- [291] R. K. Pirlo, P. Wu, J. Liu, B. Ringeisen, Biotechnol. Bioeng. 2012, 109, 262.
- [292] P. K. Wu, B. R. Ringeisen, Biofabrication 2010, 2, 014111.
- [293] Z. Xiong, H. Li, P. Kunwar, Y. Zhu, R. Ramos, S. Mcloughlin, T. Winston, Z. Ma, P. Soman, Biofabrication 2019, 11, 035005.
- [294] J. H. Slater, J. S. Miller, S. S. Yu, J. L. West, Adv. Funct. Mater. 2011, 21, 2876.
- [295] J. H. Slater, J. L. West, Methods Cell Biol. 2014, 119, 193.
- [296] Y. Aizawa, R. Wylie, M. Shoichet, Adv. Mater. 2010, 22, 4831.
- [297] J. H. Slater, P. J. Boyce, M. P. Jancaitis, H. E. Gaubert, A. L. Chang, M. K. Markey, W. Frey, ACS Appl. Mater. Interfaces 2015, 7, 4390.
- [298] A. Farrukh, J. I. Paez, A. del Campo, Adv. Funct. Mater. 2019, 29, 1807734.
- [299] K. Sarveswaran, V. Kurz, Z. Dong, T. Tanaka, S. Penny, G. Timp, Sci. Rep. 2016, 6, 21885.
- [300] H. Hocheng, C. Tseng, Opt. Commun. 2008, 281, 4435.
- [301] O. Sarig-Nadir, N. Livnat, R. Zajdman, S. Shoham, D. Seliktar, Biophys. J. 2009, 96, 4743.
- [302] K. C. Hribar, K. Meggs, J. Liu, W. Zhu, X. Qu, S. Chen, Sci. Rep. 2015, 5, 17203.
- [303] C. K. Arakawa, B. A. Badeau, Y. Zheng, C. A. DeForest, Adv. Mater. 2017, 29, 1703156.
- [304] N. Brandenberg, M. P. Lutolf, Adv. Mater. 2016, 28, 7450.
- [305] K. A. Heintz, M. E. Bregenzer, J. L. Mantle, K. H. Lee, J. L. West, J. H. Slater, Adv. Healthcare Mater. 2016, 5, 2153.
- [306] M. B. Applegate, J. Coburn, B. P. Partlow, J. E. Moreau, J. P. Mondia, B. Marelli, D. L. Kaplan, F. G. Omenetto, *Proc. Natl. Acad. Sci. USA* 2015, 112, 12052.
- [307] K. A. Heintz, D. Mayerich, J. H. Slater, J. Visualized Exp. 2017, 119, 55101.
- [308] J. Guo, K. A. Keller, P. Govyadinov, P. Ruchhoeft, J. H. Slater, D. Mayerich, Anal. Methods 2019, 11, 8.
- [309] H. Sekine, T. Shimizu, K. Sakaguchi, I. Dobashi, M. Wada, M. Yamato, E. Kobayashi, M. Umezu, T. Okano, *Nat. Commun.* 2013. 4, 1399.
- [310] H. Masumoto, T. Ikuno, M. Takeda, H. Fukushima, A. Marui, S. Katayama, T. Shimizu, T. Ikeda, T. Okano, R. Sakata, J. K. Yamashita, Sci. Rep. 2015, 4, 6716.
- [311] A. Ito, K. Ino, M. Hayashida, T. Kobayashi, H. Matsunuma, H. Kagami, M. Ueda, H. Honda, *Tissue Eng.* **2005**, *11*, 1553.
- [312] S. V. Pislaru, Circulation 2006, 114, 1314.
- [313] T. Sun, Q. Shi, Q. Huang, H. Wang, X. Xiong, C. Hu, T. Fukuda, Acta Biomater. 2018, 66, 272.
- [314] B. M. Mattix, T. R. Olsen, M. Casco, L. Reese, J. T. Poole, J. Zhang, R. P. Visconti, A. Simionescu, D. T. Simionescu, F. Alexis, *Biomaterials* 2014, 35, 949.
- [315] K. Shimizu, A. Ito, M. Arinobe, Y. Murase, Y. Iwata, Y. Narita, H. Kagami, M. Ueda, H. Honda, J. Biosci. Bioeng. 2007, 103, 472.
- [316] H. Perea, J. Aigner, U. Hopfner, E. Wintermantel, Cells Tissues Organs 2006, 183, 156.

- [317] M. F. Leong, J. K. C. Toh, C. Du, K. Narayanan, H. F. Lu, T. C. Lim, A. C. A. Wan, J. Y. Ying, *Nat. Commun.* 2013, 4, 2353.
- [318] J. Nawroth, J. Rogal, M. Weiss, S. Y. Brucker, P. Loskill, Adv. Healthcare Mater. 2018, 7, 1700550.
- [319] B. Zhang, M. Radisic, Lab Chip 2017, 17, 2395.
- [320] A. Guan, P. Hamilton, Y. Wang, M. Gorbet, Z. Li, K. S. Phillips, Nat. Biomed. Eng. 2017, 1, 0045.
- [321] S. Kim, H. Lee, M. Chung, N. L. Jeon, Lab Chip 2013, 13, 1489.
- [322] J. Paek, S. E. Park, Q. Lu, K.-T. Park, M. Cho, J. M. Oh, K. W. Kwon, Y. Yi, J. W. Song, H. I. Edelstein, J. Ishibashi, W. Yang, J. W. Myerson, R. Y. Kiseleva, P. Aprelev, E. D. Hood, D. Stambolian, P. Seale, V. R. Muzykantov, D. Huh, ACS Nano 2019. 13, 7627.
- [323] R. Ran, H. Wang, F. Hou, Y. Liu, Y. Hui, N. Petrovsky, F. Zhang, C. Zhao, Adv. Healthcare Mater. 2019, 8, 1900015.
- [324] H.-F. Wang, R. Ran, Y. Liu, Y. Hui, B. Zeng, D. Chen, D. A. Weitz, C.-X. Zhao, ACS Nano 2018, 12, 11600.
- [325] Y.-H. Hsu, M. L. Moya, P. Abiri, C. C. W. Hughes, S. C. George, A. P. Lee, Lab Chip 2013, 13, 81.
- [326] C. Del Amo, C. Borau, N. Movilla, J. Asín, J. M. García-Aznar, Integr. Biol. 2017, 9, 339.
- [327] B. M. Baker, B. Trappmann, S. C. Stapleton, E. Toro, C. S. Chen, Lab Chip 2013, 13, 3246.
- [328] L. F. Alonzo, M. L. Moya, V. S. Shirure, S. C. George, Lab Chip 2015, 15, 3521.
- [329] E. Akbari, G. B. Spychalski, K. K. Rangharajan, S. Prakash, J. W. Song, Lab Chip 2018, 18, 1084.
- [330] C. Souilhol, J. Serbanovic-Canic, M. Fragiadaki, T. J. Chico, V. Ridger, H. Roddie, P. C. Evans, Nat. Rev. Cardiol. 2020, 17, 52.
- [331] A. W. Caulk, G. Tellides, J. D. Humphrey, in *Mechanobiology in Health and Disease* (Ed: S. W. Verbruggen), Elsevier, Cambridge, MA 2018, pp. 215–248.
- [332] M. Kong, J. Lee, I. K. Yazdi, A. K. Miri, Y.-D. Lin, J. Seo, Y. S. Zhang, A. Khademhosseini, S. R. Shin, Adv. Healthcare Mater. 2019, 8, 1801146
- [333] Y. S. Zhang, F. Davoudi, P. Walch, A. Manbachi, X. Luo, V. Dell'Erba, A. K. Miri, H. Albadawi, A. Arneri, X. Li, X. Wang, M. R. Dokmeci, A. Khademhosseini, R. Oklu, *Lab Chip* 2016, 16, 4097
- [334] E. Westein, A. D. van der Meer, M. J. E. Kuijpers, J.-P. Frimat, A. van den Berg, J. W. M. Heemskerk, Proc. Natl. Acad. Sci. USA 2013, 110, 1357.
- [335] P. F. Costa, H. J. Albers, J. E. A. Linssen, H. H. T. Middelkamp, L. van der Hout, R. Passier, A. van den Berg, J. Malda, A. D. van der Meer, Lab Chip 2017, 17, 2785.
- [336] W. S. Nesbitt, E. Westein, F. J. Tovar-Lopez, E. Tolouei, A. Mitchell, J. Fu, J. Carberry, A. Fouras, S. P. Jackson, Nat. Med. 2009, 15, 665.
- [337] S. Loyau, B. Ho-Tin-Noé, M.-C. Bourrienne, Y. Boulaftali, M. Jandrot-Perrus, Arterioscler., Thromb., Vasc. Biol. 2018, 38, 2626.
- [338] T. Mathur, K. A. Singh, N. K. R. Pandian, S.-H. Tsai, T. W. Hein, A. K. Gaharwar, J. M. Flanagan, A. Jain, *Lab Chip* **2019**, *19*, 2500.
- [339] N. K. R. Pandian, R. G. Mannino, W. A. Lam, A. Jain, Curr. Opin. Biomed. Eng. 2018, 5, 29.
- [340] A. Jain, A. Graveline, A. Waterhouse, A. Vernet, R. Flaumenhaft, D. E. Ingber, Nat. Commun. 2016, 7, 10176.
- [341] L. J. Worke, J. E. Barthold, B. Seelbinder, T. Novak, R. P. Main, S. L. Harbin, C. P. Neu, *Adv. Healthcare Mater.* **2017**, *6*, 1700114.
- [342] P. Occhetta, G. Isu, M. Lemme, C. Conficconi, P. Oertle, C. Räz, R. Visone, G. Cerino, M. Plodinec, M. Rasponi, A. Marsano, *Integr. Biol.* 2018, 10, 174.
- [343] N. Kamaly, G. Fredman, J. J. R. Fojas, M. Subramanian, W. I. Choi, K. Zepeda, C. Vilos, M. Yu, S. Gadde, J. Wu, J. Milton, R. Carvalho Leitao, L. Rosa Fernandes, M. Hasan, H. Gao, V. Nguyen, J. Harris, I. Tabas, O. C. Farokhzad, ACS Nano 2016, 10, 5280.

- [344] P. A. Stapleton, M. E. James, A. G. Goodwill, J. C. Frisbee, Pathophysiology 2008, 15, 79.
- [345] J. E. Druso, C. Fischbach, Trends Cancer 2018, 4, 271.
- [346] M. Li, M. Qian, J. Xu, Front. Cardiovasc. Med. 2017, 4, 51.
- [347] N. Escobedo, G. Oliver, Cell Metab. 2017, 26, 598.
- [348] K. J. Mather, B. Mirzamohammadi, A. Lteif, H. O. Steinberg, A. D. Baron, *Diabetes* 2002, 51, 3517.
- [349] N. Shoham, A. Gefen, J. Biomech. 2012, 45, 1.
- [350] R. A. Wimmer, A. Leopoldi, M. Aichinger, N. Wick, B. Hantusch, M. Novatchkova, J. Taubenschmid, M. Hämmerle, C. Esk, J. A. Bagley, D. Lindenhofer, G. Chen, M. Boehm, C. A. Agu, F. Yang, B. Fu, J. Zuber, J. A. Knoblich, D. Kerjaschki, J. M. Penninger, *Nature* 2019, 565, 505.
- [351] J. Rogal, A. Zbinden, K. Schenke-Layland, P. Loskill, Adv. Drug Delivery Rev. 2019, 140, 101.
- [352] D. Irimia, X. Wang, Trends Biotechnol. 2018, 36, 923.
- [353] P. Kongsuphol, S. Gupta, Y. Liu, S. Bhuvanendran Nair Gourikutty, S. K. Biswas, Q. Ramadan, Sci. Rep. 2019, 9, 4887.
- [354] S. Schmitt, P. Hendricks, J. Weir, R. Somasundaram, G. S. Sittampalam, V. S. Nirmalanandhan, Assay Drug Dev. Technol. 2012, 10, 137.
- [355] O. T. Guenat, F. Berthiaume, Biomicrofluidics 2018, 12, 042207.
- [356] N. V. Dorrello, B. A. Guenthart, J. D. O'Neill, J. Kim, K. Cunningham, Y.-W. Chen, M. Biscotti, T. Swayne, H. M. Wobma, S. X. L. Huang, H.-W. Snoeck, M. Bacchetta, G. Vunjak-Novakovic, Sci. Adv. 2017, 3, e1700521.
- [357] K. Kato, R. Diéguez-Hurtado, D. Y. Park, S. P. Hong, S. Kato-Azuma, S. Adams, M. Stehling, B. Trappmann, J. L. Wrana, G. Y. Koh, R. H. Adams, *Nat. Commun.* 2018, 9, 2448.
- [358] P. B. Dieffenbach, C. M. Haeger, A. M. F. Coronata, K. M. Choi, X. Varelas, D. J. Tschumperlin, L. E. Fredenburgh, Am. J. Physiol.: Lung Cell. Mol. Physiol. 2017, 313, L628.
- [359] T. Bertero, W. M. Oldham, K. A. Cottrill, S. Pisano,
 R. R. Vanderpool, Q. Yu, J. Zhao, Y. Tai, Y. Tang, Y.-Y. Zhang,
 S. Rehman, M. Sugahara, Z. Qi, J. Gorcsan, S. O. Vargas,
 R. Saggar, R. Saggar, W. D. Wallace, D. J. Ross, K. J. Haley,
 A. B. Waxman, V. N. Parikh, T. De Marco, P. Y. Hsue, A. Morris,
 M. A. Simon, K. A. Norris, C. Gaggioli, J. Loscalzo, J. Fessel,
 S. Y. Chan, J. Clin. Invest. 2016, 126, 3313.
- [360] S. Uhlig, Am. J. Physiol.: Lung Cell. Mol. Physiol. 2002, 282, 1892
- [361] D. Huh, D. C. Leslie, B. D. Matthews, J. P. Fraser, S. Jurek, G. A. Hamilton, K. S. Thorneloe, M. A. McAlexander, D. E. Ingber, Sci. Transl. Med. 2012, 4, 159ra147.
- [362] D. Bovard, A. Sandoz, K. Luettich, S. Frentzel, A. Iskandar, D. Marescotti, K. Trivedi, E. Guedj, Q. Dutertre, M. C. Peitsch, J. Hoeng, Lab Chip 2018, 18, 3814.
- [363] K. H. Benam, R. Novak, J. Nawroth, M. Hirano-Kobayashi, T. C. Ferrante, Y. Choe, R. Prantil-Baun, J. C. Weaver, A. Bahinski, K. K. Parker, D. E. Ingber, Cell Syst. 2016, 3, 456.
- [364] D. Huh, B. D. Matthews, A. Mammoto, M. Montoya-Zavala, H. Y. Hsin, D. E. Ingber, Science 2010, 328, 1662.
- [365] K. H. Benam, R. Villenave, C. Lucchesi, A. Varone, C. Hubeau, H.-H. Lee, S. E. Alves, M. Salmon, T. C. Ferrante, J. C. Weaver, A. Bahinski, G. A. Hamilton, D. E. Ingber, *Nat. Methods* 2016, 13, 151
- [366] J. Gracia-Sancho, G. Marrone, A. Fernández-Iglesias, Nat. Rev. Gastroenterol. Hepatol. 2019, 16, 221.
- [367] J. Poisson, S. Lemoinne, C. Boulanger, F. Durand, R. Moreau, D. Valla, P.-E. Rautou, J. Hepatol. 2017, 66, 212.
- [368] Z. Song, K. Gupta, I. C. Ng, J. Xing, Y. A. Yang, H. Yu, Semin. Cell Dev. Biol. 2017, 71, 153.
- [369] C. Pastor, Hepatology 2000, 32, 786.
- [370] K. Nishii, E. Brodin, T. Renshaw, R. Weesner, E. Moran, S. Soker, J. L. Sparks, J. Cell. Physiol. 2018, 233, 4272.

- [371] A. Ozkan, N. Ghousifam, P. J. Hoopes, T. E. Yankeelov, M. N. Rylander, Biotechnol. Bioeng. 2019, 116, 1201.
- [372] H. Lee, S. Chae, J. Y. Kim, W. Han, J. Kim, Y. Choi, D.-W. Cho, Biofabrication 2019, 11, 025001.
- [373] L.-D. Ma, Y.-T. Wang, J.-R. Wang, J.-L. Wu, X.-S. Meng, P. Hu, X. Mu, Q.-L. Liang, G.-A. Luo, Lab Chip 2018, 18, 2547.
- [374] M. Gori, M. C. Simonelli, S. M. Giannitelli, L. Businaro, M. Trombetta, A. Rainer, PLoS One 2016, 11, e0159729.
- [375] Y. B. Kang, J. Eo, S. Mert, M. L. Yarmush, O. B. Usta, Sci. Rep. 2018, 8, 8951.
- [376] B. Delalat, C. Cozzi, S. Rasi Ghaemi, G. Polito, F. H. Kriel, T. D. Michl, F. J. Harding, C. Priest, G. Barillaro, N. H. Voelcker, Adv. Funct. Mater. 2018, 28, 1801825.
- [377] Y.-S. Weng, S.-F. Chang, M.-C. Shih, S.-H. Tseng, C.-H. Lai, Adv. Mater. 2017, 29, 1701545.
- [378] L. Lorenz, J. Axnick, T. Buschmann, C. Henning, S. Urner, S. Fang, H. Nurmi, N. Eichhorst, R. Holtmeier, K. Bódis, J.-H. Hwang, K. Müssig, D. Eberhard, J. Stypmann, O. Kuss, M. Roden, K. Alitalo, D. Häussinger, E. Lammert, *Nature* 2018, 562, 128.
- [379] D. Attwell, A. M. Buchan, S. Charpak, M. Lauritzen, B. A. MacVicar, E. A. Newman, *Nature* 2010, 468, 232.
- [380] A. D. Wong, M. Ye, A. F. Levy, J. D. Rothstein, D. E. Bergles, P. C. Searson, Front. Neuroeng. 2013, 6, 7.
- [381] N. J. Abbott, L. Rönnbäck, E. Hansson, Nat. Rev. Neurosci. 2006, 7. 41.
- [382] J. J. Jamieson, P. C. Searson, S. Gerecht, J. Biol. Eng. 2017, 11. 37.
- [383] M. Campisi, Y. Shin, T. Osaki, C. Hajal, V. Chiono, R. D. Kamm, Biomaterials 2018, 180, 117.
- [384] M. Ye, H. M. Sanchez, M. Hultz, Z. Yang, M. Bogorad, A. D. Wong, P. C. Searson, Sci. Rep. 2015, 4, 4681.
- [385] A. Reinitz, J. DeStefano, M. Ye, A. D. Wong, P. C. Searson, *Microvasc. Res.* 2015, 99, 8.
- [386] L. Cucullo, M. Hossain, V. Puvenna, N. Marchi, D. Janigro, BMC Neurosci. 2011, 12, 40.
- [387] B. R. Chen, M. G. Kozberg, M. B. Bouchard, M. A. Shaik, E. M. C. Hillman, J. Am. Heart Assoc. 2014, 3, 000787.
- [388] H. Yousef, C. J. Czupalla, D. Lee, M. B. Chen, A. N. Burke, K. A. Zera, J. Zandstra, E. Berber, B. Lehallier, V. Mathur, R. V. Nair, L. N. Bonanno, A. C. Yang, T. Peterson, H. Hadeiba, T. Merkel, J. Körbelin, M. Schwaninger, M. S. Buckwalter, S. R. Quake, E. C. Butcher, T. Wyss-Coray, *Nat. Med.* 2019, 25, 988.
- [389] S. M. Mueller, D. D. Heistad, Hypertension 1980, 2, 809.
- [390] K. Kisler, A. R. Nelson, S. V. Rege, A. Ramanathan, Y. Wang, A. Ahuja, D. Lazic, P. S. Tsai, Z. Zhao, Y. Zhou, D. A. Boas, S. Sakadžić, B. V. Zlokovic, *Nat. Neurosci.* 2017, 20, 406.
- [391] A. Hoffmann, T. Dege, R. Kunze, A.-S. Ernst, H. Lorenz, L.-I. Böhler, T. Korff, H. H. Marti, S. Heiland, M. Bendszus, X. Helluy, M. Pham, Stroke 2018, 49, 1479.
- [392] W. Abdullahi, D. Tripathi, P. T. Ronaldson, Am. J. Physiol.: Cell Physiol. 2018, 315. C343.
- [393] H. Cho, J. H. Seo, K. H. K. Wong, Y. Terasaki, J. Park, K. Bong, K. Arai, E. H. Lo, D. Irimia, Sci. Rep. 2015, 5, 15222.
- [394] G. Adriani, D. Ma, A. Pavesi, R. D. Kamm, E. L. K. Goh, *Lab Chip* 2017, 17, 448.
- [395] S. Mobini, Y. H. Song, M. W. McCrary, C. E. Schmidt, *Biomaterials* 2019, 198, 146.
- [396] R. Booth, H. Kim, Lab Chip 2012, 12, 1784.
- [397] T. Osaki, V. Sivathanu, R. D. Kamm, Sci. Rep. 2018, 8, 5168.
- [398] G. Li, M. J. Simon, L. M. Cancel, Z.-D. Shi, X. Ji, J. M. Tarbell, B. Morrison, B. M. Fu, Ann. Biomed. Eng. 2010, 38, 2499.
- [399] R. M. Linville, J. G. DeStefano, M. B. Sklar, Z. Xu, A. M. Farrell, M. I. Bogorad, C. Chu, P. Walczak, L. Cheng, V. Mahairaki, K. A. Whartenby, P. A. Calabresi, P. C. Searson, *Biomaterials* 2019, 190-191, 24.

- [400] A. Marino, O. Tricinci, M. Battaglini, C. Filippeschi, V. Mattoli, E. Sinibaldi, G. Ciofani, Small 2018, 14, 1702959.
- [401] Y. Shin, S. H. Choi, E. Kim, E. Bylykbashi, J. A. Kim, S. Chung, D. Y. Kim, R. D. Kamm, R. E. Tanzi, Adv. Sci. 2019, 6, 1900962.
- [402] Y. B. Arık, M. W. van der Helm, M. Odijk, L. I. Segerink, R. Passier, A. van den Berg, A. D. van der Meer, Biomicrofluidics 2018, 12, 042218.
- [403] N. Jourde-Chiche, F. Fakhouri, L. Dou, J. Bellien, S. Burtey, M. Frimat, P.-A. Jarrot, G. Kaplanski, M. Le Quintrec, V. Pernin, C. Rigothier, M. Sallée, V. Fremeaux-Bacchi, D. Guerrot, L. T. Roumenina, Nat. Rev. Nephrol. 2019, 15, 87.
- [404] T. Srivastava, H. Dai, D. P. Heruth, U. S. Alon, R. E. Garola, J. Zhou, R. S. Duncan, A. El-Meanawy, E. T. McCarthy, R. Sharma, M. L. Johnson, V. J. Savin, M. Sharma, Am. J. Physiol.: Renal Physiol. 2018, 314, F22.
- [405] L. Perico, S. Conti, A. Benigni, G. Remuzzi, Nat. Rev. Nephrol. 2016, 12, 692.
- [406] I. Shaw, S. Rider, J. Mullins, J. Hughes, B. Péault, Nat. Rev. Nephrol. 2018, 14, 521.
- [407] G. Targher, C. D. Byrne, Nat. Rev. Nephrol. 2017, 13, 297.
- [408] A. J. King, B. M. Brenner, Am. J. Physiol. 1991, 260, R653.
- [409] F. Tasnim, D. Zink, Am. J. Physiol.: Renal Physiol. 2012, 302, F1055.
- [410] S. Weinbaum, Y. Duan, L. M. Satlin, T. Wang, A. M. Weinstein, Am. J. Physiol.: Renal Physiol. 2010, 299, F1220.
- [411] S. Weinbaum, Y. Duan, M. M. Thi, L. You, Cell. Mol. Bioeng. 2011, 4, 510.
- [412] A. Petrosyan, P. Cravedi, V. Villani, A. Angeletti, J. Manrique, A. Renieri, R. E. De Filippo, L. Perin, S. Da Sacco, *Nat. Commun.* 2019, 10, 3656.
- [413] K.-J. Jang, A. P. Mehr, G. A. Hamilton, L. A. McPartlin, S. Chung, K.-Y. Suh, D. E. Ingber, *Integr. Biol.* 2013, 5, 1119.
- [414] M. J. Wilmer, C. P. Ng, H. L. Lanz, P. Vulto, L. Suter-Dick, R. Masereeuw, Trends Biotechnol. 2016, 34, 156.
- [415] X. Mu, W. Zheng, L. Xiao, W. Zhang, X. Jiang, Lab Chip 2013, 13, 1612.
- [416] A. I. Astashkina, B. K. Mann, G. D. Prestwich, D. W. Grainger, Biomaterials 2012, 33, 4700.
- [417] S. Musah, N. Dimitrakakis, D. M. Camacho, G. M. Church, D. E. Ingber, *Nat. Protoc.* 2018, 13, 1662.
- [418] S. G. Rayner, K. T. Phong, J. Xue, D. Lih, S. J. Shankland, E. J. Kelly, J. Himmelfarb, Y. Zheng, Adv. Healthcare Mater. 2018, 7, 1801120.
- [419] S. Musah, A. Mammoto, T. C. Ferrante, S. S. F. Jeanty, M. Hirano-Kobayashi, T. Mammoto, K. Roberts, S. Chung, R. Novak, M. Ingram, T. Fatanat-Didar, S. Koshy, J. C. Weaver, G. M. Church, D. E. Ingber, *Nat. Biomed. Eng.* 2017, 1, 0069.
- [420] J. S. Dutton, S. S. Hinman, R. Kim, Y. Wang, N. L. Allbritton, Trends Biotechnol. 2019, 37, 744.
- [421] C. P. Gayer, M. D. Basson, Cell. Signalling 2009, 21, 1237.
- [422] J. Bernier-Latmani, T. V. Petrova, Nat. Rev. Gastroenterol. Hepatol. 2017. 14. 510.
- [423] S. Jalili-Firoozinezhad, F. S. Gazzaniga, E. L. Calamari, D. M. Camacho, C. W. Fadel, A. Bein, B. Swenor, B. Nestor, M. J. Cronce, A. Tovaglieri, O. Levy, K. E. Gregory, D. T. Breault, J. M. S. Cabral, D. L. Kasper, R. Novak, D. E. Ingber, *Nat. Biomed. Eng.* 2019, *3*, 520.
- [424] H. J. Kim, D. Huh, G. Hamilton, D. E. Ingber, Lab Chip 2012, 12, 2165.
- [425] P. D. Cani, B. F. Jordan, Nat. Rev. Gastroenterol. Hepatol. 2018, 15, 671.
- [426] D. B. Gunasekara, J. Speer, Y. Wang, D. L. Nguyen, M. I. Reed, N. M. Smiddy, J. S. Parker, J. K. Fallon, P. C. Smith, C. E. Sims, S. T. Magness, N. L. Allbritton, *Anal. Chem.* 2018, 90, 13331.
- [427] W. Shin, H. J. Kim, Proc. Natl. Acad. Sci. USA 2018, 115, E10539.



- [429] Y. Wang, D. B. Gunasekara, M. I. Reed, M. DiSalvo, S. J. Bultman, C. E. Sims, S. T. Magness, N. L. Allbritton, *Biomaterials* 2017, 128, 44
- [430] R. Kim, Y. Wang, S.-H. J. Hwang, P. J. Attayek, N. M. Smiddy, M. I. Reed, C. E. Sims, N. L. Allbritton, Lab Chip 2018, 18, 2202.
- [431] K. Pocock, L. Delon, V. Bala, S. Rao, C. Priest, C. Prestidge, B. Thierry, ACS Biomater. Sci. Eng. 2017, 3, 951.
- [432] K. Pocock, L. C. Delon, A. Khatri, C. Prestidge, R. Gibson, C. Barbe, B. Thierry, *Biomater. Sci.* 2019, 7, 2410.
- [433] D.-Y. Yu, P. K. Yu, S. J. Cringle, M. H. Kang, E.-N. Su, Prog. Retinal Eye Res. 2014, 40, 53.
- [434] J. Cunha-Vaz, R. Bernardes, C. Lobo, Eur. J. Ophthalmol. 2011, 21,
- [435] M. Coca-Prados, J. Glaucoma 2014, 23, S36.
- [436] C. J. Pournaras, E. Rungger-Brändle, C. E. Riva, S. H. Hardarson, E. Stefansson, Prog. Retinal Eye Res. 2008, 27, 284.
- [437] S. T. Braakman, J. E. Moore, C. R. Ethier, D. R. Overby, Exp. Eye Res. 2016, 146, 17.
- [438] M. Goel, Open Ophthalmol. J. 2010, 4, 52.
- [439] P. Törnquist, A. Alm, A. Bill, Eye 1990, 4, 303.
- [440] B. Molins, A. Mora, S. Romero-Vázquez, A. Pascual-Méndez, S. Rovira, M. Figueras-Roca, M. Balcells, A. Adán, J. Martorell, Exp. Eye Res. 2019, 187, 107751.
- [441] M. Mesquida, F. Drawnel, S. Fauser, Semin. Immunopathol. 2019, 41, 427.
- [442] C. P. Ring, T. C. Pearson, M. D. Sanders, G. Wetherley-Mein, Br. J. Ophthalmol. 1976, 60, 397.
- [443] A. Ishibazawa, T. Nagaoka, H. Yokota, S. Ono, A. Yoshida, Exp. Eye Res. 2013, 116, 308.
- [444] H. Xu, A. Manivannan, K. A. Goatman, H.-R. Jiang, J. Liversidge, P. F. Sharp, J. V. Forrester, I. J. Crane, J. Leukocyte Biol. 2004, 75, 224
- [445] D. Y. Park, J. Lee, J. Kim, K. Kim, S. Hong, S. Han, Y. Kubota, H. G. Augustin, L. Ding, J. W. Kim, H. Kim, Y. He, R. H. Adams, G. Y. Koh, *Nat. Commun.* 2017, 8, 15296.
- [446] M. Chung, S. Lee, B. J. Lee, K. Son, N. L. Jeon, J. H. Kim, Adv. Healthcare Mater. 2018, 7, 1700028.
- [447] J. Ko, Y. Lee, S. Lee, S. Lee, N. L. Jeon, Adv. Healthcare Mater. 2019, 8. 1900328.
- [448] J. Yeste, M. García-Ramírez, X. Illa, A. Guimerà, C. Hernández, R. Simó, R. Villa, Lab Chip 2018, 18, 95.
- [449] D. Bennet, Z. Estlack, T. Reid, J. Kim, Lab Chip 2018, 18, 1539.
- [450] L.-J. Chen, S. Ito, H. Kai, K. Nagamine, N. Nagai, M. Nishizawa, T. Abe, H. Kaji, Sci. Rep. 2017, 7, 3538.
- [451] J. Seo, W. Y. Byun, F. Alisafaei, A. Georgescu, Y.-S. Yi, M. Massaro-Giordano, V. B. Shenoy, V. Lee, V. Y. Bunya, D. Huh, Nat. Med. 2019 25 1310
- [452] E. Brakenhielm, K. Alitalo, Nat. Rev. Cardiol. 2019, 16, 56.
- [453] L. Planas-Paz, E. Lammert, Cell. Mol. Life Sci. 2013, 70, 4341.
- [454] J. M. Rutkowski, K. C. Boardman, M. A. Swartz, Am. J. Physiol.: Heart Circ. Physiol. 2006, 291, H1402.
- [455] K. C. Boardman, M. A. Swartz, Circ. Res. 2003, 92, 801.
- [456] C. P. Ng, C.-L. E. Helm, M. A. Swartz, Microvasc. Res. 2004, 68, 258.
- [457] M. A. Swartz, A. W. Lund, Nat. Rev. Cancer 2012, 12, 210.
- [458] J. D. Shields, M. E. Fleury, C. Yong, A. A. Tomei, G. J. Randolph, M. A. Swartz, Cancer Cell 2007, 11, 526.
- [459] G. J. Randolph, V. Angeli, M. A. Swartz, Nat. Rev. Immunol. 2005, 5, 617.
- [460] S. Parlato, A. De Ninno, R. Molfetta, E. Toschi, D. Salerno, A. Mencattini, G. Romagnoli, A. Fragale, L. Roccazzello,

M. Buoncervello, I. Canini, E. Bentivegna, M. Falchi, F. R. Bertani, A. Gerardino, E. Martinelli, C. Natale, R. Paolini, L. Businaro, L. Gabriele, *Sci. Rep.* **2017**, *7*, 1093.

- [461] C.-L. E. Helm, A. Zisch, M. A. Swartz, Biotechnol. Bioeng. 2007, 96, 167
- [462] W. Sun, Z. Luo, J. Lee, H.-J. Kim, K. Lee, P. Tebon, Y. Feng, M. R. Dokmeci, S. Sengupta, A. Khademhosseini, Adv. Healthcare Mater. 2019, 8, 1801363.
- [463] P. Moura Rosa, N. Gopalakrishnan, H. Ibrahim, M. Haug, Ø. Halaas, Lab Chip 2016, 16, 3728.
- [464] S. Shim, M. C. Belanger, A. R. Harris, J. M. Munson, R. R. Pompano, Lab Chip 2019, 19, 1013.
- [465] H. Mollica, A. Coclite, M. E. Miali, R. C. Pereira, L. Paleari, C. Manneschi, A. DeCensi, P. Decuzzi, *Biomicrofluidics* 2018, 12, 042205.
- [466] H. N. Kim, N. L. Habbit, C. Su, N. Choi, E. H. Ahn, E. A. Lipke, D. Kim, Adv. Funct. Mater. 2019, 29, 1807553.
- [467] S. Liang, M. J. Slattery, D. Wagner, S. I. Simon, C. Dong, Ann. Biomed. Eng. 2008, 36, 661.
- [468] M. De Palma, D. Biziato, T. V. Petrova, Nat. Rev. Cancer 2017, 17, 457.
- [469] D. Rodenhizer, T. Dean, E. D'Arcangelo, A. P. McGuigan, Adv. Healthcare Mater. 2018, 7, 1701174.
- [470] X.-Y. Wang, Y. Pei, M. Xie, Z.-H. Jin, Y.-S. Xiao, Y. Wang, L.-N. Zhang, Y. Li, W.-H. Huang, Lab Chip 2015, 15, 1178.
- [471] V. Kumar, S. Varghese, Adv. Healthcare Mater. 2019, 8, 1801198.
- [472] H. J. Lee, M. F. Diaz, K. M. Price, J. A. Ozuna, S. Zhang, E. M. Sevick-Muraca, J. P. Hagan, P. L. Wenzel, *Nat. Commun.* 2017, 8, 14122.
- [473] M. K. Shin, S. K. Kim, H. Jung, Lab Chip 2011, 11, 3880.
- [474] J. S. Jeon, S. Bersini, M. Gilardi, G. Dubini, J. L. Charest, M. Moretti, R. D. Kamm, Proc. Natl. Acad. Sci. USA 2015, 112, 214.
- [475] W. J. Polacheck, J. L. Charest, R. D. Kamm, Proc. Natl. Acad. Sci. USA 2011, 108, 11115.
- [476] M. B. Chen, J. M. Lamar, R. Li, R. O. Hynes, R. D. Kamm, Cancer Res. 2016, 76, 2513.
- [477] A. C. Shieh, H. A. Rozansky, B. Hinz, M. A. Swartz, Cancer Res. 2011, 71, 790.
- [478] S. H. Au, B. D. Storey, J. C. Moore, Q. Tang, Y.-L. Chen, S. Javaid, A. F. Sarioglu, R. Sullivan, M. W. Madden, R. O'Keefe, D. A. Haber, S. Maheswaran, D. M. Langenau, S. L. Stott, M. Toner, *Proc. Natl. Acad. Sci. USA* 2016, 113, 4947.
- [479] M. Dabagh, A. Randles, PLoS One 2019, 14, 0211418.
- [480] E. M. Balzer, Z. Tong, C. D. Paul, W.-C. Hung, K. M. Stroka, A. E. Boggs, S. S. Martin, K. Konstantopoulos, FASEB J. 2012, 26, 4045
- [481] G. Follain, N. Osmani, A. S. Azevedo, G. Allio, L. Mercier, M. A. Karreman, G. Solecki, M. J. Garcia Leòn, O. Lefebvre, N. Fekonja, C. Hille, V. Chabannes, G. Dollé, T. Metivet, F. D. Hovsepian, C. Prudhomme, A. Pichot, N. Paul, R. Carapito, S. Bahram, B. Ruthensteiner, A. Kemmling, S. Siemonsen, T. Schneider, J. Fiehler, M. Glatzel, F. Winkler, Y. Schwab, K. Pantel, S. Harlepp, J. G. Goetz, Dev. Cell 2018, 45, 33.
- [482] Y. Xin, X. Chen, X. Tang, K. Li, M. Yang, W. C.-S. Tai, Y. Liu, Y. Tan, Biophys. J. 2019, 116, 1803.
- [483] M. J. Mitchell, C. Denais, M. F. Chan, Z. Wang, J. Lammerding, M. R. King, Am. J. Physiol.: Cell Physiol. 2015, 309, C736.
- [484] V. C. Shukla, T. Kuang, A. Senthilvelan, N. Higuita-Castro, S. Duarte-Sanmiguel, S. N. Ghadiali, D. Gallego-Perez, *Trends Biotechnol.* 2018, 36, 549.
- [485] C. F. Buchanan, S. S. Verbridge, P. P. Vlachos, M. N. Rylander, Cell Adhes. Migr. 2014, 8, 517.
- [486] F. De Sanctis, S. Ugel, J. Facciponte, A. Facciabene, Semin. Immunol. 2018, 35, 35.

- [487] A. C. Dudley, Cold Spring Harbor Perspect. Med. 2012, 2, a006536.
- [488] K. Ghosh, C. K. Thodeti, A. C. Dudley, A. Mammoto, M. Klagsbrun, D. E. Ingber, Proc. Natl. Acad. Sci. USA 2008, 105, 11305.
- [489] M. Tichet, V. Prod'Homme, N. Fenouille, D. Ambrosetti, A. Mallavialle, M. Cerezo, M. Ohanna, S. Audebert, S. Rocchi, D. Giacchero, F. Boukari, M. Allegra, J.-C. Chambard, J.-P. Lacour, J.-F. Michiels, J.-P. Borg, M. Deckert, S. Tartare-Deckert, Nat. Commun. 2015, 6, 6993.
- [490] M. W. Dewhirst, T. W. Secomb, Nat. Rev. Cancer 2017, 17, 738.
- [491] S. G. Mina, P. Huang, B. T. Murray, G. J. Mahler, Biomicrofluidics 2017, 11, 044104.
- [492] T. Stylianopoulos, L. L. Munn, R. K. Jain, Trends Cancer 2018, 4, 258.
- [493] S. Pradhan, A. M. Smith, C. J. Garson, I. Hassani, W. J. Seeto, K. Pant, R. D. Arnold, B. Prabhakarpandian, E. A. Lipke, Sci. Rep. 2018, 8, 3171.
- [494] F. Meng, C. M. Meyer, D. Joung, D. A. Vallera, M. C. McAlpine, A. Panoskaltsis-Mortari, Adv. Mater. 2019, 31, 1806899.
- [495] Y. Xiao, D. Kim, B. Dura, K. Zhang, R. Yan, H. Li, E. Han, J. Ip, P. Zou, J. Liu, A. T. Chen, A. O. Vortmeyer, J. Zhou, R. Fan, Adv. Sci. 2019, 6, 1801531.
- [496] S. Nagaraju, D. Truong, G. Mouneimne, M. Nikkhah, Adv. Health-care Mater. 2018, 7, 1701257.
- [497] M. B. Chen, J. A. Whisler, J. Fröse, C. Yu, Y. Shin, R. D. Kamm, Nat. Protoc. 2017, 12, 865.
- [498] C. D. Edington, W. L. K. Chen, E. Geishecker, T. Kassis, L. R. Soenksen, B. M. Bhushan, D. Freake, J. Kirschner, C. Maass, N. Tsamandouras, J. Valdez, C. D. Cook, T. Parent, S. Snyder, J. Yu, E. Suter, M. Shockley, J. Velazquez, J. J. Velazquez, L. Stockdale, J. P. Papps, I. Lee, N. Vann, M. Gamboa, M. E. LaBarge, Z. Zhong, X. Wang, L. A. Boyer, D. A. Lauffenburger, R. L. Carrier, C. Communal, S. R. Tannenbaum, C. L. Stokes, D. J. Hughes, G. Rohatgi, D. L. Trumper, M. Cirit, L. G. Griffith, Sci. Rep. 2018, 8, 4530.
- [499] V. S. Shirure, Y. Bi, M. B. Curtis, A. Lezia, M. M. Goedegebuure, S. P. Goedegebuure, R. Aft, R. C. Fields, S. C. George, *Lab Chip* 2018. 18, 3687.
- [500] Y. S. Zhang, J. Aleman, S. R. Shin, T. Kilic, D. Kim, S. A. Mousavi Shaegh, S. Massa, R. Riahi, S. Chae, N. Hu, H. Avci, W. Zhang, A. Silvestri, A. Sanati Nezhad, A. Manbohi, F. De Ferrari, A. Polini, G. Calzone, N. Shaikh, P. Alerasool, E. Budina, J. Kang, N. Bhise, J. Ribas, A. Pourmand, A. Skardal, T. Shupe, C. E. Bishop, M. R. Dokmeci, A. Atala, A. Khademhosseini, *Proc. Natl. Acad. Sci.* USA 2017, 114, E2293.
- [501] M. S. Nikshoar, M. A. Khayamian, S. Ansaryan, H. Sanati, M. Gharooni, L. Farahmand, F. Rezakhanloo, K. Majidzadeh-A, P. Hoseinpour, S. Dadgari, L. Kiani-M, M. Saqafi, M. Gity, M. Abdolahad, *Nat. Commun.* 2017, 8, 2175.
- [502] H. Li, Y. Fan, R. Kodzius, I. G. Foulds, Microsyst. Technol. 2012, 18, 373.
- [503] P. P. Shiu, G. K. Knopf, M. Ostojic, S. Nikumb, J. Micromech. Microeng. 2008, 18, 025012.
- [504] D. A. Bartholomeusz, R. W. Boutte, J. D. Andrade, J. Microelectromech. Syst. 2005, 14, 1364.
- [505] D. J. Guckenberger, T. E. de Groot, A. M. D. Wan, D. J. Beebe, E. W. K. Young, *Lab Chip* 2015, 15, 2364.
- [506] U. N. Lee, X. Su, D. J. Guckenberger, A. M. Dostie, T. Zhang, E. Berthier, A. B. Theberge, Lab Chip 2018, 18, 496.
- [507] D. A. Mair, E. Geiger, A. P. Pisano, J. M. J. Fréchet, F. Svec, *Lab Chip* 2006, 6, 1346.
- [508] Y. Temiz, R. D. Lovchik, G. V. Kaigala, E. Delamarche, Microelectron. Eng. 2015, 132, 156.
- [509] E. A. Jaffe, R. L. Nachman, C. G. Becker, C. R. Minick, J. Clin. Invest. 1973, 52, 2745.
- [510] S. Hauser, F. Jung, J. Pietzsch, Trends Biotechnol. 2017, 35, 265.



ADVANCED HEALTHCARE MATERIALS

www.advhealthmat.de

- [511] H. Patel, J. Chen, K. C. Das, M. Kavdia, Cardiovasc. Diabetol. 2013, 12, 142.
- [512] A. Müller, Exp. Mol. Pathol. 2002, 73, 171.
- [513] J.-T. Chi, H. Y. Chang, G. Haraldsen, F. L. Jahnsen, O. G. Troyanskaya, D. S. Chang, Z. Wang, S. G. Rockson, M. van de Rijn, D. Botstein, P. O. Brown, *Proc. Natl. Acad. Sci.* USA 2003, 100, 10623.
- [514] R. Marcu, Y. J. Choi, J. Xue, C. L. Fortin, Y. Wang, R. J. Nagao, J. Xu, J. W. MacDonald, T. K. Bammler, C. E. Murry, K. Muczynski, K. R. Stevens, J. Himmelfarb, S. M. Schwartz, Y. Zheng, iScience 2018, 4, 20.
- [515] R. E. Unger, V. Krump-Konvalinkova, K. Peters, C. J. Kirkpatrick, Microvasc. Res. 2002, 64, 384.
- [516] A. Cochrane, H. J. Albers, R. Passier, C. L. Mummery, A. van den Berg, V. V. Orlova, A. D. van der Meer, Adv. Drug Delivery Rev. 2019, 140, 68.
- [517] J. A. Jiménez-Torres, M. Virumbrales-Muñoz, K. E. Sung, M. H. Lee, E. J. Abel, D. J. Beebe, EBioMedicine 2019, 42, 408.
- [518] J. S. Mohammed, Y. Wang, T. A. Harvat, J. Oberholzer, D. T. Eddington, Lab Chip 2009, 9, 97.
- [519] S. H. Lee, S. Hong, J. Song, B. Cho, E. J. Han, S. Kondapavulur, D. Kim, L. P. Lee, Adv. Healthcare Mater. 2018, 7, 1701111.
- [520] T. Tao, Y. Wang, W. Chen, Z. Li, W. Su, Y. Guo, P. Deng, J. Qin, Lab Chip 2019, 19, 948.
- [521] A. L. Glieberman, B. D. Pope, J. F. Zimmerman, Q. Liu, J. P. Ferrier, J. H. R. Kenty, A. M. Schrell, N. Mukhitov, K. L. Shores,

- A. B. Tepole, D. A. Melton, M. G. Roper, K. K. Parker, *Lab Chip.* **2019**, *19*, 2993.
- [522] K. Shik Mun, K. Arora, Y. Huang, F. Yang, S. Yarlagadda, Y. Ramananda, M. Abu-El-Haija, J. J. Palermo, B. N. Appakalai, J. D. Nathan, A. P. Naren, *Nat. Commun.* 2019, 10, 3124.
- [523] Y. Torisawa, C. S. Spina, T. Mammoto, A. Mammoto, J. C. Weaver, T. Tat, J. J. Collins, D. E. Ingber, Nat. Methods 2014, 11, 663.
- [524] S. G. M. Uzel, R. J. Platt, V. Subramanian, T. M. Pearl, C. J. Rowlands, V. Chan, L. A. Boyer, P. T. C. So, R. D. Kamm, Sci. Adv. 2016, 2, e1501429.
- [525] S. Levenberg, J. Rouwkema, M. Macdonald, E. S. Garfein, D. S. Kohane, D. C. Darland, R. Marini, C. A. van Blitterswijk, R. C. Mulligan, P. A. D'Amore, R. Langer, *Nat. Biotechnol.* 2005, 23, 879.
- [526] T. Osaki, V. Sivathanu, R. D. Kamm, Biomaterials 2018, 156, 65.
- [527] L. Vernetti, A. Gough, N. Baetz, S. Blutt, J. R. Broughman, J. A. Brown, J. Foulke-Abel, N. Hasan, J. In, E. Kelly, O. Kovbasnjuk, J. Repper, N. Senutovitch, J. Stabb, C. Yeung, N. C. Zachos, M. Donowitz, M. Estes, J. Himmelfarb, G. Truskey, J. P. Wikswo, D. L. Taylor, Sci. Rep. 2017, 7, 42296.
- [528] S. Baratchi, K. Khoshmanesh, O. L. Woodman, S. Potocnik, K. Peter, P. McIntyre, Trends Mol. Med. 2017, 23, 850.
- [529] M. C. Lampi, C. A. Reinhart-King, Sci. Transl. Med. 2018, 10, eaao0475.